**Title**

Investigating the Regulation of Translational Stress Responses in S. cerevisiae



**Author**

Baum, Rachel

**Publication Date**

2024

Peer reviewed|Thesis/dissertation

# Investigating the Regulation of Translational Stress Responses in *S. cerevisiae*

By

Rachel Baum

A dissertation submitted in partial satisfaction of the

requirements for the degree of

Doctor of Philosophy

in

Molecular and Cell Biology

in the

Graduate Division

of the

University of California, Berkeley

Committee in charge:

Professor Nicholas Ingolia, Chair
Professor Elçin Ünal
Professor David Savage
Professor James Olzmann

Fall 2024

Abstract

Investigating the Regulation of Translational Stress Responses in *S. cerevisiae*

by

Rachel Baum

Doctor of Philosophy in Molecular and Cell Biology

University of California, Berkeley

Professor Nicholas Ingolia, Chair

Cells are dynamic systems that respond to changes in their environment by sensing these changes and transducing signals to drive gene expression changes that maintain homeostasis. Stresses are fluctuations in the environment that threaten the survival of the cell by impeding its ability to grow and proliferate. Cells respond to stress by adaptively modifying gene expression, transcript abundance, mRNA stability, protein expression, and many other aspects of their physiology, which allows continued growth and proliferation. As a unicellular organism, the budding yeast *Saccharomyces cerevisiae* (*S. cerevisiae*) has evolved to adapt to fluctuations in nutrient availability on a timescale of minutes to hours. This rapid response is crucial for yeast to remain viable during sudden, unfavorable environmental changes; indeed, *S. cerevisiae* has served as a model organism to study the complexity of cellular responses to stress.

In chapter 1, we investigated how differences in nitrogen source quality affects mRNA stability. Nitrogen metabolism is regulated to prefer the use of certain nitrogen sources over others through the nitrogen catabolite repression (NCR) response. Prior work has demonstrated the importance of mRNA destabilization on the NCR. We used a metabolic labeling approach to profile differences in mRNA stability between different quality nitrogen sources. We performed a comprehensive global analysis of transcript stability in S288C and Σ1278b yeast strains. Our data mapped out mRNA transcripts that underwent changes in stability between different quality nitrogen sources. These work exemplify how cells control the stability of pre-existing mRNAs as part of integrated responses to metabolic changes.

In chapter 2, we explored the regulatory role of Gta1, a strongly repressive post-transcriptional regulator. Gta1 is a relatively uncharacterized protein that has been shown to play a role in Golgi and vesicle transport, localizes to the ER, and copurifies with translational machinery. In our work, we profiled the effect of Gta1 overexpression on mRNAs by RNA-seq. We found that Gta1 drives the downregulation of ER and Golgi-localized mRNA transcripts. We also identified a conserved motif within Gta1 that is necessary for its repressor activity.

In chapter 3, we developed new approaches to understand how the rapid translational shutoff in response to glucose starvation is regulated. Compared to other stress responses,

glucose withdrawal leads to the most dramatic translation inhibition based on the magnitude and rapidness of this response. We used a genome-scale CRISPRi based approach, CiBER-seq, to identify gene knockdowns that lead to global resistance to translation inhibition after glucose withdrawal. We optimized the conditions for this assay by modifying the pre-stress growth conditions and the reporter system. The CiBER-seq screen identified several genes that may participate in this response, which will be pursued in future work. This promises new insights into the mechanism of the unique glucose starvation translation inhibition response.

In chapter 4, we interrogated the genetic architecture that regulates the adaptive dynamics of the integrated stress response (ISR). The ISR is a conserved eukaryotic signaling pathway that responds to diverse stress stimuli to restore cellular proteostasis. By pairing a titratable activator of the ISR with a high-throughput CRISRPi based approach, we measured how ISR dynamics change in response to genetic perturbations. We mapped these effects for a subset of CRISPRi guides that we previously demonstrated to affect the ISR. Our data revealed that perturbations of ribosome biogenesis factors shift ISR dynamics due to decreased ribosome availability. We also profiled the combined effects of two CRISPRi guides to look for epistatic interactions that shift ISR dynamics, though we did not analyze these dual-guide data here. We hope that this data will provide useful insight into how ISR dynamics are regulated.

# Acknowledgments

This acknowledgment can never do justice to how much everyone's support has helped carry me through this journey, but I hope this rambly mess conveys at least a little bit of that.

*To Nick*— Before I started graduate school, the main advice I got from friends was that I needed to prioritize finding a great mentor and I feel like I got lucky in joining your lab. Thank you for being such a fountain of knowledge, for having such great advice, and for helping me pivot more than once. Aside from the science, you have been extremely supportive anytime I've told you I was struggling and that is a quality I want to extend to people I mentor in the future.

*To my thesis committee*— To Elçin, Dave, and James, thank you for your continued guidance, even when I felt unsure of myself, you all reassured me and offered words of encouragement and scientific support.

*To my lab*— It's been such an incredible place to do research, largely due to all the people I've had the opportunity to work with over the years. I've seen the lab change so much over the years but our commitment to being the antisocial lab of Barker Hall is unwavering. To Jinyoung, thank you for being so supportive and always offering me your help. I'm going to miss our late-night chats where we always found new ways to express how tired we were. To Anna, thank you for being such a sweet, caring person and for teaching me all the things about KPop. To Wren, I always appreciate our breakroom chats and the wise advice and fun stories you share. To Joe and Paige, thank you for always asking great questions and providing so much scientific support. To Sam, you've been such a pivotal part of my growth as a scientist and in giving me such helpful advice whenever I felt stuck. I also loved your impeccable music taste (potatoes and molasses forever). To Zuriah, thank you for always being such a good friend to me in lab, for being so kind through all my ups and downs, and for letting me know every time I repeated a story. To Mia, you've been a big part of helping me unwind and destress during our pottery classes and I'm forever grateful for that. To Kendra, you've been such a supportive friend, especially over the last year, and I'm so glad we reconnected. To Ryan, thank you for bringing such great ideas into the lab and for making it a more fun place to be.

*To my former mentors*— To Tim, when I finally decided to move away from being premed so late in college, you were the first person to accept me into your lab even though I had no real research experience. You taught me that "science is about self-expression" and I've carried a lot of your philosophies on mentorship with me. To Adam, I learned so much by working with you, and you opened my eyes to a whole world of RNA that I knew so little about. I appreciate you being so supportive and having so much patience in teaching me many of the skills I used throughout graduate school.

*To Dina, my pottery teacher*— I always wanted to be the type of person who had a cool hobby. Trying pottery on a whim brought me more joy than I could've ever expected. Thank you, Dina, for being such a gracious, fun, and encouraging teacher, for bestowing me with "the queen of

Halloween" title, and for being such an incredible potter to aspire to. Your classes were always the bright spot of my week, and I always left in a better headspace than I came in.

*To my Berkeley peeps*—Dylan, Bere and Carolina, you all have been such an amazing support system to me outside of the lab. Thank you for always being there to listen.

*To my found family*— Jenny, thank you for always being my biggest cheerleader, for helping me pursue my California journey, for always celebrating with me, and for sending the most thoughtful care packages. Sonia, thank you for always checking in on me, for giving me more of your energy than you even have available, and for your continuous guidance. To Suleman, thank you for constant encouragement, for always being there for me in a split seconds notice, and for the meals and love you and KT have provided me over the years.

*To my other family*— Gigi and Raymond, thank you both for always being so supportive and helping me through some of my hardest times in life with so much love. To my little Dexteypoo, the first dog I ever loved, thank you for eventually loving me back, and for ushering me off to graduate school. I miss you everyday.

*To my pups*— To my Kunichi, "the divine lady", thank you for being the most grumpy, silly little puppy who will turn any shirt, sweater, sock, or sheet into a blanket for yourself to lay on. Thank you for always reminding me (and demanding) that I need to take breaks to play rope toy with you. To Seki, aka "the baby" aka "the rambunctious little lamb", you were an unexpected little miracle that none of us knew we needed. You bring such a sense of light and goofiness to whatever you're doing. You're also the best little cuddlebug and I'm so happy Kunichi made you a part of our family.

*To my partner*— RC, thank you endlessly and overwhelmingly for all the ways you've supported me over the past decade (or however long we've been together). Your enormous love for me doesn't always make sense to me, but I'm so grateful that we chose each other and get to experience life together. For every new challenge I've thrown your way, for every time I've put more on your plate, you've always accepted it all with all the support in the world. I never imagined being in a relationship could be this much fun and unserious, but I'm so happy we get to do life together. I love you so much and never could have done this without you.

## Table of Contents

# List of Figures

## List of Tables

Chapter 1

# Profiling the Effects of Different Nitrogen Sources on mRNA Stability and Reprogramming the Transcriptome

## 1.1 Abstract

*S. cerevisiae* have evolved the ability to process a wide variety of compounds as nitrogen sources due to heterogeneity in their environment. Nitrogen metabolism is regulated to prefer the use of certain nitrogen sources over others through the nitrogen catabolite repression (NCR) response. In the presence of favored nitrogen sources, the genes needed to break down alternate nitrogen sources are repressed through the NCR. The transcriptional component of this response has been studied extensively, but the destabilization of mRNA has also been implicated in the NCR. Such post-transcriptional regulation is useful for accelerating reprogramming of the transcriptome. By using a metabolic labeling approach, TimeLapse-seq, I profiled both total mRNA abundance and new mRNA transcript abundance in discrete nitrogen sources. Using this method, I was able perform a comprehensive global analysis to map out genes that display the largest changes of stability between conditions of "good" nitrogen sources and "poor" nitrogen sources.

## 1.2 Introduction

Nitrogen is one of the most essential nutrients for biogenic processes, therefore regulation of nitrogen metabolism is complex. *S. cerevisiae* can metabolize a wide variety of compounds as nitrogen sources due to heterogeneity in their environment, selectively favoring certain nitrogen sources over others through activation of Nitrogen Catabolite Repression (NCR) (Magasanik and Kaiser 2002). The NCR works by effecting a physiological response through the inactivation or repression of genes that are utilized for catabolizing the poorer nitrogen source in the presence of a better nitrogen source, which is degraded into building blocks of nitrogen metabolism (Hofman-Bang 1999; ter Schure, van Riel, and Verrips 2000). A "good", or preferred, nitrogen source is characterized by a high specific growth rate and highly active NCR control while a "poor" nitrogen source has a low specific growth rate. The NCR is regulated by selective transcription of genes that encode proteins involved in scavenge, uptake and catabolism of non-preferential nitrogen sources.

Despite the extensive study of the transcriptional regulation of nitrogen metabolism, there is limited understanding of post-transcriptional mRNA regulation in this response. The destabilization of mRNAs is a useful mechanism for accelerating reprogramming of the transcriptome since it occurs on a shorter timescale than transcription and can eliminate existing mRNAs. This reprogramming is likely important to increase the nucleotide pool and facilitate the reallocation of translational capacity (Shachrai et al. 2011; Giordano et al. 2016; Kief and Warner 1981). The importance of mRNA turnover has also been demonstrated in other model systems such as *C. elegans* where selective mRNA stabilization was characterized to play a role in gene expression during development (West et al. 2018). In *S. cerevisiae*, changes in

mRNA stability can result from both starvation, by inducing the environmental stress response, or an upshift in nutrient conditions (Scheffler, de la Cruz, and Prieto 1998; Canadell et al. 2015).

Recently, mRNA stability was identified to play a key role in accelerating reprogramming during an "upshift" from a disfavored nitrogen source to a more favored one, after which 78 mRNA transcripts were subject to destabilization (Miller, Brandt, and Gresham 2018). While this work was important for identifying a role for mRNA stability in reprogramming nitrogen metabolism, it was limited by focusing on a single nitrogen transition upshift and only followed-up by analyzing factors affecting the destabilization of a single mRNA, *GAP1*, which was attributed to modulators of decapping activity and core degradation factors. We were interested in comparing global regulation of mRNA stability in *S. cerevisiae* grown in different nitrogen conditions. We performed a metabolic labeling experiment using TimeLapse-Seq for cells grown in three different nitrogen sources and compared mRNA stability between these conditions. By tracking the formation of new mRNA transcripts with the abundance of preexisting transcripts using TimeLapse-seq, we identified mRNA transcripts that are stabilized in specific nitrogen conditions.

## 1.3 Materials and methods

*Yeast Strains*

Strains used in this study are listed in Table 1.1. Strains were either derived from *S. cerevisiae* BY4741 or Σ1278b using standard genetic techniques. Prototrophic BY4741 (NIY434) was generated by integrating pNTI694 into the X-3 locus with NotI-linearized vector from the Easyclone 2.0 toolkit for yeast genomic integration(Stovicek et al. 2015). Prototrophic Σ1278b (NIY438) was generated by integrating pRB001 into the X-3 locus with NotI-linearized vector from the Easyclone 2.0 toolkit for yeast genomic integration (Stovicek et al. 2015). Gene deletion strain for YLR136C (NIY440) was generated by using one-step-replacement with LEU2 marker cassette (Goldstein and McCusker 1999; Hentges et al. 2005; Stovicek et al. 2015). PCR amplification of *Kluyveromyces lactis* LEU2 cassette from pCfB2189 easyclone 2.0 vector with primers RB110 and RB111 primers with flanking sequence homology to the 5' and 3' ends of target gene coding YLR136C. A second round of PCR amplification with primers RB112 and RB113 to add 45 basepairs of homology to YLR136C on 5' and 3' end. PCR amplification product transformed into yeast using LEU2 selection marker. YLR136C gene deletion was validated by RT-qPCR with qRB007 and qRB008 primers. Plasmids and primers used in strain construction are listed in Table 1.2 and 1.3, respectively.

*Plasmids*

Plasmids used in this study are listed in Table 1.2. Plasmids were generated by Gibson assembly from amplicons made with primers listed in Table 1.2. Amplicons corresponding to HIS3, LEU2, MET17, and URA3 cassettes was subcloned from pNTI599. This was assembled with amplicon of easyclone pCfB2223 vector by Gibson assembly (Stovicek et al. 2015; Gibson et al. 2009). TRP1 amplicons were made by PCR amplification of S288C genomic DNA.

*Nitrogen Media Recipes*

Yeast media composed of 1X Yeast Nitrogen Base without Amino Acids and Ammonium Sulfate (BD, 233520), 2% dextrose, and single nitrogen source of (1) 10 mM ammonium sulfate (2) 10 mM urea or (3) 10 mM methionine.

*Growth Assays*

Cells were grown overnight in YEPD, or ammonium sulfate, urea, methionine nitrogen media to saturation. Cells were back-diluted to 0.2 and grown to mid-log phase (typically 5 mL culture at $OD_{600}$ 0.5 - 1.0), and then further back-diluted to $OD_{600}$ 0.01 in triplicate in a 96-well plate. Absorbance measurements at $OD_{595}$ were taken every 15 minutes, with shaking in between measurements, and temperature maintained at 30℃ (Tecan SPARK Multimode Microplate Reader). Growth rates were fit using the R package 'growthcurver' (Sprouffske and Wagner 2016). Growth assay for *cth2Δ* strain performed using the same method.

*In vitro transcription of TimeLapse-seq reporters*

In vitro transcription of *Renilla Luciferase (RLuc)* and *Firefly Luciferase (ffLuc)* were used to measure conversion efficiency in TimeLapse-seq experiment (Schofield et al. 2018). *RLuc and ffLuc* were amplified from psiCheck2 plasmid by PCR (AP1120 and AP1121, RB5 and RB6 respectively) and PCR product was cleaned up with clean and concentrator kit (Zymo #D4004). DNA template was used for in vitro-transcription reaction (IVT) using T7 RNA polymerase kit (Cell Script #C-AS3107). *RLuc* DNA template was in vitro-transcribed using 0.015 µM s4U (Sigma # 440736) in place of UTP nucleotide in 20µl reaction volume. *ffLuc* was in vitro-transcribed using standard ATP, CTP, GTP, and UTP nucleotides. IVT reactions were incubated at 37℃ for 2 hours. The reaction mixture was treated with TURBO DNase for 15 minutes at 37℃. RNA was purified using oligo clean and concentrate kit (Zymo #D4060), eluted in 10µl 10 mM Tris pH 8.0. Reporters were used as spike-in controls in TimeLapse-seq experiment.

*TimeLapse-seq*

Prototrophic BY4741/Σ1278b yeast cultures were grown to saturation overnight in minimal media containing ammonium sulfate, urea (BY4741 only), or methionine nitrogen sources. Cells were back-diluted to 0.05 in 30 mL volume ang grown to $OD_{600}$ ~0.8. Ammonium sulfate grown cells reached this $OD_{600}$ after 14 hours of growth, urea grown cells reached this $OD_{600}$ after 16 hours of growth, methionine grown cells reached this $OD_{600}$ after 26 hours of growth.

A 500 mM 4sU stock was prepared in DMSO. Cells at $OD_{600}$ 0.8 were treated with 500 µM 4sU (Sigma # 440736) for 5 minutes and immediately harvested. Harvesting was done by adding 5 mL culture to 7.5mL pre-cooled methanol, inverted to mix and incubated on dry ice for 5 minutes. Cells were centrifuged at 6000rpm/5minutes/4℃, methanol was decanted, and pellets were used for RNA isolation. RNA extraction using standard phenol/chloroform protocol.

For TimeLapse chemistry, 5 µg of isolated RNA was mixed with 5ng *RLuc* and 5ng *ffLuc* IVT reporters. RNA samples with reporters were TimeLapse chemistry using published protocol followed by RNA cleanup with RNA clean and concentrator kit (Zymo #R1013) (Schofield et al. 2018). We depleted rRNA using the Ribo-Zero Gold rRNA Removal Kit (Illumina #MRZY1324, discontinued). Libraries were prepared according to NEBNext Ultra II Directional RNA Library Prep Kit for Illumina (NEB #E7760S). TimeLapse-seq libraries were sequenced on an Illumina NovaSeq 4000 using 100 base pair single-end reads.

Sequencing reads were trimmed using cutadapt to remove Illumina adapter sequences and aligned to the S288C R64.1 or Σ1278b reference genomes with added annotations for *RLuc* and *ffLuc* IVT reporter sequences using HISAT2 (Martin 2011; D. Kim, Langmead, and Salzberg 2015). Trimmed reads were further processed into labeled and total reads similarly to TimeLapse-seq paper and reads were counted using HTSeq-count (Anders, Pyl, and Huber 2015). Differential expression analysis was performed with DESeq2 (Love, Huber, and Anders 2014). Data is available upon request.

*RT-qPCR*

Σ1278b cells were grown to saturation overnight in minimal media with nitrogen media source of (1) 10 mM ammonium sulfate (2) 10 mM ammonium chloride (3) 10 mM leucine (4) 10 mM methionine. Cells maintained in ammonium sulfate and ammonium chloride were back-diluted to 0.01 and cells maintained in leucine and methionine were back-diluted to 0.1 due to their slower growth. Harvested cultures grown to $OD_{600}$ mid log phase ~0.5 for cells in ammonium sulfate and ammonium chloride and $OD_{600}$ 1.0 for cells in leucine and methionine. RNA isolated using phenol/chloroform extraction method. Complementary DNA was synthesized using ProtoScript II reverse transcriptase (NEB #M0368L) and random primers according to manufacturers protocol. Quantitative PCR was conducted using the DyNAmo HS SYBR Green qPCR kit (Fisher Scientific #F-410L) and the primers listed in Table 1.3 (BioRad-CFX96 qPCR System instrument).

## 1.4 Validating the quality of nitrogen sources: ammonium, urea, and methionine

To investigate the role of different nitrogen sources on mRNA stability, we chose three different quality nitrogen sources based on growth and NCR activity (Godard et al. 2007). The three sources we chose in order of best to worst were (1) ammonium sulfate, (2) urea, and (3) methionine. Ammonia can be used to synthesize both glutamate and glutamine directly, while all other nitrogen sources must first be degraded into ammonia or glutamate. Urea is degraded to ammonia in a single step while methionine requires at least three steps of degradation to release ammonia. Ammonia also transcriptionally inhibits the synthesis of many proteins required to use poorer nitrogen sources.

We validated the quality of the nitrogen sources by measuring growth in yeast grown in minimal media containing ammonium sulfate, urea, or methionine as the sole nitrogen source. As expected, there is an inverse relationship between cell fitness and quality of nitrogen source (Figure 1.1). The doubling time in ammonium is ~1.25 hours, urea is ~3 hours, and methionine is

~4 hours. Yeast grown in ammonium sulfate still showed a fitness defect when compared to their growth in rich media (YEPD), however.

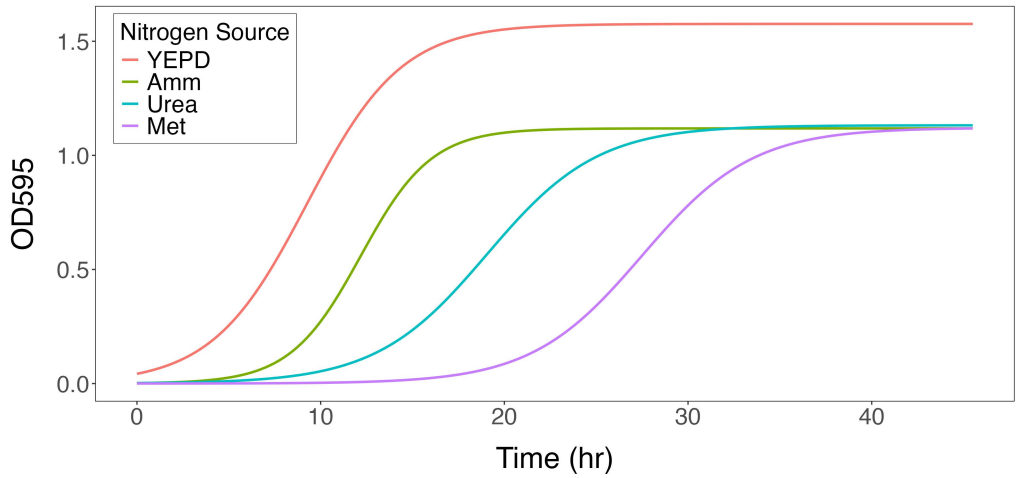


**Figure 1.1: Growth differences between nitrogen sources quality in yeast.** Growth curves of S288C yeast grown in YEPD, or minimal media containing ammonium sulfate, urea, or methionine as the sole nitrogen source.

## 1.5 TimeLapse-seq metabolic labeling to measure mRNA stability under different nitrogen conditions in S288C strain

To measure how different nitrogen sources affected mRNA stability, we used a metabolic pulse labeling method, TimeLapse-seq, to measure this. TimeLapse-seq profiles the abundance of both newly transcribed mRNAs and pre-existing mRNAs jointly in a single sequencing library by using oxidative-nucleophilic-aromatic substitution to convert 4-thiouridine (4sU) into cytidine analogs, which read as U-to-C mutations upon sequencing (Schofield et al. 2018). We used this method in yeast grown in each of the discrete nitrogen conditions and carried out pulse labeling with 4-thiouracil (4TU) for 3 minutes. We chose this timepoint because mRNA has been shown to have an average half-life of 4.8 minutes, so a 3 minute timepoint should be sufficient to observe the synthesis and decay rates for a diverse population of mRNA transcripts (Chan et al. 2018). To control for differences in U-to-C conversion efficiency, we used spike-in synthetic control *luciferase* transcripts that were transcribed in vitro with either 4TU or UTP prior to the conversion reaction. The 4TU *luciferase* measured the U-to-C conversion efficiency and the UTP *luciferase* measured spontaneous U-to-C conversion in the absence of 4TU.

In our analysis for each condition, we distinguished changes in transcription from mRNA stability by comparing newly synthesized transcripts to total transcripts. For each condition, we generated a (1) labeled dataset, which profiled the abundance of newly transcribed mRNAs with 1 or more U-to-C conversions and (2) total dataset, which profiled total mRNA transcript abundance. By tracking the formation of new mRNA transcripts with the abundance of

preexisting transcripts, we were able to look for differences in mRNA stability. More explicitly, transcripts with a larger fraction of new transcripts are less stable and exhibit higher turnover.

The percentage of U-to-C conversions were similar between biological replicates and different nitrogen conditions (Figure 1.2A). We also compared the ratio of labeled reads to total reads with published *S. cerevisiae* mRNA half-lives generated by metabolic labeling and isolation of labeled mRNA (Chan et al. 2018). We anticipated that more stable mRNA, which have longer half-lives, should a smaller fraction of transcripts with U-to-C conversions. We found that the fraction of new mRNA corresponds directly with the reported half-lives of these transcripts, confirming that our experiment does measure mRNA stability (Figure 1.2B).

Analysis of the total mRNA sequencing dataset revealed differences in mRNA abundance between different nitrogen sources. Pairwise comparisons showed many significant differences in mRNA abundance for yeast grown on methionine relative to ammonium or urea (Figure 1.2C). This is expected since methionine is a disfavored nitrogen source that relieves NCR and thus leads to transcriptional reprogramming (Godard et al. 2007).

We next measured differences in mRNA stability between conditions by jointly analyzing the labeled and total datasets. To quantify these differences in mRNA stability, we used a general linear model in DESeq2 to infer the log2 fold-change between the ratio of labeled reads/total reads in one condition versus another condition. A lower ratio of newly-synthesized, labeled reads relative to toal reads indicates greater mRNA stability. We found that many transcripts were significantly and substantially stabilized in methionine (log2 fold-change < -1, $p_{adj}$ <0.05) when compared to either ammonium sulfate or urea (Figure 1.2D). In contrast, we saw few differentially stabilized transcripts comparing ammonium versus urea (Figure 1.2D).

Our stability analysis turned up mRNA transcripts that were stabilized in methionine compared with ammonium, which were previously validated to be destabilized during a nitrogen upshift (Figure 1.3A) (Miller, Brandt, and Gresham 2018). We found that three mRNAs encoding metabolite transporters, *GAP1*, *DAL5*, and *MEP2*, are all stabilized in methionine, in addition to being NCR targets. *GAP1* encodes a general amino acid permease; *DAL5* encodes an allantoate permease; and *MEP2* encodes an ammonium permease. In methionine, the cellular demand for alternative nitrogen source uptake and metabolism leads to the stabilization of these permeases to import nitrogen-containing compounds. *GDH2*, which encodes an NAD(+)-dependent glutamate dehydrogenase that degrades glutamate to ammonia and α-ketoglutarate, is also stabilized in methionine. Expression of *GDH2* and glutamate catabolism is needed to utilize methionine as a nitrogen source. *GCN4*, a transcription factor that activates genes involved in amino acid biosynthesis by activating the ISR, is stabilized in methionine, enabling cells to adapt to this perceived nitrogen starvation condition.

In urea, we found destabilization of the transcripts *GLT1* and *LEU1* compared to ammonium (Figure 1.3B). *GLT1* encodes glutamate synthase and is an essential part of the GS-GOGAT nitrogen assimilation pathway. *LEU1* is an NAD(+)-dependent glutamate synthase that synthesizes glutamate from glutamine and alpha-ketoglutarate. Cth1 and Cth2, a pair of paralogous RNA-binding proteins, respond to iron limitation by destabilizing their target transcripts, which include *GLT1* and *LEU1* (Puig, Askeland, and Thiele 2005; Puig, Vergara, and Thiele 2008). Since these transcripts are regulated by Cth2, we compared growth in ammonium, urea, and methionine in *wildtype* vs *cth2*Δ cells (Figure 1.3C). The growth rate per hour increased slightly in *cth2*Δ cells grown in urea, which suggests that Cth2 might also play a

role in nitrogen assimilation. New literature has come out since this work was completed which found an additional role for Cth1 and Cth2 in inhibiting translational regulation during iron starvation (Barlit et al. 2024). While we have not followed-up on whether this destabilization we noticed stemmed from the iron regulon response or the nitrogen source, it would be interesting to further elucidate the mechanism of this response.

*HXT3*, a low affinity glucose transporter, was another transcript we found destabilized in urea versus ammonium (Figure 1.3B). This is likely because cells grown in ammonium can prioritize glycolysis, maintaining the need for *HXT3*. In contrast, cells grown in urea need to balance glucose uptake needs with nitrogen assimilation, leading to its destabilization.

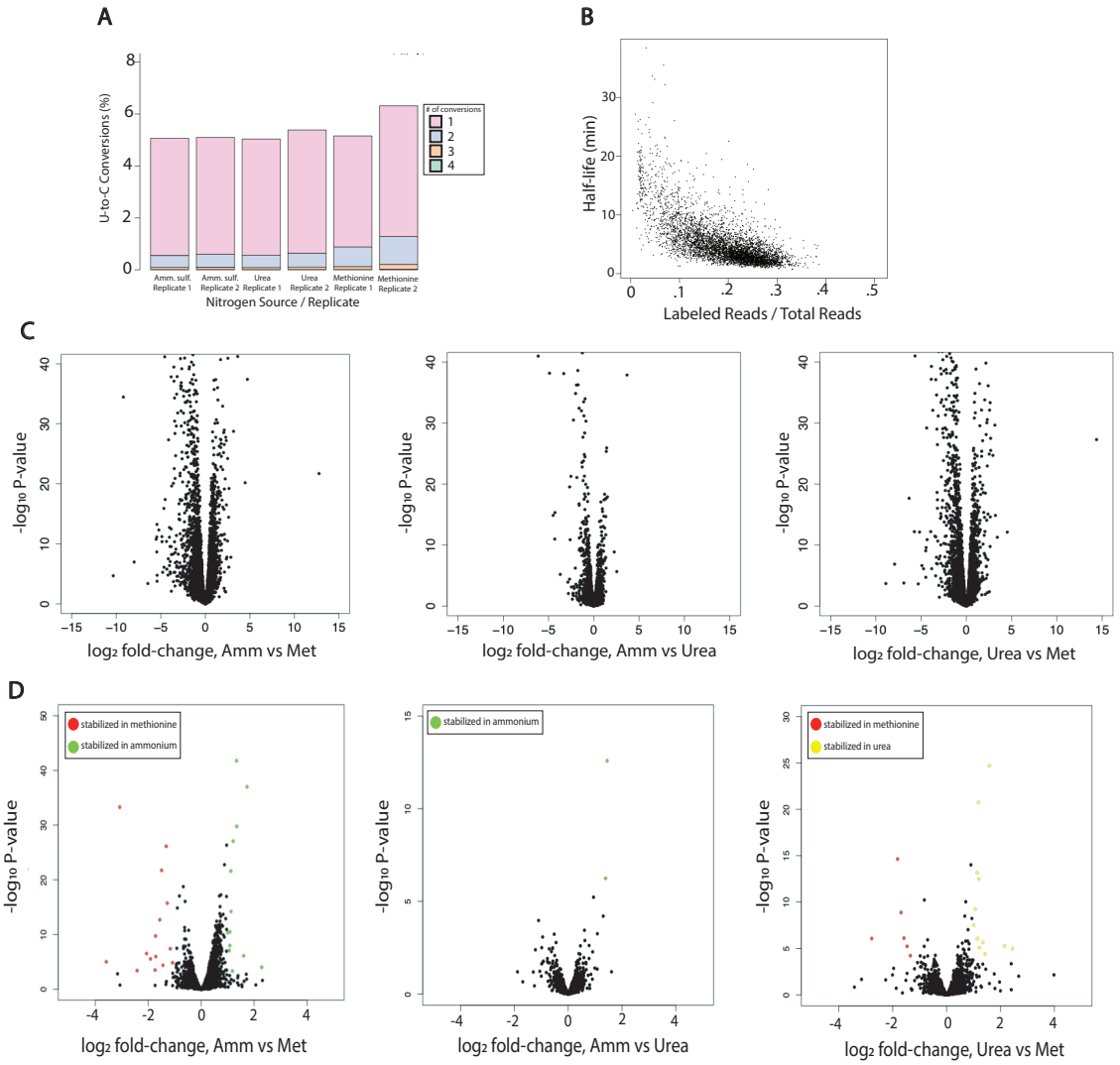

**Figure 1.2: S288C TimeLapse-seq analysis (A)** U-to-C conversion rates per 100 bp SR (single-read) for TimeLapse-Seq in ammonium sulfate, urea, and methionine nitrogen conditions. **(B)** Scatterplot of Timelapse-seq labeled reads / total reads and steady-state mRNA half life (Chan et al. 2018). **(C)** Volcano plots show differential expression (DE) analysis of two conditions of nitrogen source growth (left) ammonium versus methionine conditions (center) ammonium versus urea conditions (right) urea versus methionine conditions. **(D)** Volcano plots show DE analysis changes in mRNA stability in two conditions of nitrogen source growth (left) ammonium versus methionine conditions (center) ammonium versus urea conditions (right) urea versus methionine conditions. Each point represents mRNA. Red points represent mRNA stabilized in methionine, green points represent mRNA stabilized in ammonium, yellow points represent mRNA stabilized in urea.

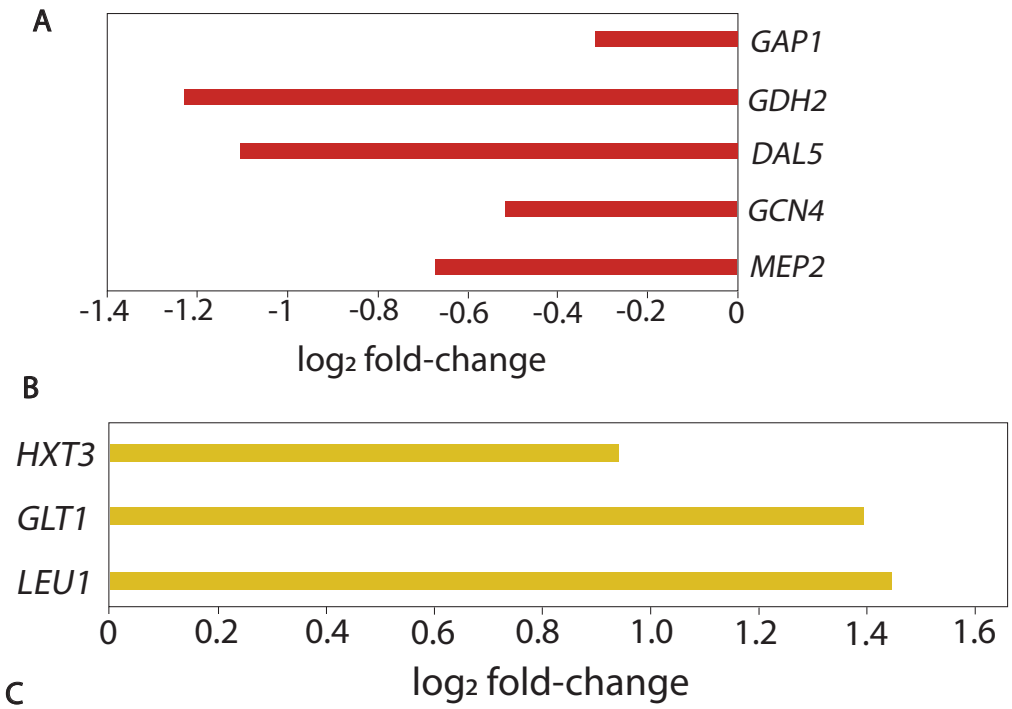
A
GAP1
GDH2
DAL5
GCN4
MEP2
-1.4
-1.2
-1
-0.8
-0.6
-0.4
-0.2
0
log2 fold-change
B
HXT3
GLT1
LEU1
0
0.2
0.4
0.6
0.8
1.0
1.2
1.4
1.6
log2 fold-change

C

N2 source

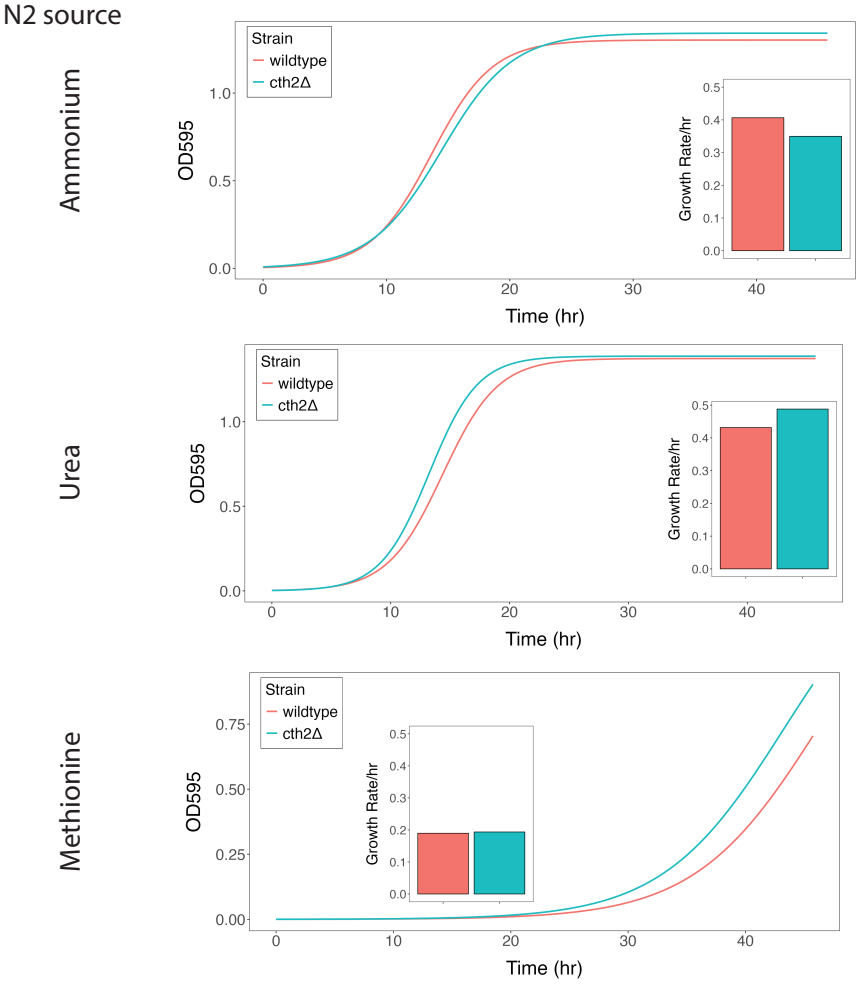
Ammonium
Urea
Methionine
Strain
wildtype
cth2Δ
OD595
Growth Rate/hr
Time (hr)

**Figure 1.3: mRNA Stability Changes (A)** $\log_2$ fold-change mRNA transcripts stabilized in methionine compared to ammonium grown cells (padj <0.05). **(B)** $\log_2$ fold-change mRNA transcripts destabilized in urea compared to ammonium grown cells (padj <0.05). **(C)** Growth curves of *wildtype* and *cth2Δ* cells maintained in ammonium, urea, or methionine nitrogen sources. Growth rate/hour calculated for each strain and condition.

## 1.6 TimeLapse-seq metabolic labeling to measure mRNA stability under different nitrogen conditions in Σ1278b strain

We performed TimeLapse-seq to look for nitrogen-dependent stability differences in the yeast strain Σ1278b, a more commonly used reference strain in nitrogen regulation studies. Strain Σ1278b was used in studies that led to the concept of NCR and pseudohyphal growth induced by limiting the ammonium supply to diploid cells (Wiame, Grenson, and Arst 1985; Gimeno et al. 1992). In addition to NCR, strain Σ1278b exhibits an additional negative regulatory effect exerted by ammonium on genes involved in the use of poor nitrogen sources, which occurs to a lesser degree in S288C (Rytka 1975).

For the Σ1278b strain, the minimal differences between ammonium and urea observed in S288C prompted us to only compare stability changes in ammonium and methionine. We carried out TimeLapse-seq experiment as in S288C, but comparing only ammonium and methionine as sole nitrogen sources, excluding urea. We again saw that the percentage of U-to-C conversions per 100 basepair read were similar between biological replicates and different nitrogen conditions (Figure 1.4A). Analysis of the total RNA-seq dataset, reflecting changes in both stability and transcription, showed that many mRNAs were significantly shifted in this comparison (Figure 1.4B).

We saw increased abundance of *MET6* and *MET14* driven both by increased transcription and stabilization (Figure 1.4C). *MET6* encodes a methionine synthase and *MET14* an adenylylsulfate kinase required for sulfate assimilation. We used our datasets to distinguish between changes in transcription and stability for *MET14* (Figure 1.4D). We found that *MET14* increases in both transcription and stability, with a bigger contribution for this shift coming from stability. Since we used ammonium sulfate as our source of ammonium, we were interested in whether this shift in *MET14* was due to its role in sulfur assimilation. We did this by growing cells with either ammonium chloride or ammonium sulfate as the sole nitrogen source and quantifying *MET14* transcript expression by RT-qPCR (Figure 1.4E). While we did not find any significant difference between *MET14* expression levels, this method does not distinguish between transcription and stability. We also observed that growing cells in leucine as a poor nitrogen source showed a higher level of *MET14* expression than cells grown in methionine. Since methionine is a part of sulfur assimilation as an essential sulfur amino acid, it can be catabolized to other sulfur-containing compounds. Therefore, it is still a possibility that the observed change in mRNA stability is due to sulfur assimilation rather than nitrogen metabolism. We have not followed up on this further, but it would be interesting to dissect the role of *MET14* stability in sulfur assimilation.

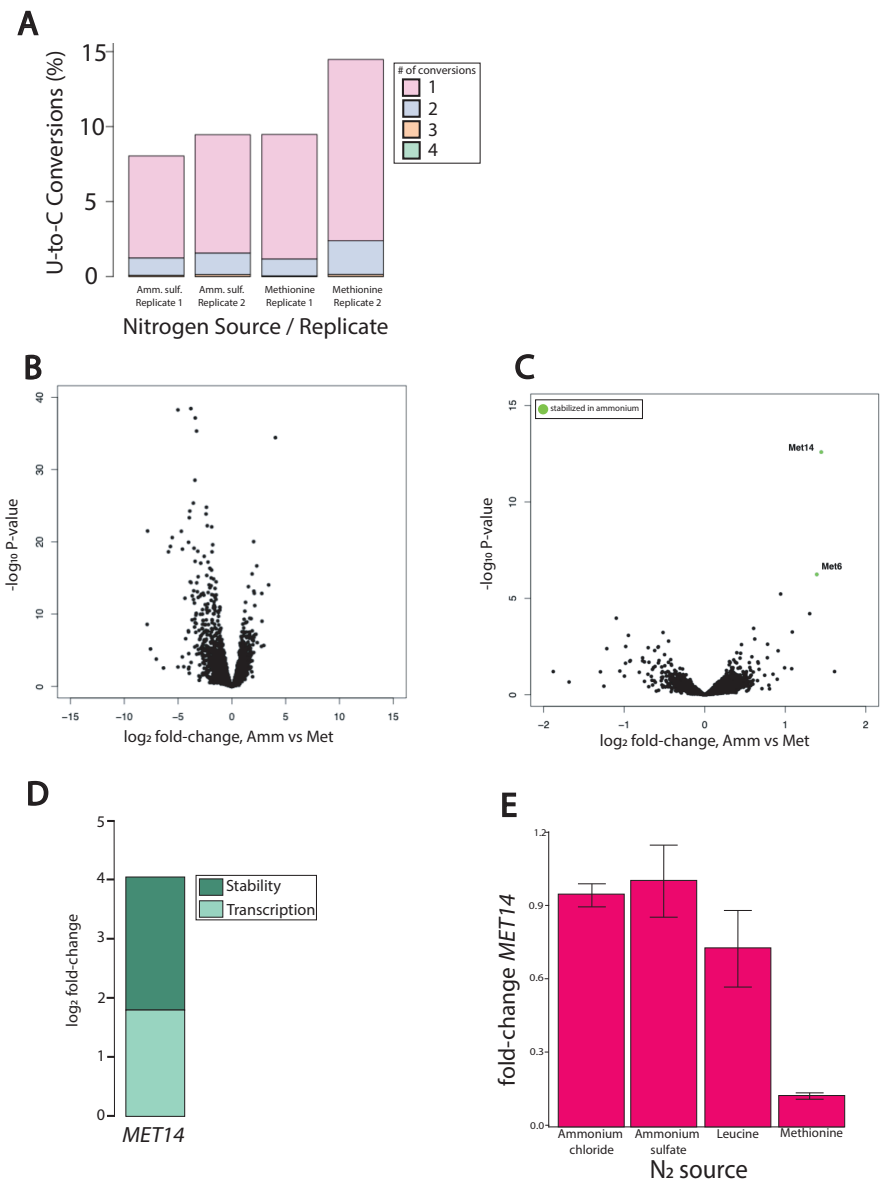


**Figure 1.4: Σ1278b strain TimeLapse-seq analysis (A)** U-to-C conversion rates per 100 bp SR (single-read) for TimeLapse-Seq in ammonium sulfate and methionine nitrogen conditions. **(B)** Volcano plot shows DE analysis of two conditions of nitrogen source growth in ammonium versus methionine conditions in total mRNA. **(C)** Volcano plot shows DE analysis changes in mRNA stability in ammonium versus methionine condition. Each point represents mRNA. Green points represent mRNA stabilized in ammonium. **(D)** *MET14* $\log_2$ fold-change contributions of transcription and stability in cells containing ammonium **(E)** RT-qPCR *MET14* fold-change (normalized to *ACT1*) for cells maintained in nitrogen sources ammonium chloride, ammonium sulfate, leucine, or methionine

## 1.7 Conclusions

We conducted TimeLapse-seq metabolic labeling in S288C and Σ1278b yeast strains to identify global changes in mRNA stability stemming from different quality nitrogen sources. From our datasets we were able to disentangle changes in transcription from changes in stability. The stability changes we identified reinforced transcriptional changes and increased the expression of genes needed under these different growth conditions. Further work needs to be done to distinguish the stability responses of nitrogen metabolism from other types of cellular responses such as the iron regulon response or sulfur assimilation.

**Table 1.1: Yeast strains used in this study.** (NIY434 and NIY440 derived from BY4741; NIY438 derived from Σ1278b)

| Strain Number | Genotype | Source |
|---|---|---|
| NIY434 | MATa his3Δ1 leu2Δ0 lys2Δ0 met15Δ0 ura3Δ0 XII-2::dCas9-Mxi1::TetR::kanMXsyn X-3::HIS3 LEU2 MET15 URA3 | This work |
| NIY440 | MATa his3Δ1 leu2Δ0 lys2Δ0 met15Δ0 ura3Δ0 XII-2::dCas9-Mxi1::TetR::kanMXsyn X-3::HIS3 LEU2 MET15 URA3 [*ylr136c*Δ LEU2] | This work |
| NIY438 | MATa his3D::hisG, leu2D::hisG, trp1D::hisG, ura3-52 XII-2::dCas9-Mxi1::TetR::kanMXsyn X-3::HIS3 LEU2 URA3 TRP1 | This work |

**Table 1.2: Plasmids used in this study**

| Plasmid Name | Description | Source |
|---|---|---|
| pNTI599 | CEN/ARS HIS3 MET17 URA3 LEU2 | AddGene #64166 |
| pTNI694 | HIS3 LEU2 MET17 URA3 markers in pCfB2223 | This work |
| pNTI698 | HIS3 MET17 URA3 markers in pCfB2223 | This work |
| pRB001 | HIS3 LEU2 URA3 TRP1 | This work |
| APp32 | psiCHECK-2 | Promega (#C8021) |

**Table 1.3: Oligonucleotides used in this study**

| Oligo Number | Sequence | Notes | Source |
|---|---|---|---|
| AP1119 | taatacgactcactataggGCAAATGAACGTGCTGGAC | psiCheck2 renilla luciferase amplification PCR primer | Alex Padron |
| AP1120 | TTCGTCGTGTTGTCTGGTTC AAGAAGTTATTCTCAAGCACCATTTTC | psiCheck2 renilla luciferase amplification PCR primer | Alex Padron |
| AP1121 | TTCGTCGTGTTGTCTG | RT primer for 4sU reporter RNA | This work |
| RB5 | taatacgactcactataggTTCGACAGGGACAAAACCATTG | psiCheck2 firefly luciferase amplification PCR primer | This work |
| RB6 | CAGAATGGCGCTGGTTGTCT | psiCheck2 firefly luciferase amplification PCR primer | This work |
| RB68 | agatagggttgagtgttgttaaaaccctggcgttaccct | pCfB2223 gibson assembly primer | This work |
| RB69 | aatttatggtgcactctcagatcgcacgcattccatgcga | pCfB2223 gibson assembly primer | This work |
| RB70 | tcgcatggaatgcgtgcgatctgagagtgcaccataaattc | pNTI694 gibson assembly primer | This work |

| | | | |
|---|---|---|---|
| RB71 | aggggtaacgccagggttttaacaacactcaaccctatct | pNTI694 gibson assembly primer | This work |
| RB110 | AAAAAATAACGCAATATGGCTGTGAAGATCCCAGCAAA | ylr136c knockout uptag | This work |
| RB111 | GCAGGCTAACCGGAACCTGTATTAGGCCAGGAATTGTTTCA | ylr136c knockout dntag | This work |
| RB112 | CGAAACAGTGCTGCAAACTCAATACGTAAAAAATAACGCAATATG | ylr136c knockout up45 | This work |
| RB113 | AGTTTAGTTGAGACGCCGGTCTTCGCCAGGCCAGGAATTGTTTCA | ylr136c knockout dn45 | This work |
| qRB007 | GTCAGTTTGCTCACGGACTC | *CTH2* RT-qPCR | This work |
| qRB008 | TTGTCGTCGCCATGTTTGAA | *CTH2* RT-qPCR | This work |
| qRB013 | GAAAGCTAGGGAGGGTGTAATC | *MET14* RT-qPCR | This work |
| qRB014 | GCACATTCTTCAACCGTCTTC | *MET14* RT-qPCR | This work |

Chapter 2

Elucidating the Role of the RNA Binding Protein Gta1

## 2.1 Abstract

We identified a C-terminal disordered region of Gta1 with strong repressive activity in an unbiased FACS-based tethering assay screening for activity of post-transcriptional regulators in S*accharomyces cerevisiae*. Gta1 is a relatively uncharacterized protein that has been shown to play a role in Golgi and vesicle transport, localizes to the ER, and copurifies with translational machinery. The overexpression of Gta1 alters the morphology of cells to an elongated phenotype. We investigated the role of Gta1 by performing a time-course of an inducible Gta1 overexpression strain and carrying out RNA-seq across a time-course of Gta1 overexpression. GO analysis identified the downregulation of Golgi- and ER-specific mRNA transcripts, suggesting Gta1 might promote mRNA destabilization due to its localization. Additionally, we identified a conserved motif within the repressor peptide that abolishes its repressor activity upon deletion.

## 2.2 Introduction

Cells utilize post-transcriptional regulation as a major control point for regulating mRNA translation to produce a dynamic proteome that meets the changing needs of the cell. RNA binding proteins (RBPs) play an important role in post-transcriptional regulation by controlling mRNA translational activation or repression, localization, and degradation. RBPs can also play a role in remodeling RNA structure to make it accessible to other RBPs or enzymes, and act as chaperones to prevent RNA aggregation and misfolding (Gerstberger, Hafner, and Tuschl 2014; Ott 2016). Previously in the Ingolia lab, a novel high-throughput tethering screen was used to identify proteins that functionally activate or repress post-transcriptional regulation (Reynaud et al. 2023).

Gta1 (YEL043W), a relatively uncharacterized protein, was identified from this screen as having potent repressor activity in the C-terminus, found in several overlapping C-terminal fragments (Reynaud et al. 2023). In targeted experiments motivated by the tethering screen, full-length Gta1 and C-terminal Gta1(603-767) both reduced median reporter expression and produced a strongly bimodal distribution of reporter expression, a distinctive phenotype stemming from the repressor fragment Gta1(603-767). Overexpression of Gta1 also leads to an elongated cell morphology phenotype. Gta1 is relatively uncharacterized, but is known to play a role in golgi and vesicle transport, localizes to the ER, and copurifies with translational machinery (Mattiazzi Usaj et al. 2020; Costanzo et al. 2016; Huh et al. 2003; Fleischer et al. 2006). To follow up on the surprising observation of regulatory activity in this uncharacterized protein, we wanted to elucidate the role of Gta1 in destabilizing mRNAs. We investigated the role of Gta1 by performing a time-course of inducible Gta1 or Halo-tag overexpression strains and looking for differential RNA expression by RNA-seq. Gene-ontology (GO) enrichment analysis identified transcripts encoding Golgi and ER localized proteins. Golgi-localized proteins are translated at the ER and then trafficked to the Golgi. Given that Gta1 protein is localized to

Golgi and ER, it could be destabilizing mRNAs associated with these compartments. Additionally, we identified a conserved motif in the Gta1 repressor fragment that is required for its repressive activity.

## 2.3 Methods

*Yeast Strains*

Strains used in this study are listed in Table 2.1. Strains were derived from *S. cerevisiae* BY4741 using standard genetic techniques. Parent strain with ZIF268 transcription factor (pNTI729) generated from NotI-linearized construct integrated into the XII-5 locus of BY4741 from Easyclone 2.0 toolkit (Aranda-Díaz et al. 2017; Stovicek et al. 2015). Gal1 inducible Gta1 or Halo overexpression constructs were generated by integrating SwaI-linearized pNTI784 or pNTI784 into the X-4 locus from the Easyclone 2.0 toolkit for yeast genomic integration (Stovicek et al. 2015). C-terminal HA Tag (sec13-HA) strain was generated by amplifying the HA tag that included 40 basepairs of sequence identity with either side of the insertion and integrated using CRISPR-Cas9 technology as described in (Brothers and Rine 2019). YFP-GTA1 constructs were integrated by NotI-linearization into X-2 locus in BY4741 strain from the Easyclone 2.0 toolkit for yeast genomic integration (Stovicek et al. 2015).

*Plasmids*

Plasmids used in this study are listed in Table 2.2. Plasmids were generated by Gibson assembly from amplicons made from plasmids listed in Table 2.2 (Gibson et al. 2009).

*Western Blot*

Gta1 or Halo overexpression cells were grown to saturation overnight in YEPD and back diluted to $OD_{600}$ 0.05 and grown to $OD_{600}$ 0.3. Cells were collected for uninduced samples. Cells were induced with 150 nM β-estradiol and collected at 1, 2, 3, and 4 hour timepoints. Cell pellets were resuspended in 5 mL 5% TCA (Sigma-Aldrich #T6399) and incubated at 4℃ for 10 minutes. Resuspension was centrifuged at 4000rpm for 5 minutes and supernatant was removed. The pellet was resuspended in 1 mL acetone, vortexed, centrifuged, and supernatant was removed. Pellet was dried overnight in 30℃ incubator. Dried pellets were lysed by adding glass beads (Sigma-Aldrich #Z250465) and protein lysis buffer (50 mM Tris pH 7.5, 1 mM EDTA, 10 mM DTT, protease inhibitor (Sigma-Aldrich #11836170001). Added LDS sample buffer (Sigma-Aldrich #NP0007) to final concentration of 1X.

Protein lysates were denatured at 95℃ for 5 minutes and loaded onto a 4-12% polyacrylamide Bis-Tris gel (Life Technologies # NW04125BOX). The gel was run at 165V for ~45 minutes in 1X Bolt MOPS SDS running buffer (Thermo Fisher Scientific #B0001). The protein was transferred to a nitrocellulous membrane (Thermo Fisher Scientific #88018) according to manufacturers guidelines at 20V for ~1 hour. Membranes were blocked for 1 hour in TBST (0.05% Tween-20) with 5% milk, shaking 1 hour at room temperature. Primary antibody was diluted 1:2000 in TBST with 5% milk and added to the membrane, shaking overnight at 4℃.

Membranes were washed three times in TBST by shaking for 10 minutes. Secondary antibody was diluted 1:10000 in TBST with 5% milk and added to the membrane, shaking 1 hour at room temperature. Membranes were washed three times in TBST by shaking for 10 minutes. Membrane blots were developed with Pierce ECL Western Blotting Substrate (Thermo Fisher Scientific #32209) and visualized using a FluorChem R imaging system (ProteinSimple). **Primary antibodies**: rabbit anti-FLAG (Cell Signaling Technologies #2368S); mouse anti-Actin (Cell Signaling Technologies # 12620S); rabbit anti-HA (Cell Signaling Technologies #3724S). **Secondary antibodies**: Anti-rabbit IgG, HRP-linked Antibody (Cell Signaling Technologies #7074); Anti-Mouse IgG, HRP-linked Antibody (Cell Signaling Technologies #7076S).

*RT-qPCR*

Gta1 or Halo overexpression cells were grown to saturation overnight in YEPD and back diluted to $OD_{600}$ 0.05 and grown to $OD_{600}$ 0.3. Cells were collected for uninduced samples. Cells were induced with 150 nM β-estradiol and collected at the 1 hour timepoint. RNA was extracted from cell pellets using standard phenol/chloroform protocol. Complementary DNA was synthesized using ProtoScript II reverse transcriptase (NEB #M0368L) and random primers according to manufacturers protocol. Quantitative PCR was conducted using the DyNAmo HS SYBR Green qPCR kit (Fisher Scientific #F-410L) and the primers listed in Table 2.3 (BioRad-CFX96 qPCR System instrument).

*RNA-seq*

Gta1 and Halo inducible yeast strains were grown to saturation overnight in YEPD media. Cells were back-diluted to $OD_{600}$ 0.05 for final volume of 150mL culture and grown for 6 hours until they reached $OD_{600}$ ~0.3-0.4. Cells were collected for preinduction sample. Remaining culture was induced with 150 nM β-estradiol and cells were collected at 1 and 3 hour timepoints post-induction. RNA was extracted from cell pellets using standard phenol/chloroform protocol. We depleted rRNA using the QIAseq FastSelect –rRNA yeast kit (Qiagen #334215). Libraries were prepared according to NEBNext Ultra II Directional RNA Library Prep Kit for Illumina (NEB #E7760S). RNA-seq libraries were sequenced on an Illumina NovaSeq 4000 using 100 base pair single-end reads.

Sequencing reads were trimmed using cutadapt to remove Illumina adapter sequences (Martin 2011). Trimmed reads were aligned using HISAT2 to the S288C reference genome R64.1 (D. Kim, Langmead, and Salzberg 2015). Samtools software was used to process and prepare the alignment and reads were counted using HTSeq-count (Li et al. 2009; Anders, Pyl, and Huber 2015). Differential expression analysis was performed with DESeq2 (Love, Huber, and Anders 2014). Data is available upon request.

*Immunofluorescence microscopy*

Gta1 inducible yeast strain with sec13-HA (yRB003) were grown to saturation overnight in YEPD media. Cells were back-diluted to $OD_{600}$ 0.05 and grown to $OD_{600}$ 0.3, pre-induction samples were collected. Cells were then induced with 150 nM β-estradiol for 1 hours and

collected. Cells were fixed by resuspending in 3.7% formaldehyde in 0.1 mM KPi, pH 6.4 and nutated overnight at 4℃. Cell pellets were washed in 1 mL 0.1M KPi. Cell pellet was resuspended in 1.2M sorbitol-citrate and stored at -20℃ until further use. Samples were thawed on ice. Cell wall was digested using zymolase and glusalase and put on a rotating rack at 30℃ for 15 minutes. Cells were resuspended in 30µl of sorbitol citrate.

Cell slides were prepared by incubating wells with 5µl polylysine for 5 minutes and then aspirated. 5µl of cells were added to each well and incubated for 10 minutes before washing with sorbitol citrate. Slide was dehydrated in pre-cooled methanol bath for 3 minutes at -20℃ and then moved to an acteone bath at -20℃ for 10 seconds. Primary antibody was diluted 1:200 and incubated in a humid chamber for 1 hour in the dark. Wells were washed five times with PBS/BSA. Preabsorbed secondary antibodies was diluted 1:200 and incubated in a humid chamber for 1 hour in the dark. Wells were washed five times with PBS/BSA. DAPI was added to each well. Coverslip was sealed with nailpolish and slides were left to dry before imaging. Images were visualized with confocal microscopy. **Primary antibodies:** rabbit anti-FLAG (Cell Signaling Technologies #2368S); mouse anti-HA (Sigma-Aldrich #H3663). **Secondary antibodies** (gifted from Professor Elçin Ünal)**:** Anti-mouse-Cy3 (preabsorbed 1:5); Anti-rabbit-FITC (preabsorbed 1:6).

*Flow Cytometry*

Expression of YFP and RFP constructs in the tethering assay was measured using flow cytometry instrument (BD Bioscience LSR Fortessa). Excitation by the 488mm blue laser and 561mm yellow-green laser, captured the FITC and PE-TexasRed channels, respectively.

### 2.4 Profiling kinetic changes in mRNA expression during Gta1 overexpression

Since we determined that tethering Gta1 to a reporter transcript reduces mRNA abundance, we wanted to examine how Gta1 overexpression affected endogenous mRNAs. To investigate this, we analyzed the impact of Gta1 on mRNA expression. We integrated an inducible copy of Gta1 into S288C to capture changes in endogenous mRNA expression over time, using an inducible HaloTag as a control. First, we verified expression of FLAG-tagged Gta1 and Halo 1-4 hours post-induction, and saw a strong, consistent expression of FLAG-tagged protein (Figure 2.1A, B). We saw a ~3 to 4-fold change in endogenous *GTA1* mRNA levels post-induction compared to pre-induction levels, and a ~7-fold change in *HALO* mRNA levels post-induction measured by RT-qPCR (Figure 2.1C).

We performed RNA-seq on pre-induction cells and on cells induced for 1 or 3 hours. We then performed differential expression (DE) analysis comparing Gta1 and Halo at each timepoint. In the pre-induction analysis, we identified Gta1 as the most significantly differentially expressed ($\log_2$ fold-change of 1) mRNA versus Halo, which suggests some level of leaky expression of our overexpression construct (Figure 2.1D). However, at the 1 and 3 hour post-induction timepoints, we saw a 16-fold induction of Gta1, validating increased induction in our overexpression strain (Figure 2.1E, F). In our analysis, we found that increasingly from the 1 to 3 hour timepoint, more transcripts were significantly ($p_{adj} < 0.05$) differentially expressed, with a greater number transcripts of downregulated transcripts than upregulated (Figure 2.1E,

F). To validate our RNA-seq analysis, we measured the change of mRNA expression for one upregulated and one downregulated transcript by RT-qPCR. *HXK1*, which catalyzes the phosphorylation of glucose during glucose metabolism, was significantly upregulated based on our RNA-seq dataset 3 hours post-induction of Gta1 ($log_2$ fold-change 1.90). We validated this increase in expression of *HXK1* by RT-qPCR, which led to a 4-fold increase after 1 hour, and a 16-fold increase after 3 hours of Gta1 overexpression (Figure 2.1G). This qualitative agreement between the RNA-seq and RT-qPCR results confirm the robust upregulation of *HXK1*. *HXT1*, a low-affinity glucose transporter, is significantly downregulated in our RNA-seq analysis 3 hours post-induction of Gta1 ($log_2$ fold-change -2.88). We observed the a similar level of downregulation by RT-qPCR after 3 hours of Gta1 overexpression with a 4-fold decrease in *HXT1* expression (Figure 2.1H). This increase in glucose phosphorylation and utilization and decrease in glucose uptake after Gta1 overexpression suggests that Gta1 drives metabolic reprogramming in cells.

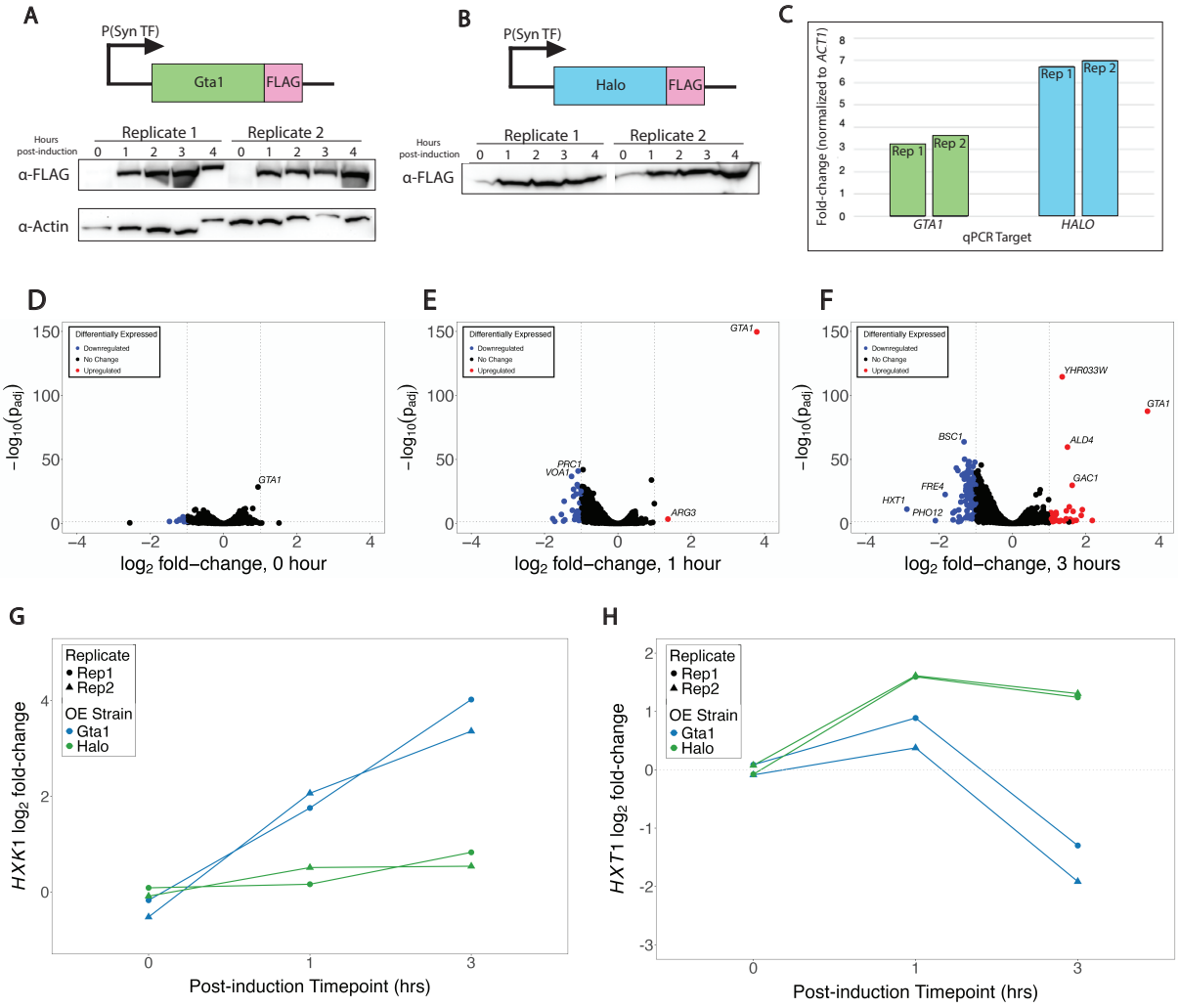

**Figure 2.1: Gta1 overexpression RNA-seq analysis (A)** (top) Schematic of β-estradiol inducible Gta1-FLAG construct (bottom) Western blot for S288C cells expressing inducible FLAG-tagged Gta1 relative to β-actin for various timepoints post-induction. **(B)** (top) Schematic of β-estradiol inducible Halo-FLAG construct (bottom) Western blot for S288C cells expressing inducible FLAG-tagged Halo for various timepoints post-induction **(C)** RT-qPCR shows mRNA induction of Gta1 / Halo expression 1 hour post-induction compared to pre-induction. **(D-F)** Volcano plots of Gta1 vs Halo RNA-seq analysis; colored points represent $p_{adj} < 0.05$, $-1 < \log_2$ fold-change $> 1$ **(D)** Uninduced comparison **(E)** 1 hour post-induction comparison **(F)** 3 hour post-induction comparison. **(G)** RT-qPCR *HXK1* expression for Gta1 and Halo inducible strains in pre-induction, 1 and 3 hour post-induction timepoints. *HXK1* is induced in Gta1 overexpression strain. **(H)** RT-qPCR *HXT1* expression for Gta1 and Halo inducible strains in pre-induction, 1 and 3 hour post-induction timepoints. *HXT1* is reduced in Gta1 overexpression strain at 3 hour timepoint.

## 2.5 Gta1 overexpression leads to destabilization of many different ER and Golgi specific mRNA

Since so many genes were downregulated after prolonged overexpression of Gta1, we performed a Gene Ontology (GO) analysis to identify whether these transcripts had any enrichment patterns. Among significantly downregulated genes (log2 fold-change ≤-1, $p_{adj}$ <0.05) at 3 hours of Gta1 overexpression, GO analysis terms were enriched for transcripts localized to the endoplasmic reticulum (ER) and Golgi (Figure 2.2A). We hypothesized that Gta1 could be promoting mRNA degradation due to its localization. We performed immunofluorescence (IF) on FLAG-tagged Gta1 overexpressed cells with an ER marker, Sec13, a subunit of the COPII vesicle coat required for ER-to-Golgi transport. We did not see colocalization of FLAG-Gta1 with Sec13 by IF (Figure 2.2B). Since Sec13 has a dual function as part of the nuclear pore complex, it may not be a representative ER marker. We were not able to definitively map the localization of Gta1, but further work should be done to look at whether Gta1 localizes to the ER or Golgi.

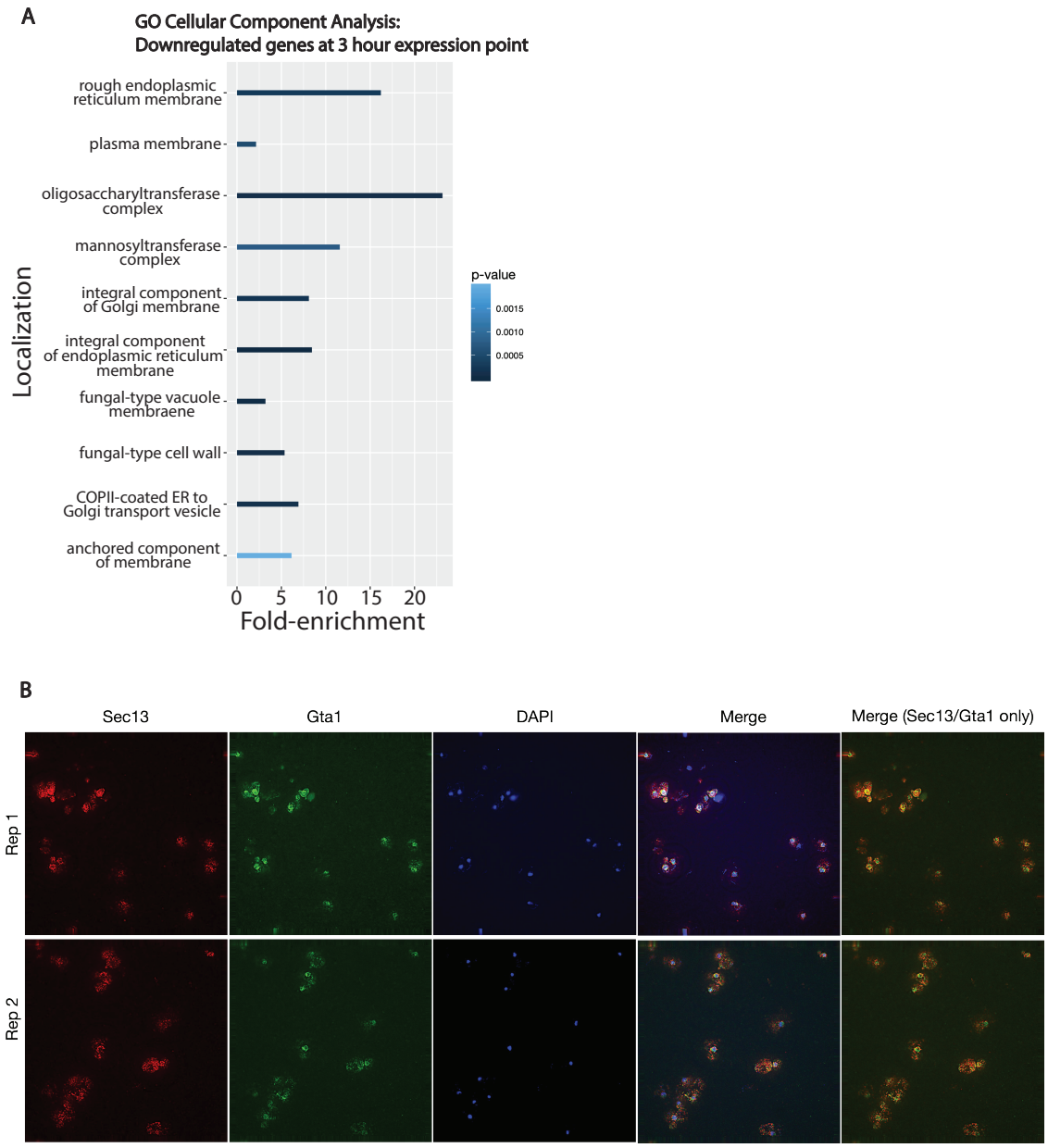


**Figure 2.2: ER and Golgi localization of downregulated Gta1 transcripts (A)** Gene Ontology localization analysis for genes which were significantly ($p_{adj} < 0.05$) downregulated ($log_2$ fold-change ≤ -1) following 3-hour overexpression in RNA-seq analysis. Enrichment for transcripts localized to ER and Golgi. **(B)** Fluorescence microscopy of yeast overexpressing Gta1. Cells were probed with Sec13 (ER marker), FLAG (Gta1-FLAG marker), and DAPI stain. Merged images of DAPI/Sec13/Gta1 and Sec13/Gta1.

## 2.6 A conserved motif in the Gta1 repressor fragment is required for its repressive activity

Genome alignment of full length Gta1 sequence with other fungal sequences identified a conserved motif within the repressor region of Gta1 (Figure 2.3A). Since this motif is conserved, we hypothesized that it could drive repressive activity of the larger fragment. We designed three different constructs of Gta1 (1) Gta1(603-767) repressor fragment (2) Gta1(603-653, 692-767) repressor fragment Δ conserved motif, and (3) Gta1(654-691) conserved motif (Figure 2.3B). We measured repressor activity by tethering these query sequences using the dual reporter tethering assay (Reynaud et al. 2023). Deletion of the conserved motif within the repressor fragment abolished repressor activity, demonstrating this motif is necessary for repressor activity (Figure 2.3C-F). The conserved motif is necessary but not sufficient to engender the repressor phenotype which suggests there are additional factors at play (Figure 2.3C-F).

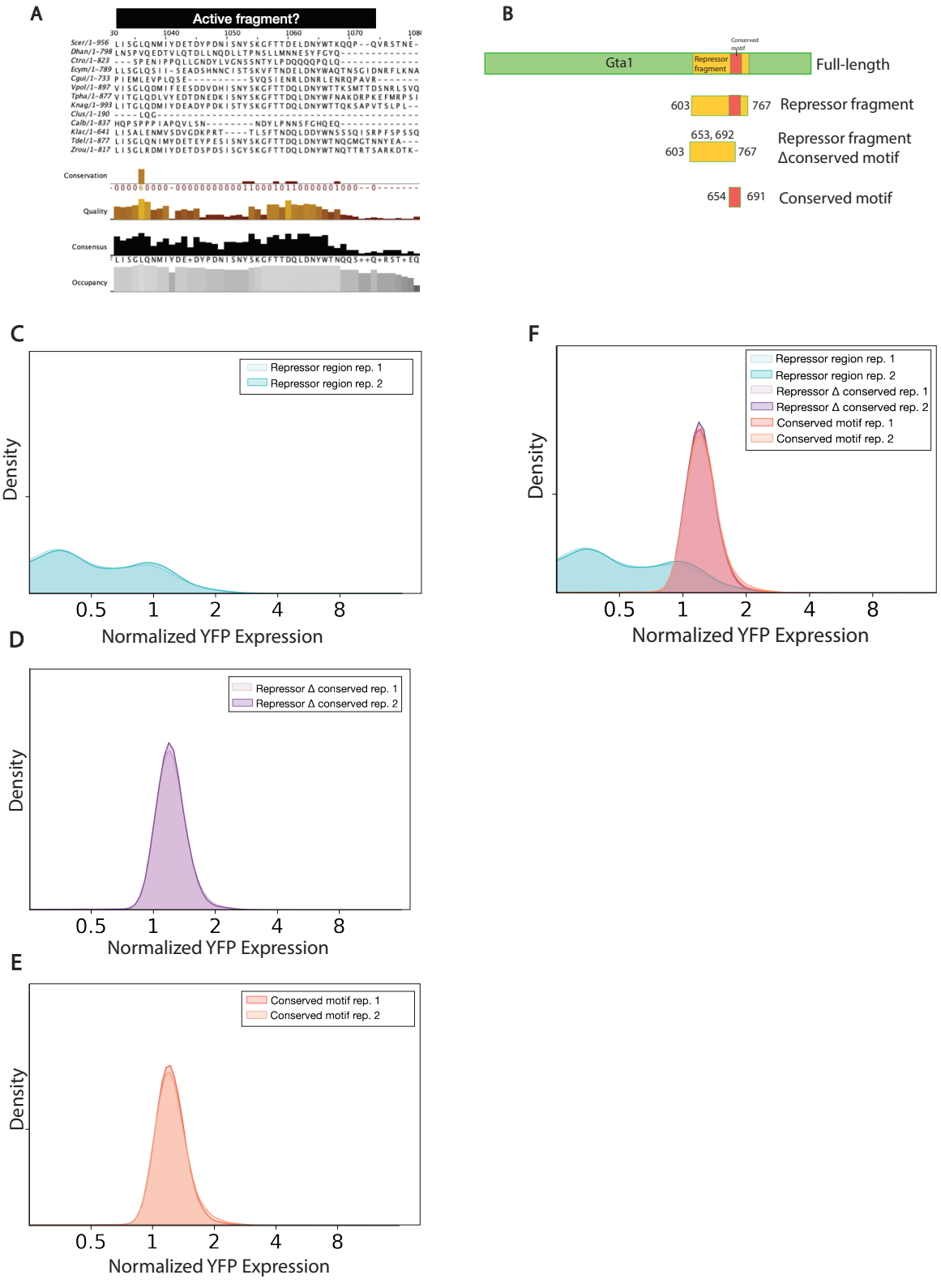
A
Active fragment?
Conservation
Quality
Consensus
Occupancy
B
Conserved motif
Repressor fragment
Gta1
Full-length
603
767
Repressor fragment
653, 692
603
767
Repressor fragment
Δconserved motif
654
691
Conserved motif
C
Repressor region rep. 1
Repressor region rep. 2
Density
0.5
1
2
4
8
Normalized YFP Expression
D
Repressor Δ conserved rep. 1
Repressor Δ conserved rep. 2
Density
0.5
1
2
4
8
Normalized YFP Expression
E
Conserved motif rep. 1
Conserved motif rep. 2
Density
0.5
1
2
4
8
Normalized YFP Expression
F
Repressor region rep. 1
Repressor region rep. 2
Repressor Δ conserved rep. 1
Repressor Δ conserved rep. 2
Conserved motif rep. 1
Conserved motif rep. 2
Density
0.5
1
2
4
8
Normalized YFP Expression

**Figure 2.3: Characterizing Gta1 repressor activity and localization (A)** Alignment of fungal sequences reveals conserved motif within the repressor region of Gta1 **(B)** Schematic of query motifs used to measure activity by tethering assay **(C-F)** Flow cytometry of tethering screen measuring activity of **(C)** Gta1 repressor region (603-767) **(D)** Gta1 repressor region Δ conserved motif (603-653, 692-767) **(E)** Gta1 conserved motif (654-691); repressor activity of Gta1(603-767) is abolished when conserved motif is deleted from repressor fragment; conserved motif alone is not sufficient to produce repressor activity **(F)** Overlay C-E flow cytometry data

## 2.7 Conclusions

We investigated the repressive activity of Gta1, a candidate post-transcriptional regulator identified in a fluorescent reporter tethering screen. By overexpressing Gta1, we found that a significant number of transcripts that are downregulated encode proteins localized to the ER and Golgi. While we were not able to completely characterize the localization pattern for Gta1, we hypothesize that this might play a role in its repressor activity. Additionally, we characterized a conserved motif within the repressor region which is essential for its repressive activity. We hope that future work can follow up on further characterizing the role of Gta1 activity within cells.

**Table 2.1: Yeast strains used in this study.** All strains are derived from *S. cerevisiae* BY4741.

| Strain Number | Genotype | Source |
|---|---|---|
| yRB001 | MATa his3Δ1 leu2Δ LYS2 met15Δ ura3Δ0 X-4::spHIS4:P(Gal1)::GTA1-1xFLAG:T(ADH1) XII-5::hphMX:pADH1-ZIF268 TF | This work |
| yRB002 | MATa his3Δ1 leu2Δ LYS2 met15Δ ura3Δ0 X-4::spHIS4:P(Gal1)::Halo-1xFLAG:T(ADH1) XII-5::hphMX:pADH1-ZIF268 TF | This work |
| yRB003 | MATa his3Δ1 leu2Δ LYS2 met15Δ ura3Δ0 X-4::spHIS4:P(Gal1)::GTA1-1xFLAG:T(ADH1) XII-5::hphMX:pADH1-ZIF268TF sec13-HA | This work |
| yRB004 | MATa his3Δ1 leu2Δ LYS2 met15Δ ura3Δ0 X-2::KIURA3:pPGK1::YFP-GTA1-3xFLAG::tADH1 | This work |
| yRB005 | MATa his3Δ1 leu2Δ LYS2 met15Δ ura3Δ0 X-2::KIURA3:pPGK1::YFP-GTA1(603-767)-3xFLAG::tADH1 | This work |
| yRB006 | MATa his3Δ1 leu2Δ LYS2 met15Δ ura3Δ0 X-2::KIURA3:pPGK1::YFP-GTA1(603-653,692-767)-3xFLAG::tADH | This work |
| yRB007 | MATa his3Δ1 leu2Δ LYS2 met15Δ ura3Δ0 X-2::KIURA3:pPGK1::YFP-GTA1(654-691)-3xFLAG::tADH1 | This work |

**Table 2.2: Plasmids used in this study.**

| Plasmid Name | Description | Source |
|---|---|---|
| pNTI729 | pADH1-ZIF268 TF in Easyclone vector pCfB2337 | Muller et al. 2020 |
| pKS139 | pGAL-Cit_LB tethering | Kendra Reynaud |
| pKS183 | pPGK1::GTA1-λN-T2A*-1xFLAG-BFP-NES::tADH1 pAgTEF::SpHIS5::tAgTEF ARS/CEN | Reynaud et al. 2023 |
| pNTI784 | pGal1::GTA1-1xFLAG:tADH1 in easyclone pCfB2226 | This work |
| pKS187 | Halo control-LN-T2A*-3xFLAG-BFP | Kendra Reynaud |
| pNTI785 | pGal1::Halo-1xFLAG:tADH1 in easyclone pCfB2226 | This work |
| pNTI292 | pFA6a P(PGK1)::yECitrine::boxb::T(ADH1) CaURA3 URA3int | Anna McGeachy |
| pRB004 | pPGK1::yECitrine-GTA1-3xFLAG::tADH1 in Easyclone vector pCfB2188 | This work |
| pRB005 | pPGK1::yECitrine-GTA1(603-767)-3xFLAG::tADH1 in Easyclone vector pCfB2188 | This work |
| pRB006 | pPGK1::yECitrine-GTA1(603-653,692-767)-3xFLAG::tADH1 in Easyclone vector pCfB2188 | This work |
| pRB007 | pPGK1::yECitrine-GTA1(654-691)-3xFLAG::tADH1 in Easyclone vector pCfB2188 | This work |

**Table 2.3: Primers used in this study.**

| Oligo Number | Sequence | Notes | Source |
|---|---|---|---|
| qRB084 | GCATGTCTGTGGCTCTCTTATAG | *GTA1* RT-qPCR | This work |
| qRB085 | TTGTTGCCGGTGGAGTTT | *GTA1* RT-qPCR | This work |
| qRB088 | GAAGTCGAGATGGACCATTACC | Halo RT-qPCR | This work |
| qRB089 | GCAGCCAGTCCATGTATTCT | Halo RT-qPCR | This work |
| RB832 | gactttAATGTACTAGCTCTTTCCGG | Sec13 gRNA oligo1 | This work |
| RB836 | ttCCGGAAAGAGCTAGTACATTgttt | Sec13 gRNA oligo2 | This work |

Chapter 3

# Genetic Regulation of Polysome Collapse During Glucose Starvation in *S. Cerevisiae*

## 3.1 Abstract

Glucose starvation in *S. cerevisiae* leads to a bulk translation inhibition response that occurs very rapidly. This response inhibits translation initiation and leads to polysome collapse. Although we understand adaptation glucose withdrawal on longer timescales, the mechanism underlying the early response remains unknown. We were interested in understanding how the rapid polysome collapse is regulated. We addressed this question using a genome-scale experiment, using CiBER-seq to measure the effect of genetic perturbations on the abundance of the reporter in polysome fractions in a high-throughput manner. We sought to identify genes that, when depleted, lead to global resistance of the translation inhibition response. We optimized the conditions for performing this screen by modifying the growth conditions prior to glucose withdrawal and the reporter system. The CiBER-seq screen identified several genes that likely participate in this response, which will be followed-up on in future work.

## 3.2 Introduction

Glucose is the preferred carbon source in yeast, which encodes several signal transduction pathways that perceive its levels and initiate the appropriate responses. When yeast are starved of glucose, cells undergo a bulk inhibition of translation initiation during which transcripts dissociate from polysomes as rapidly as 1 minute post-starvation (Ashe, De Long, and Sachs 2000). The response is characterized by a shift of ribosomes out of polysomes region into monosomes, indicative of reduced protein synthesis (Arribere, Doudna, and Gilbert 2011). Translational inhibitory responses in response to many different environmental stresses are common in yeast to maintain energy reserves and catalyze a stress-specific gene expression response. Despite the ubiquitous nature of translation inhibition as a response to different types of stress, the mechanism of inhibition during glucose starvation differs from other stress responses. Mechanisms that regulate other translation inhibition responses include the amino acid starvation pathway and the TOR signaling pathway, but these have no effect on translation shutoff after glucose starvation, nor is it driven by mRNA decay (Ashe, De Long, and Sachs 2000). The polysome withdrawal phenotype during glucose starvation does not require new transcription, and the environmental stress response is still activated (Gasch et al. 2000).

The glucose starvation response is also accompanied by a unique transcriptional signature of two classes of mRNAs. The first class includes many heat-shock inducible transcripts and are diffusely localized to the cytoplasm; the second class co-localize with P-bodies and stress granules. The first class of transcripts, which are both transcriptionally and translationally upregulated, are enriched for heat shock elements in their promoters that bind Hsf1 (Zid and O'Shea 2014). The second class of transcripts, which are transcriptionally upregulated but translationally downregulated mRNAs, are enriched in Rvb1 and Rvb2 binding in their promoters. Rvb1 and Rvb2 are conserved ATPase proteins involved in chromatin remodeling (Chen et al. 2022). Sequestration of these transcripts likely allows for cells to

recover more efficiently after glucose re-addition. More recent work has also shown that glucose stress leads to global mRNA retention in the nucleus dependent on the RNA binding protein Nab2. The formation of Nab2 condensates blocks bulk mRNA export while selectively allowing stress-induced mRNAs to pass into the cytoplasm (Heinrich et al. 2024).

The re-addition of glucose after starvation only reactivates a subpopulation of fewer than 400 transcripts in the absence of new transcription (Arribere, Doudna, and Gilbert 2011). Inhibiting transcription upon glucose re-addition still allows for substantial polysome recovery. Polysome (P) to total mRNA (T) ratios (P/T), a readout for ribosome occupancy, was found to be a good predictor for whether a gene would reassociate with ribosomes after glucose readdition. Specifically, genes with a high P/T ratio during glucose starvation returned to polysomes after readdition of glucose. Such genes were depleted from the total mRNA population while genes with low P/T ratios after glucose starvation were depleted specifically from the polysomal pool compared to the non-polysomal pool. Ribosomal protein genes make up a large pool of genes with a high P/T ratio (Arribere, Doudna, and Gilbert 2011).

The translation inhibition response to glucose withdrawal is the most dramatic inhibitory effect based on the scale and time of response. We were interested in understanding how this rapid reduction in translation initiation is regulated after polysome collapse and movement into the monosome. There are already some characterized mutants from the glucose repression pathway that are known to prevent polysome collapse upon glucose starvation (Ashe, De Long, and Sachs 2000). However, we were interested in looking at other potential genetic regulators outside of this pathway. We used CiBER-seq, a CRISPRi barcoded expression readout approach, to perturb all genes in the yeast genome and identify which mutants regulate mRNAs leaving polysomes after glucose withdrawal (Muller et al. 2020). By fractionating monosomes and polysomes using sucrose gradients, we identified which transcripts have decreased polysome association after glucose withdrawal. We used this same technique to find mutants that regulate transcripts loading back onto polysomes after glucose refeeding.

## 3.3 Methods

*Yeast strains*

Strains used in this study are listed in Table 3.1. Strains were derived from *S. cerevisiae* BY4741 using standard genetic techniques. Gene deletion strains were generated by using one-step-replacement with KanMX marker cassette (Goldstein and McCusker 1999). PCR amplification of KanMX from pCfB2223 easyclone 2.0 vector with primers gene_uptag and gene_dntag with 25 basepairs flanking sequence homology to the 5’ and 3’ ends of the target gene. A second round of PCR amplification with primers gene_up45 and gene_dn45 to add 45 basepairs of homology to target gene on 5’ and 3’ ends. PCR amplification product was transformed into yeast using KanMX selection marker. Gene deletions were validated by RT-qPCR with primers listed in Table 3.2. Plasmids and primers used in strain construction are listed in Table 3.2 and 3.3, respectively.

*Plasmids*

Plasmids used in this study are listed in Table 3.2.

*Sucrose Gradients*

Cells were grown to mid-log phase in a volume of at least 150 mL ($OD_{600}$ ~0.5 - 1.0). Cells were harvested by vacuum filtrated with 0.45 µM Whatman cellulose nitrate membrane filters (Fisher Scientific #09-744-75). Yeast cells were immediately scraped off with a pre-chilled metal spatula and plunged into a conical tube with holes poked into the cap and filled with liquid nitrogen. Drip 2 mL of freshly prepared ice cold polysome buffer (20 mM Tris-HCl pH 7.4, 150 mM NaCl, 5 mM MgCl2, 1 mM DTT, 1% Triton X-100, .02 U/µl Turbo DNase) into conical tube with cells so that it forms droplets. Store conical tubes in -80℃ overnight.

Frozen yeast and polysome buffer were lysed by cryogrinding with the MM400 Mixer mill (Retsch #20.745.0001). Cryogrinding yeast for six cycles of 3 minutes at 15 Hz. The powder was moved from the grinding chamber using a pre-chilled metal spatula into a conical tube with holes poked into the cap, filled with liquid nitrogen. Store conical in -80℃ overnight. Lysates were thawed slowly on an ice bucket (~2 hours). Lysates were clarified by centrifuging conical tube at 3000g/5min/4℃. Supernatant was transferred to Eppendorf tubes and clarified at 14000rpm/15min/4℃. Supernatant was transferred to Eppendorf tubes. Lysate was quantified by isolating 100µl RNA using a Direct-zol RNA Purification Kit (Zymo #R2060) and treating with TurboDNase for 15 minutes. Clarified lysates were used for sucrose gradients.

Sucrose gradients were prepared using a Gradient Master (BioComp Instruments) using Seton Open-Top Polyclear Centrifuge Tubes (Seton Scientific #7030). Normalized lysates (220µl) were loaded onto a 10-50% sucrose gradient prepared in polysome buffer. Gradients were centrifuged at 35000rpm/3 hours/4℃ in a Beckman SW41 Ti rotor using an XL-70 ultracentrifuge (Beckman Coulter). The sucrose gradients were run through the gradient master system and the absorbance was monitored using a UV monitor (BioRad EM-1 Econo UV monitor). Distinct fractions were collected manually by monitoring the polysome traces.

RNA was isolated from sucrose gradients using protocol adapted from Professor Stephen Floor (Extracting RNA from polysome profile fractions for qPCR or TrIP-seq sequencing, Benchling). Phase separation portions of protocol were carried out using phase lock gel tubes (VWR #2302830) to minimize interphase contamination. RNA was eluted in water and quantified using Nanodrop.

*RT-qPCR*

RNA was extracted from sucrose gradient fractions according to method in sucrose gradient section. Complementary DNA was synthesized using ProtoScript II reverse transcriptase (NEB #M0368L) and oligo $d(T)_{23}VN$ according to manufacturers protocol. Quantitative PCR was conducted using the DyNAmo HS SYBR Green qPCR kit (Fisher Scientific #F-410L) and the primers listed in Table 3.3 (BioRad-CFX96 qPCR System instrument).

*Plasmid library transformation*

The divergent P(Z)-mScarlet and P(*TFC1*)-citrine plasmid library was gifted by Paige Diamond and generated as detailed in (Diamond, McGlincy, and Ingolia 2024; Muller et al. 2020). The library was retransformed into ElectroMax DH10β cells (Thermo Scientific #18290015) by electroporation according to manufacturers protocol. Serial dilutions of transformations were plated to ensure sufficient library diversity (>50x coverage of 240,000 unique barcodes).

*CiBER-seq Screen Setup*

Plasmid library was transformed into NIY443 yeast cells using standard lithium acetate transformation (Gietz and Schiestl 2007). Serial dilutions of transformations were plated onto URA selection plates to ensure sufficient library diversity (>5x coverage of 240,000 unique barcodes).

CiBER-seq experiments are usually carried out in a continuous-culture turbidostat, but due to volume limitations and the rapid nature of the stress experiment, we modified this protocol to use batch culture instead (Muller et al. 2020; McGeachy, Meacham, and Ingolia 2019). Yeast populations transformed with plasmid libraries were inoculated into SCD -URA selection media with 10 mM β-estradiol (200 mL total culture volume). Cells were grown about 5 hours until $OD_{600}$ of ~4.5. Cells were back-diluted into prewarmed SCD -URA media with 10 mM β-estradiol to starting $OD_{600}$ of 0.05. After 10 hours of growth, cells reached $OD_{600}$ of ~0.3. Cells were back-diluted again to $OD_{600}$ of 0.05 in SCD -URA media (800 mL culture volume) and guides were induced with 250 ng/mL tetracycline. Once cells reached $OD_{600}$ of 0.8, cells were centrifuged and resuspended in prewarmed YEPD media to $OD_{600}$ of 0.2 (1.6 L culture volume) with 10 mM β-estradiol and 250 ng/mL tetracycline. Yeast were grown in YEPD for one population doubling (~4 hours). Cells were collected for unperturbed condition. Remaining cells were centrifuged and resuspended in prewarmed YP with 10 mM β-estradiol and 250 ng/mL tetracycline for glucose starvation condition. After 10 minutes, cells were harvested by vacuum filtration as described in sucrose gradient methods section. For the refed condition, dextrose with with 10 mM β-estradiol and 250 ng/mL tetracycline was added to culture for final concentration of 2% dextrose. Refed cells were harvested by vacuum filtration. Cell lysates were prepared for sucrose gradients by cryogrinding and fractionating using the gradient master (see method described in sucrose gradient section).

RNA for CiBER-seq library input was prepared from input lysate and sucrose gradient monosome and heavy polysome fractions using method described in sucrose gradient section. Barcode library preparation was prepared according to protocol described in (Muller et al. 2020). The cDNA products was amplified with RM-810 and RM-511 for P(TFC1)-citrine libraries. Libraries were sequenced on an Illumina NovaSeq 4000 using 100 base pair single-end reads.

*CiBER-seq Analysis*

Sequencing data were trimmed using cutadapt to remove Illumina adapter sequences and deconvolve multiplexed libraries based on embedded nucleotide indices (Martin 2011).

Trimmed barcodes were counted as described in (Muller et al. 2020). Barcodes with fewer than 32 average counts in across all fractions were excluded from the analysis. The remaining barcodes were evaluated by differential expression analysis using DESeq2 (Love, Huber, and Anders 2014). Data is available upon request.

### 3.4 Complete polysome collapse after glucose starvation requires rich media conditions

To identify genetic perturbations that alter mRNAs leaving ribosomes after glucose withdrawal, we used CiBER-seq followed by polysome gradient fractionation (Muller et al. 2020). More specifically, we tracked the abundance of a barcoded reporter in the input, monosome, and heavy polysome (≥5 polysomes) fractions to see which perturbations led to decreased polysome association and a concurrent increase in monosome association by sequencing the barcode abundance (Figure 3.1A). We further measured how polysome association changed across glucose withdrawal and re-addition to identify perturbations that changed this response.

Plasmid-based CiBER-seq requires cells to be maintained under constant selection of a *URA3*-marked plasmid in synthetic complete media minus uracil. To profile translational changes during stress, yeast were grown under Ura selection (unperturbed condition), followed by removal of glucose for 10 minutes (glucose-starved condition), followed by re-addition of glucose for 10 minutes (re-fed condition). Polysome profiling by sucrose gradient density ultracentrifugation demonstrated that glucose starved cells showed a dramatic reduction in polysomes compared with the unperturbed cells, and an increase in polysomes after cells were re-fed glucose (Figure 3.1B). The polysome (P) to monosome (M) P/M ratio in unperturbed cells is 0.38, 0.07 in starved cells, and 0.44 in refed cells, reflecting the changing translation levels. While these data reflective the polysome collapse phenotype we expect, prior work demonstrated a more substantial change in polysome levels. We reasoned that protein synthesis may be lower in selective synthetic media than in rich YEPD. We thus performed the same stress experiment, using rich media (YEPD), mimicking the seminal glucose starvation paper (Ashe, De Long, and Sachs 2000). Performing the stress experiment in rich media led to far more dramatic polysome collapse (P/M ratio 0.0043) and the refed condition closely mirrored the unperturbed condition (P/M unperturbed condition is 0.66; P/M refed condition is 0.50) (Figures 3.1 D,E).

These results confirm that, indeed, yeast growing rapidly in rich media respond more strongly to glucose depletion. In contrast, cells grown in synthetic complete media depend somewhat less on rapid glucose metabolism, making them less sensitive to glucose withdrawal. We amended the design of our CiBER-seq experiment so that we could deplete glucose from cells growing in rich media conditions. We transformed yeast with our CiBER-seq library, selected transformants in synthetic media, and then transferred the cells into rich media for one population doubling before performing the stress experiment (Figure 3.1F). We collected RNA from each fraction in the polysome profile. Quantification of the total amount of RNA isolated from each of the fractions also reflects the shifts between polysomes and monosomes occurring in response to glucose withdrawal and repletion (Figure S3.1A,B).

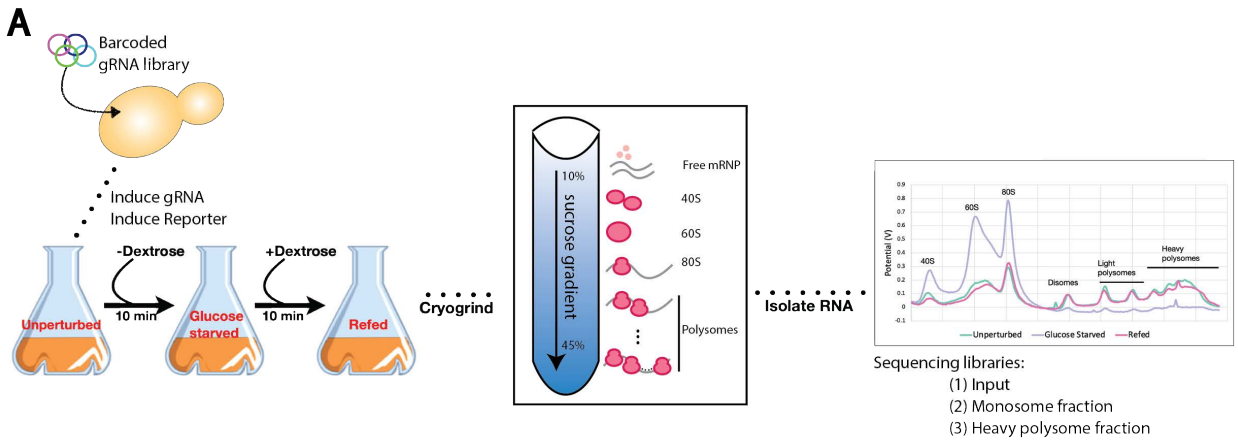
A
Barcoded
gRNA library
Induce gRNA
Induce Reporter
-Dextrose
10 min
+Dextrose
10 min
Unperturbed
Glucose starved
Refed
Cryogrind
10%
sucrose gradient
45%
Free mRNP
40S
60S
80S
Polysomes
Isolate RNA
Sequencing libraries:
(1) Input
(2) Monosome fraction
(3) Heavy polysome fraction

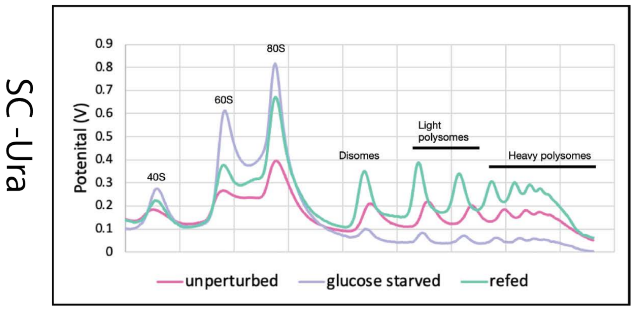
B
SC -Ura
Potenital (V)
40S
60S
80S
Disomes
Light polysomes
Heavy polysomes
unperturbed
glucose starved
refed

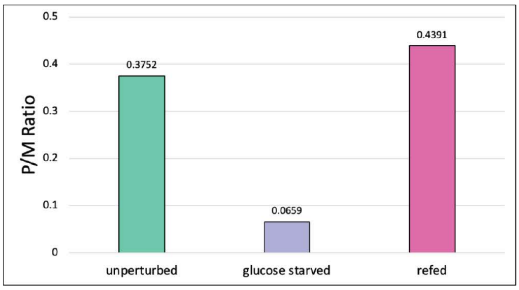
C
P/M Ratio
0.3752
0.0659
0.4391
unperturbed
glucose starved
refed

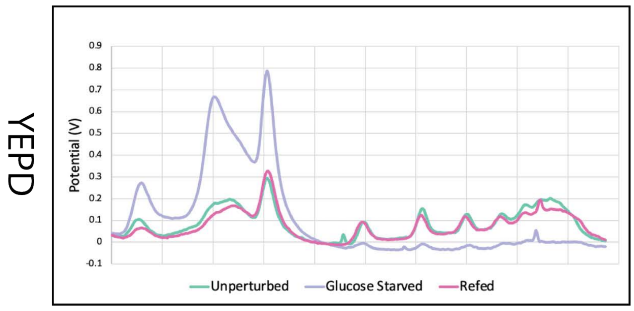
D
YEPD
Potenital (V)
Unperturbed
Glucose Starved
Refed

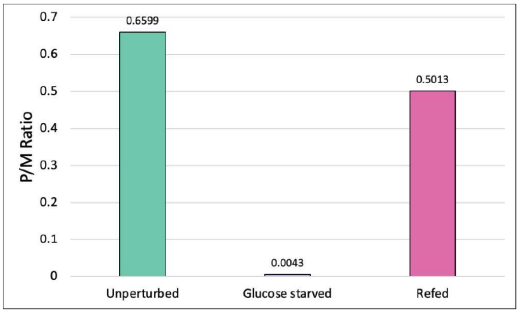
E
P/M Ratio
0.6599
0.0043
0.5013
Unperturbed
Glucose starved
Refed

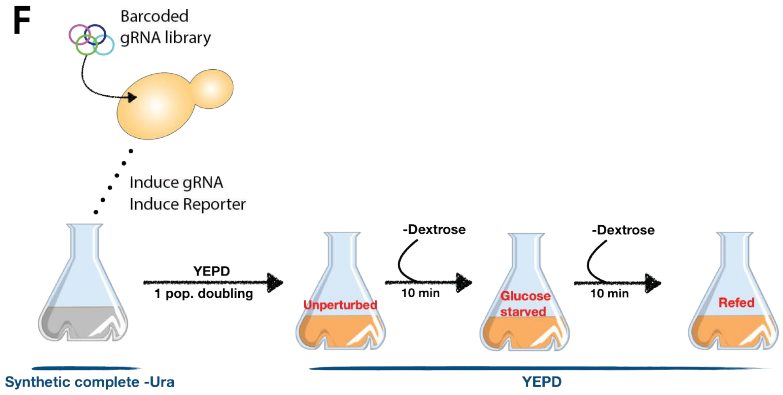
F
Barcoded
gRNA library
Induce gRNA
Induce Reporter
YEPD
1 pop. doubling
Unperturbed
-Dextrose
10 min
Glucose starved
-Dextrose
10 min
Refed
Synthetic complete -Ura
YEPD

**Figure 3.1: Glucose withdrawal polysome collapse phenotype is dependent on media conditions (A)** Schematic of CiBER-seq and polysome gradient experimental setup. Barcoded CiBER-seq libraries are transformed into yeast; induction of synthetic reporter and gRNAs; stress experiment followed by 10-45% sucrose fractionation; RNA isolation from input, monosome, and heavy polysome fractions. **(B)** Polysome gradients for glucose-replete, glucose-starved, and glucose refed yeast grown in Synthetic Complete (SC) minus Ura media conditions. **(C)** Polysome (P) to Monosome (M) P/M ratio in SC minus Ura media conditions shows decrease in P/M ratio after glucose starvation **(D)** Polysome gradients for glucose-replete, glucose-starved, and glucose refed yeast grown in rich media conditions, YEPD. **(E)** P/M ration in rich media condition shows more substantial decrease in P/M ratio after glucose starvation. **(F)** Amended CiBER-seq protocol; yeast cultures grown in SC minus Ura are transferred cultures into YEPD for one final population doubling, followed by the stress experiment.

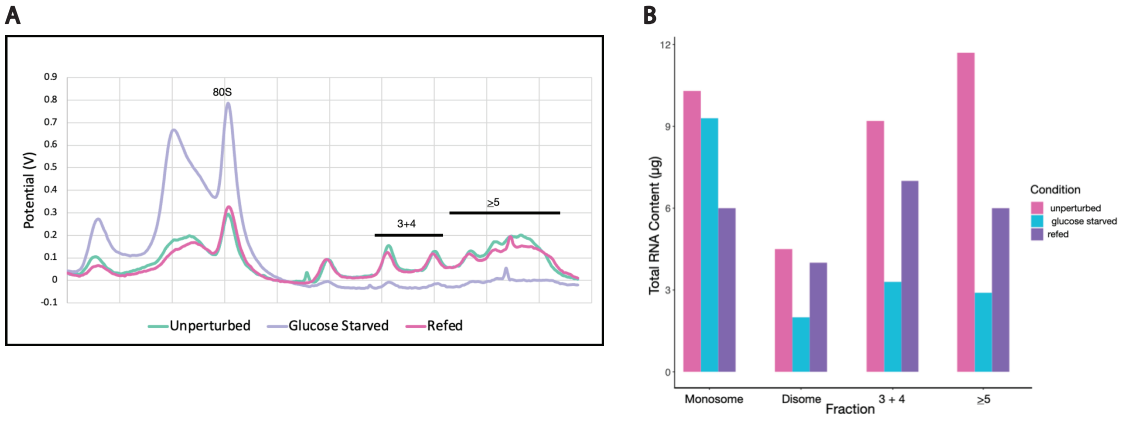


**Figure S3.1: Total RNA content corresponds with polysome fractionation phenotypes (A)** Polysome traces from 10-45% sucrose gradients for unperturbed, glucose-starved, and refed conditions demonstrate changing polysome phenotype. **(B)** Quantification of RNA in unperturbed, glucose starved, refed conditions reflects peak sizes in polysome traces.

## 3.5 *TFC1* driven reporter shows polysome withdrawal phenotype during glucose starvation

We were interested in identifying genetic perturbations that altered polysome collapse during glucose starvation. Specifically, if a genetic perturbation prevents translation shutoff, we expect an increased abundance of the associated reporter in the polysome fraction (Figure 3.2). Since we depended on a single reporter as a readout for overall polysome collapse, we looked at whether both reporters in our CiBER-seq library reflected this phenotype.

An optimal reporter should reflect the polysome shifts of endogenous transcripts. It should be depleted from the heavy polysome fraction and increase in abundance in the monosome fraction following glucose withdrawal. In the background of a genetic perturbation that prevents polysome collapse, we would expect an increase in reporter abundance in the

heavy polysome fraction. HXK2 is a hexokinase that phosphorylates glucose in the cytosol and its deletion was demonstrated to prevent polysome collapse after glucose starvation (Ashe, De Long, and Sachs 2000). To track reporter distributions in both conditions, we performed the glucose stress experiment in wildtype and *hxk2*Δ cells (Figure 3.3A). We transformed the divergent reporter construct, which consisted of the *TFC1* promoter driving a Citrine reporter and an inducible synthetic transcription factor (*SynTF*) promoter driving an mScarlet reporter, into wildtype and *hxk2*Δ yeast (Figure 3.3B). We then set up an experiment allowing us to test reporters from a small fraction of non-inhibited cells in the context of a wildtype population. To do this, we then grew three cultures: (1) wildtype yeast, (2) wildtype yeast with reporters, and (3) *hxk2*Δ yeast with reporters. We mixed each of the cultures containing the reporters individually with wildtype yeast so that the reporter strains made up 20% of the population while the background wildtype strain made up the remaining 80% right before performing glucose withdrawal and repletion (Figure 3.3C). Comparing polysome profiles between these cultures showed a slight upshift in the *hxk2*Δ strain for 40S, 60S, and monosomes compared with the wildtype strain but the polysome collapse phenotype overlapped seamlessly (Figure 3.3D). We calculated the relative number of RNA copies of the reporters in each fraction by performing RT-qPCR and using the following equation:

$$Relative\ RNA\ copy\ \# = 2\text{^}(30 - Ct_{reporter}) \times cDNA\ dilution\ factor \div Amount\ RNA\ reverse\ transcribed\ x\ Total\ RNA\ in\ fraction$$

The *TFC1* derived citrine reporter mimicked the glucose withdrawal phenotype, whereas the *SynTF* derived mScarlet reporter did not. In wildtype yeast, the citrine reporter showed higher abundance in the lighter fractions than the heavier polysome fractions. In *hxk2Δ* yeast, the citrine reporter still showed a high abundance in the earlier fraction but a comparably higher abundance in the later polysome fractions (Figure 3.3E). By comparing relative citrine copy number between wildtype and *hxk2Δ* cells, we found that the citrine transcript shifted out of polysomes, following the general trend seen across endogenous transcripts. The *SynTF* derived mScarlet reporter had nearly 1000 times greater expression than the citrine reporter. However, in the wildtype strain, the mScarlet abundance is constant across all fractions except somewhere in the middle fraction, likely representing the disomes. We saw an overall increase in the relative copies of mScarlet in *hxk2Δ* in most fractions after glucose withdrawal (Figure 3.3F). While it does appear that wildtype and *hxk2Δ* have different distributions of the mScarlet reporter, this distribution does not reflect the shift of the reporter out of polysomes following glucose withdrawal. Based on this data, we decided to only proceed with sequencing the citrine reporter libraries.

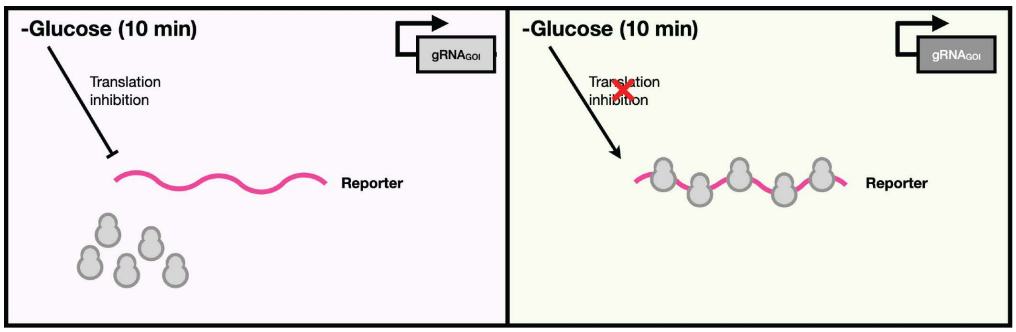


**Figure 3.2: Schematic of expected reporter phenotype for genetic perturbations that effect polysome collapse** The left panel represents a guide RNA for a gene of interest (*GOI*) that has no effect on polysome collapse during glucose starvation. Removing glucose for 10 minutes in this background still leads to translation inhibition and complete polysome loss from the reporter construct. The right panel represents a guide RNA for a *GOI* that prevents translation inhibition. Removing glucose for 10 minutes in this background prevents translation inhibition and the polysomes remain on the reporter transcript.

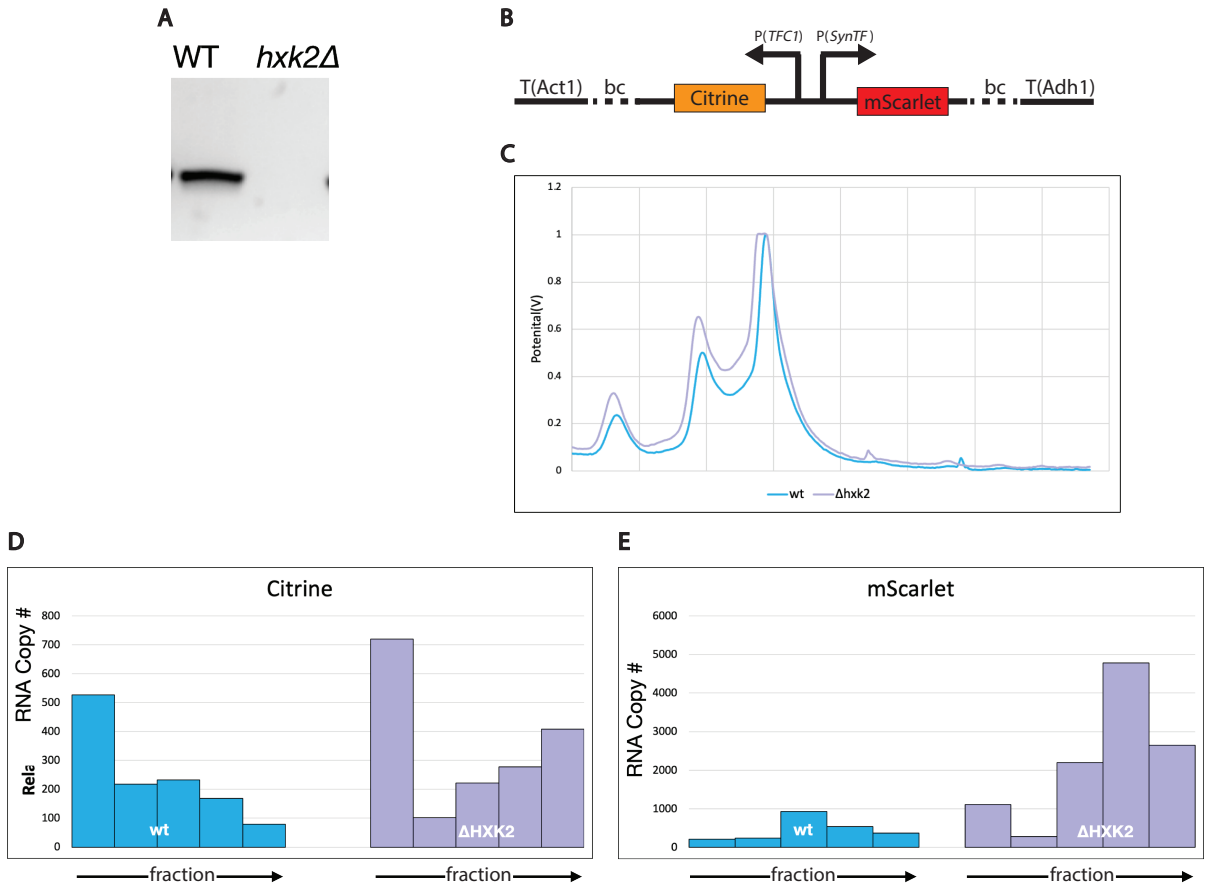

**Figure 3.3: Tracking reporter abundance across fractions to validate polysome collapse phenotype (A)** 1% agarose gel of genotyping PCR in *wildtype* (WT) and *hxk2*Δ yeast. WT PCR shows band for HXK2; *hxk2*Δ PCR shows no band, validating its deletion. **(B)** Schematic of divergent reporter setup; *TFC1* promoter is driving the citrine reporter with an *Act1* terminator sequence; inducible synthetic transcription factor (*SynTF*) promoter is driving the mScarlet reporter with an *Adh1* terminator. **(C)** Schematic for experimental setup to track reporter abundance. Wildtype yeast culture is mixed with (1) wildtype culture transformed with reporters or (2) *hxk2*Δ culture transformed with reporters in a 1:5 ratio. Each of these cultures then undergo glucose starvation and the lysate from these cultures are used for sucrose gradients. **(D)** Polysome traces for lysates from (C) show polysome withdrawal phenotype **(E)** RT-qPCR to track TFC1 driven citrine reporter abundance across fractions in *wildtype* and *hxk2*Δ strains. The *hxk2*Δ strain derived citrine reporter shows increased polysome association compared to the *wildtype* strain. (F) RT-qPCR to track *SynTF* driven mScarlet reporter abundance across fractions in *wildtype* and *hxk2*Δ strains. The *hxk2*Δ and *wildtype* strain derived mScarlet reporter abundance do not reflect a polysome collapse phenotype.

### 3.6 CiBER-seq to identify genetic perturbations that regulate polysome withdrawal phenotype

We performed CiBER-seq by sequencing barcodes from the citrine reporter in sucrose gradient fractions from glucose-replete, glucose starved, and refed conditions. We performed short-read sequencing on the barcodes from input lysate, monosome and heavy polysome fractions for two biological replicates and three conditions, for a total of 18 libraries. Our libraries contained ~240,000 barcodes. While a robust analysis required an average coverage of 100 reads per barcode, or sequencing depth of $2.4 \times 10^7$ reads, we obtained only $5–12 \times 10^6$ reads per library, which is 2–4 fold lower than our target barcode coverage (Figure S3.2A).

Given the lower barcode coverage, we moved forward with analyzing the input and heavy polysome fractions, excluding the monosome fractions that were most affected by low coverage. We saw strong correlation between each of the input and heavy polysome fractions across the different conditions (Figure S3.2B-G). We filtered the data to only include guides with more than 32 reads and used a general linear model in DESeq2 to infer the differences in barcode abundance between the input and heavy polysome fraction in one condition versus another condition. We looked for significant differences based on this comparison $\log_2$ fold-change < -1 or >1, $p_{adj}$ <0.05). The unperturbed versus refed analysis showed only five significant guides, which is unsurprising since cells restore translation after the re-addition of glucose (Figure 3.4C). In comparison, the analysis of unperturbed versus starved and starved versus refed showed more significant guides (Figure 3.4A,B).

We picked guides to pursue based on the $\log_2$ fold-change, target gene function, and whether they showed significant changes in multiple comparisons. To validate our results, we deleted the gene of interest, performed glucose withdrawal, and then compared polysome profiles from sucrose gradients for glucose-replete and glucose starvation conditions. We expected that, if a genetic perturbation prevented polysome collapse, the unperturbed and starved conditions polysome traces should look similar. First, to confirm that we could use this

approach for validating our hits, we performed this experiment using *hxk2*Δ cells. We did in fact see that glucose withdrawal in *hxk2*Δ cells did not lead to polysome collapse, though starvation did lead to an increase in the monosome fraction, likely indicating that there is a residual effect on translation initiation (Figure 3.4C). We then performed this experiment on a guide targeting *KSS1*, which encodes a mitogen-activated protein kinase that induces transcription of filamentation genes in response to nutrient limitation (Winters and Pryciak 2018). The *KSS1* guide showed a $\log_2$ fold-change of 2.86 ($p_{adj}$ 0.0294) in the unperturbed versus starved condition, indicating that knockdown of *KSS1* prevented polysome collapse. However, polysome traces in *kss1*Δ glucose-starved yeast still showed nearly complete polysome collapse compared with the unperturbed condition (Figure 3.4D). We also tested a guide targeting *GAL83*, which encodes a subunit of the Snf1 kinase complex that allows for its nuclear localization in low glucose conditions (Hedbacker and Carlson 2006; Bendrioua et al. 2014). Relatedly, an *hxk2*Δ *snf1*Δ strain prevents polysome collapse in glucose starved cells (Ashe, De Long, and Sachs 2000). The guide targeting *GAL83* had a $\log_2$ fold-change of 7.00 ($p_{adj}$ 0.061) in the unperturbed versus starved condition, and also showed a reciprocal shift in the starved versus refed conditions with a $\log_2$ fold-change of -6.94 ($p_{adj}$ 0.058). Polysome traces in *gal83*Δ glucose starved yeast also showed nearly complete polysome collapse compared to the glucose-replete condition, indicating that knockout of *GAL83* does not prevent polysome collapse (Figure 3.4E).

One key difference between the CiBER-seq experiment and our follow-up validation was the use of genetic knockdowns versus knockouts. It is possible that the phenotype we were measuring may have a layer of regulation that requires some amount of the gene to be transcribed, therefore explaining why our follow-up experiments didn't show the expected phenotype. Another limitation in our data was the lower barcode coverage, which added statistical noise. This is reflected by many of the significant hits only returning one guide with a significant log2 fold-change and $p_{adj}$ values even though our library contained multiple guides per gene.

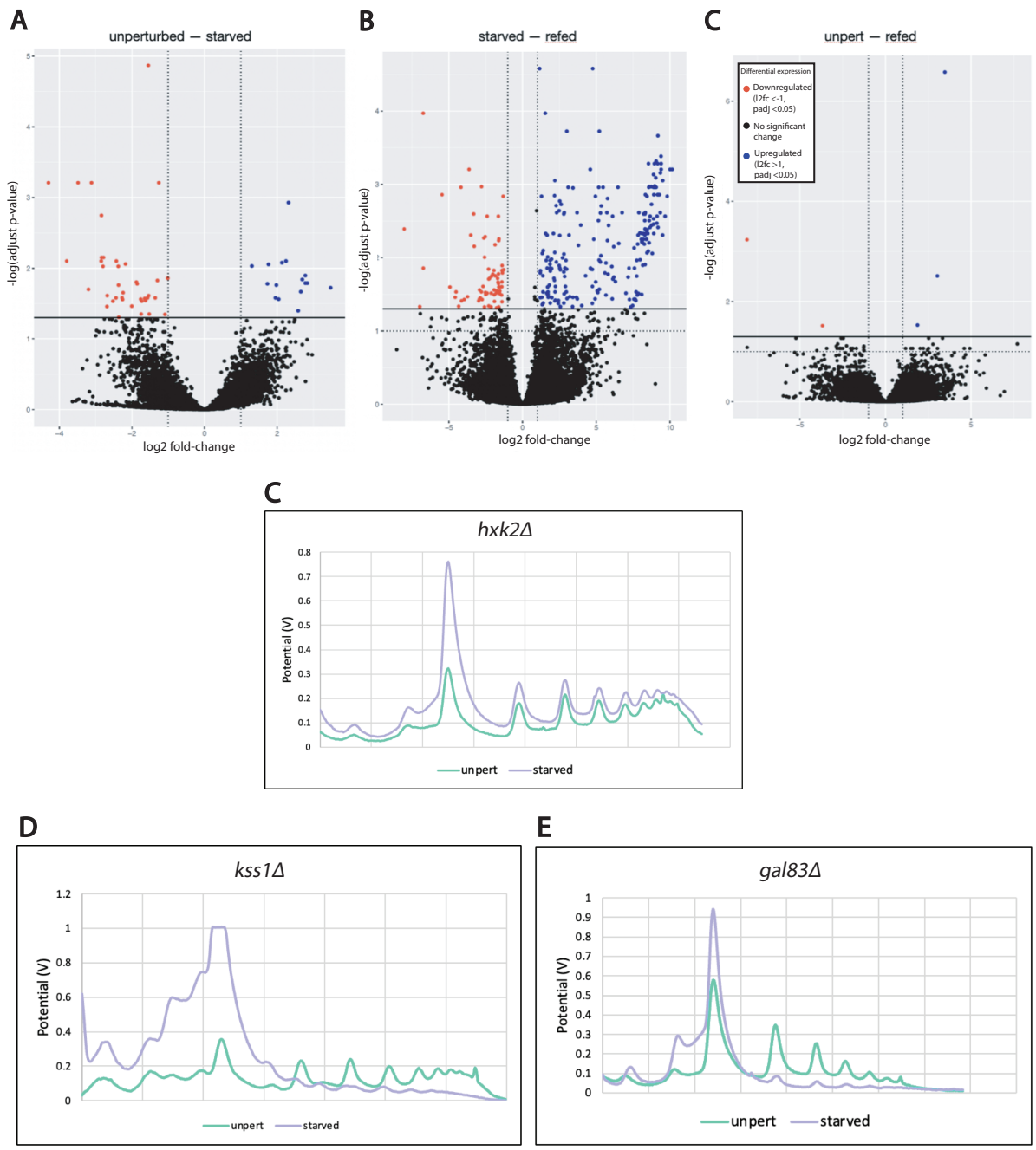


**Figure 3.4: CiBER-seq library analysis and validation experiments (A-C)** Volcano plots of DESeq2 analysis of input and heavy polysome fractions in different conditions; colored points represent $p_{adj} < 0.05$ **(A)** Unperturbed versus starved conditions **(B)** Starved versus refed conditions **(C)** Unperturbed versus refed conditions **(D)** Polysome traces for unperturbed and 10 min glucose starved *hxk2*Δ yeast shows polysome collapse response is prevented after starvation. **(E)** Polysome traces for unperturbed and 10 min glucose starved *kss1*Δ yeast shows polysome collapse still occurs after starvation. (F) Polysome traces for unperturbed and 10 min glucose starved *gal83*Δ yeast shows polysome collapse still occurs after starvation.

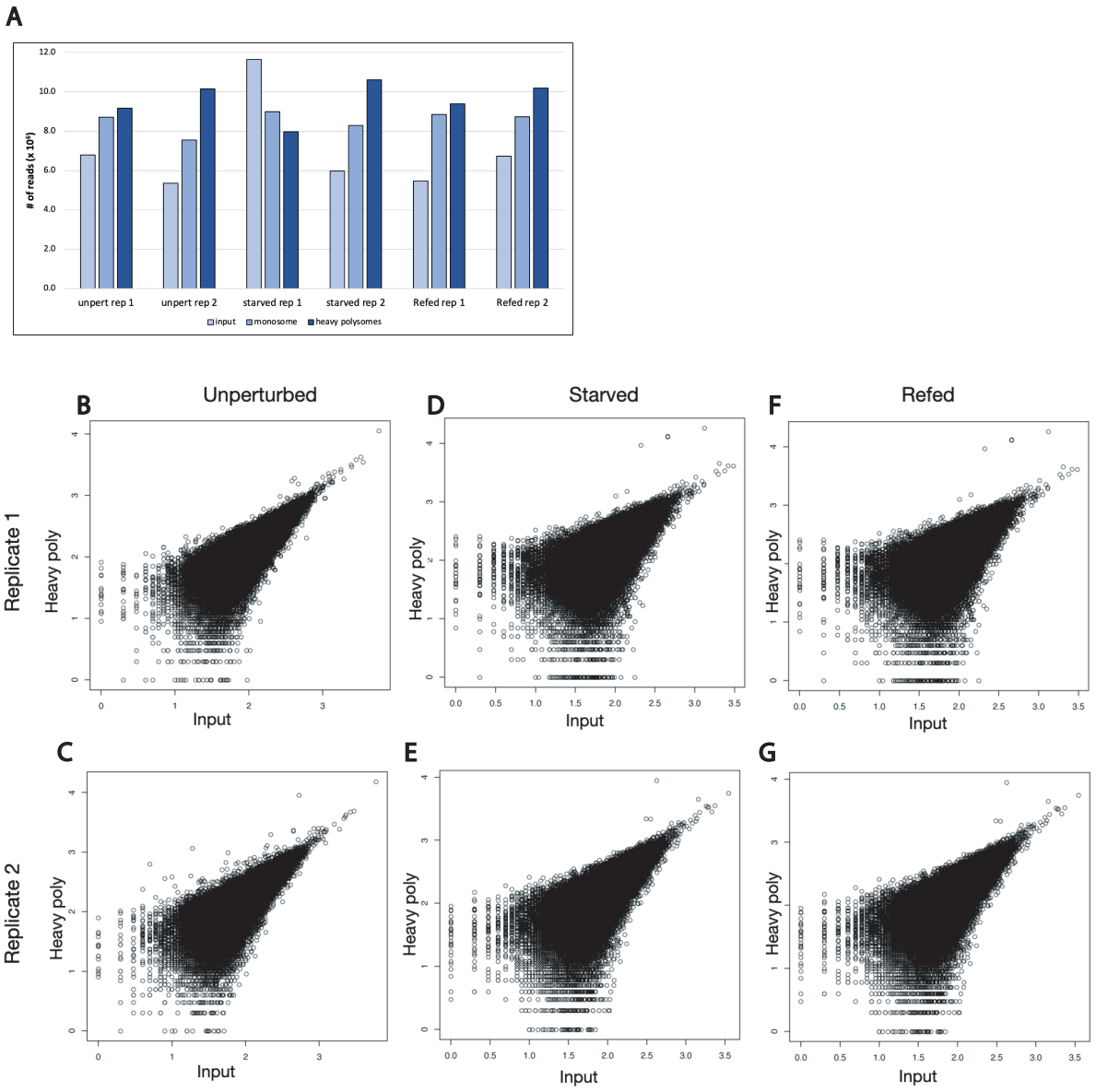


**Figure S3.2: CiBER-seq library sequencing depth and correlation plots (A)** Bar plot for total number of sequencing reads in the input, monosome, and heavy polysome fractions for each condition (unperturbed, glucose starved, glucose refed) and two biological replicates; number of reads scaled by $10^6$ **(B-G)** Barcode correlation plots for input versus heavy polysome fraction data **(B)** Unperturbed, replicate 1 **(C)** Unperturbed, replicate 2 **(D)** Glucose starved, replicate 1 **(E)** Glucose starved, replicate 2 **(F)** Glucose refed, replicate 1 **(G)** Glucose refed, replicate 2.

## 3.7 Conclusions

We optimized conditions to perform a CiBER-seq experiment to identify genetic perturbations that reduce translational shutoff during glucose starvation. We found that rich media growth ensures the most dramatic polysome collapse during glucose starvation. We also validated a reporter that reflects the polysome collapse phenotype. Further work should be done to characterize why the endogenous promoter driven reporter undergoes polysome collapse while the inducible reporter did not. However, it is also possible that the global translation shutoff response is specific to certain types of transcripts that we were unable to capture with our reporters.

**Table 3.1: Yeast strains used in this study.** All strains are derived from *S. cerevisiae* BY4741.

| Strain Number | Genotype | Source |
|---|---|---|
| NIY443 | MATa his3Δ1 leu2Δ LYS2 met15Δ ura3Δ0 [dCas9 tetR, G418R] [p(PGK1)-ZEM Transcription Factor, HygR] | Muller et al. 2020 |
| NIY552 | MATa his3Δ1 LYS2 met15Δ ura3Δ0 leu2Δ0 [ygl253wΔ:G418] [p(ADH1)-ZEM Transcription Factor, HygR] | This work |
| NIY554 | MATa his3Δ1 LYS2 met15Δ ura3Δ0 [ypl026cΔ:leu2] [dCas9 tetR, G418R] [p(PGK1)-ZEM Transcription Factor, HygR] | This work |
| NIY555 | MATa his3Δ1 LYS2 met15Δ ura3Δ0 [ygr040wΔ:leu2] [dCas9 tetR, G418R] [p(PGK1)-ZEM Transcription Factor, HygR] | This work |

**Table 3.2: Plasmids used in this study.**

| Plasmid Name | Description | Source |
|---|---|---|
| pNTI647 | Yeast dCas9-Mxi1 TetR KanMx | McGlincy et al. 2017 |
| pNTI729 | pADH1-ZIF268 TF in pCfB2337 | Muller et al. 2020 |
| pNTI730 | pPGK1-ZIF268 TF in pCfB2337 | Muller et al. 2020 |

**Table 3.3 Primers used in this study.**

| Oligo Number | Sequence | Notes | Source |
|---|---|---|---|
| RM-511 | GTGACTGGAGTTCAGACGTGTGCTCTTCCGATCTT GGTCCAGTCTTGTTACCAGACAACC | CiBER-seq barcode amplification | Muller et al. 2020 |
| RM-810 | ACACTCTTTCCCTACACGACGCTCTTCCGATCT | CiBER-seq barcode amplification | Muller et al. 2020 |

| | | | |
|---|---|---|---|
| qRB199 | GGTGATGGTCCAGTCTTGTT | Citrine RT-qPCR | Muller et al. 2020 |
| qRB200 | GGGTAATACCAGCAGCAGTAA | Citrine RT-qPCR | Muller et al. 2020 |
| qRB193 | CAGATGCCTGGAGCCTATAAC | mScarlet RT-qPCR | Paige Diamond |
| qRB194 | TTGAATGCCTACCCTCAGAAC | mScarlet RT-qPCR | Paige Diamond |
| qRB011 | AGTGTGATGTCGATGTCCGT | *Act1* RT-qPCR | This work |
| qRB012 | TCGGCAATACCTGGGAACAT | *Act1* RT-qPCR | This work |
| qRB229 | CTGGACTCAAACCTCACTAGAC | *Hxk2* RT-qPCR | This work |
| qRB230 | GGGCCAAAGCAGCAATAAC | *Hxk2* RT-qPCR | This work |
| qRB247 | GCCGGAATATCCTCCACTTAAT | *Kss1* RT-qPCR | This work |
| qRB248 | AGCATTTCTATGGGCACTTCT | *Kss1* RT-qPCR | This work |
| qRB245 | CAGCAAGTCCAAGAACAAGAAC | *Sks1* RT-qPCR | This work |
| qRB246 | GGAATATCACTCTCCGGTTCAG | *Sks1* RT-qPCR | This work |
| RB790 | cgctaattaaataaaatggGGTCTAGAGATCTGTTTAGCTTGCCTCGTC | ygl253w knockout uptag | This work |
| RB791 | atttacaaattaagtttaCTCGAGAGCTCGTTTTCGACACTGGATG | ygl253w knockout dntag | This work |
| RB792 | AATATAATTCTCCACACATAATAAGTACGCTAATTAAATAAAATG | ygl253w knockout up45 | This work |
| RB793 | AGGGCACCTTCTTGTTGTTCAAACTTAATTTACAAATTAAGTTTA | ygl253w knockout dn45 | This work |
| RB1148 | AAATTTTGTGTACAAATGgctgtgaagatcccagcaaa | ypl026c knockout uptag | This work |
| RB1149 | AAAGGTGAGACCTGCTCAgcaggctaaccggaacctgtatt | ypl026c knockout dntag | This work |
| RB1150 | AAAACATCAAATAAGAACACAGACAAGAAATTTTGTGTACAAATG | ypl026c knockout up45 | This work |
| RB1151 | TAGAACATAAGATAATACAGTGAGTATAAAGGTGAGACCTGCTCA | ypl026c knockout dn45 | This work |
| RB1132 | TTCAACAATTCAAAGATGGgctgtgaagatcccagcaaa | ygr040w knockout uptag | This work |
| RB1133 | ATGTTCTTGTGAATACTAgcaggctaaccggaacctgtatt | ygr040w knockout dntag | This work |
| RB1134 | AAAAAAGTATCTTTTCTTCACTTTTCTTTCAACAATTCAAAGATG | ygr040w knockout up45 | This work |
| RB1135 | TAGGGAAATTTTAGAAGTATGGCAGAAATGTTCTTGTGAATACTA | ygr040w knockout dn45 | This work |

Chapter 4

# Mapping the Genetic Architecture of the Adaptive Integrated Stress Response in *S. cerevisiae*

## 4.1 Abstract

The Integrated Stress Response (ISR) is a conserved eukaryotic signaling pathway that responds to diverse stress stimuli to restore cellular proteostasis. Adaptive responses require that cells respond differently depending on the strength of the stress stimulus. To explore the dynamics underlying adaptive responses, we investigated the genetic architecture underlying ISR dynamics in *S. cerevisiae* using a high-throughput, CRISPRi-based approach. We measured the strength and speed of ISR adaptation following treatment with sulfometuron methyl, a titratable inhibitor of branched-amino acid synthesis. We measured ISR dynamics using a reporter derived from the *PCL5* native promoter and profiled how ISR dynamics change in response to a subset of guides that we previously demonstrated to affect the ISR. Perturbations to translation such as depletion of aminoacyl-tRNA synthetases or tRNA biogenesis factors reduced cell growth and caused a strikingly proportionate activation of the ISR activation. In contrast, impaired ribosome biogenesis reduced basal ISR activity and weakened ISR dynamics. We followed-up on exploring ribosome biogenesis factors as important regulators of the ISR, highlighting the interplay between ribosome biogenesis and ISR dynamics. Our work provides insight into the genetic regulation of the adaptive nature of the ISR to further understand how eukaryotic cellular stress responses are regulated.

## 4.2 Introduction

The Integrated Stress Response (ISR) is a conserved, adaptive signaling pathway that responds to translational stresses to maintain or restore cellular proteostasis (A G Hinnebusch 1984). Classically, this response is triggered by increased levels of uncharged tRNAs, although we and others have found that other translational defects including ribosome collisions and tRNA insufficiency can also trigger the ISR (Muller et al. 2020; Ishimura et al. 2014; Wu et al. 2020). ISR activation leads to the inhibitory phosphorylation of the translation initiation factor eIF2α, which reduces overall translation, and induction of the transcription factor Gcn4, which drives adaptive gene expression (Alan G. Hinnebusch 2005). Historically, the ISR has been studied by treating cells with lethal challenges. However, the ISR, like most stress response pathways, has evolved to enable adaptation to sublethal challenges. This adaptation depends on the strength and timing of ISR activation.

To interrogate how the dynamic response of the ISR is genetically encoded, we used a high-throughput, CRISPRi-based approach to map how genetic perturbations affect the ISR under different conditions. By using a titratable inhibitor of amino acid biosynthesis, sulfometuron methyl (SM), we were able to track ISR adaptivity. We used a reporter-based CRISPRi screen, CiBER-seq (Muller et al. 2020), to profile ISR activation across different SM doses and treatment times. We observed genetic perturbations that shifted ISR dynamics based on dose sensitivity, alterations to adaptation after prolonged exposure, and alterations to ISR induction at early timepoints.

Recent work has demonstrated that peroxisomal stress in humans and fruit flies concurrently increase the ISR while decreasing ribosome biogenesis (J. Kim et al. 2024). Other work in *S. cerevisiae* has highlighted the acute loss of proteostasis stemming from disrupting ribosome biogenesis (Tye et al. 2019). In our own work, we found that perturbing ribosome biogenesis genes had a negative effect on cellular fitness and shifted ISR dynamics in a dose-dependent manner. Decreased ribosome levels and increased demand for amino acids after a high dose of SM treatment led to increased ISR activation. Our work highlights the importance of ribosome biogenesis in reshaping ISR dynamics.

## 4.3 Methods

*Yeast Strains*

Strains used in this study are listed in Table 4.1. Strains were derived from *S. cerevisiae* BY4741 using standard genetic techniques and CRISPR-Cas9 technology (Lee et al. 2015). Yeast transformations were carried out using standard LiAc/PEG protocol and grown at 30℃ (Gietz and Schiestl 2007). Strain with dCas9-Mxi, TetR, and attP genomic landing pad was previously validated in (Lobel and Ingolia 2024; Muller et al. 2020).

The gRNA validation strains made were either made by integration using the Bxb1 recombinase system or integration into the X-4 locus with NotI-linearized vector using the Easyclone 2.0 vector genomic integration system (Matreyek et al. 2020; Matreyek, Stephany, and Fowler 2017; Durrant et al. 2023; Lobel and Ingolia 2024; Stovicek et al. 2015). All strains used for CiBER-seq screen and gRNA validation experiments were prototrophic and grown in minimal media. Minimal media composition: Yeast nitrogen base without amino acids (Thomas Scientific #C994M99) + 2% dextrose.

*Plasmids*

Plasmids used in this study are listed in Table 4.2. Divergent promoter reporter plasmids with guides were made using a standard Gibson cloning protocol and NEB HiFi assembly (NEB #E2621L) (Gibson et al. 2009). Individual guide plasmids in Easyclone vectors were made using standard Gibson cloning into Easyclone 2.0 vectors with NEB HiFi assembly (Gibson et al. 2009). Plasmids were validated with whole plasmid sequencing performed by Plasmidsaurus using Oxford Nanopore Technology with custom analysis and annotation.

*Library guide choice*

Script for picking guides for this CiBER-seq screen is available upon request. Guides were mostly chosen from previous screens of *HIS4*, *MET6* or *ARO10* reporters based on the strength of response and significance value. A small number of guides were handpicked. Six negative control guides targeting the *HO* endonuclease. In total there are 224 guides targeting 185 distinct genes. Guide sequences are listed in Table 4.4.

We excluded following up on some guides based on our analysis of the GC content of the spacer sequence. GC content is a factor that is correlated with cleavage efficiency, with

spacer sequences requiring an optimal GC content of 40-60% (Konstantakos et al. 2022). Lower GC content is indicative of more off-target effects. There were some spacer sequences in our library of guides that fell below this threshold, therefore we avoided following-up on any guides where the GC% is below 25% (Figure S4.1D). GC content for each guide is listed in Table 4.4.

*Library construction*

We setup the dual guide library using four sub-pools (P, Q, R, and S) of guide pairs. We generated separate libraries for each of the four sub-pools and transformed them separately into yeast. P had 87,000 barcodes for 14,000 guide pairs; Q had 30,000 barcodes for 12,000 guide pairs; R had 42,000 barcodes for 12,000 guide pairs; and S had 49,000 barcodes for 10,000 guide pairs.

We cloned the divergent P(*UBC6*)-mScarlet and P(*PCL5*)-citrine reporters into the barcoded libraries in four separate pools. For the barcoded-libraries, we digested 2 µg with BsmBI-v2 (NEB #R0580) overnight at 44℃. For reporter vector (pNTI929), we digested 2.7 µg with BsmBI-v2 (NEB #R0580) overnight at 44℃. The digested barcoded-libraries and reporter constructs were purified with the Zymo clean and concentrator kit (Zymo #D4004) according to the manufacturers protocol. We performed a HiFi assembly (NEB #E2621L) with 150 fmole of the digested barcoded-libraries and 304 ng of the digested reporters at 50℃ for 1 hour. This reaction was purified with the Zymo clean and concentrator kit (Zymo #D4004) and eluted in 6µl of water. Each of these assemblies was electroporated by adding 2 µl of the Gibson assembly into 2 x 25 µl MegaX DH10B T1R Electrocomp cells (Thermo Fisher #C640003) according to the manufacturer's protocol. Cells were recovered by adding 975µl of SOC media and shaken at 37℃ for 1 hour. Serial dilutions of transformations were plated to ensure sufficient library diversity (>100 unique transformants for each barcode). Culture was transferred into 400 mL LB-Kan and grown overnight to final $OD_{600}$ of 1.8-2.5. Transformation efficiencies ranged from $3.1x10^7$ – $1.0x10^8$. Each of the CiBER-seq libraries were purified using Qiagen HiSpeed midiprep kit (Qiagen #12143).

*CiBER-seq screen*

Plasmid libraries were transformed separately into NIY539 using standard lithium acetate transformation (Gietz and Schiestl 2007). Yeast strain with attP landing pad was grown overnight to saturation in YEPD. Yeast was back-diluted to $OD_{600}$ 0.1 into 1L YEPD. Cells were grown up for 5.5 hours to mid-log phase ($OD_{600}$ 0.5 - 0.7). Cells were washed 3x with water, spun at 3000g/5min. Using LiAc/Peg transformation protocol, 20µg of each CiBER-seq library was transformed and heat shocked at 42℃ for 40 minutes, mixing by inversion every 5 minutes. Cells were spun at 3000g/5min and resuspend in 2 mL SCD -URA media. Serial dilutions were used to ensure sufficient library diversity (≥10X coverage of library unique barcodes). Culture was transferred to 450 mL 1X SCD -URA media and grown at 22℃ until $OD_{600}$ of ~1.0. After reaching target density, 90 OD units of library P, 30 OD units of library Q, 40 OD units of library R, and 50 OD units of library S were harvested by centrifugation and stored at -80℃ in YEPD + 15% glycerol. Transformation efficiencies ranged from $3.0x10^5$ – $2.4 x 10^6$.

CiBER-seq experiments are usually carried out in a continuous-culture turbidostat, but due to volume limitations and the rapid nature of the stress experiment, we modified this protocol to use batch culture instead (Muller et al. 2020; McGeachy, Meacham, and Ingolia 2019). Yeast populations transformed with plasmid libraries were inoculated in a pooling ratio that matches the barcode ratio of 9P:3Q:4R:5S for a total of 200 OD units. Harvested pellets were combined, spun at 3000g/3min, washed in 10 mL minimal media and then resuspended in 5 mL minimal media. Cells were added into 200 mL prewarmed minimal media and grown for 5 hours until $OD_{600}$ of ~1.5 - 2. Cells were back-diluted to $OD_{600}$ of 0.05 for 5.5 hours until OD ~0.1 – 0.15. Pre-induction cells were harvested by centrifuging 50 mL culture at 3000g/5min and stored at -80℃. Cells were back-diluted to $OD_{600}$ of 0.05 in minimal media with 500 ng/mL tetracycline to induce guides. After cells reach target $OD_{600}$ of 0.7, post-induction cells were harvested. Cells were divided into two flasks and treated with 0.56µM (low dose) or 14µM of sulfometuron methyl (Millipore Sigma #34224). Cells were harvested after .25 hours, 1 hour, and 4 hours of treatment.

RNA barcodes were isolated using amended protocol from (Ares 2012). Cell pellets were resuspended in 400µl AE buffer (50 mM NaOAc, pH5.2, 10 mM EDTA), 40 µl 10% SDS, and 400µl Phenol:Chloroform:Isoamyl alcohol (Fisher Scientific #bp1752i-100) and then incubated on a thermomixer at 65℃/15min/2000rpm. Samples were incubated on ice for 5 minutes. Samples were centrifuged at 14000rpm/4℃/5min. We added 400µl of chloroform to aqueous phase, shaken, centrifuged at 14000rpm/4℃/5min (repeat step 2x). The aqueous phase was transferred to a new tube, we added 50µl of 3M NaOAc, 1µl glycoblue (Invitrogen #AM9516), and 100% ethanol until tube was filled. Tubes were mixed by inversion, centrifuged 14000rpm/4℃/20min. Supernatant was removed, pellet was washed with 70% ethanol, centrifuged 14000rpm/4℃/5min and supernatant was removed again. The pellets were air dried for 5 minutes and resuspended in water.

We treated 20 µg of RNA with Turbo DNase (Thermo Fisher Scientific #AM2239) for 30 minutes at 37℃. RNA was cleaned up with RNA clean and concentrator kit (Zymo #R1017) according to the manufacturers protocol and eluted in 30µl water. 4 µg was reverse transcribed using ProtoScript II reverse transcriptase (NEB #M0368L) and 0.25µM gene-specific priming (P(*UBC6*)-mScarlet: NI-1267; P(*PCL5*)-citrine: NI-1268) according to manufacturers protocol. Reaction volume scaled up to account for input (x20 reactions). RT reaction was carried out at 42℃/1hour and 80℃/5min. RT reactions were purified using Zymo clean and concentrator kit (Zymo #D4004) with 7:1 protocol for ssDNA. Round I PCR was performed using Q5 High-Fidelity 2X Master Mix (NEB #M0492S) with primers NI-1272/NI-1273 for the citrine reporter and NI-1271/NI-1273 for the mScarlet reporter. Primers are listed in Table 4.3. The PCR was scaled up to 20 reactions and run 7 cycles for citrine amplicons and 10 cycles for mScarlet amplicons with Tm 68℃. The PCR reaction was purified using the Zymo clean and concentrator kit (Zymo #D4004) with 5:1 protocol and eluted in 15µl water. We quantified the first round PCR product by qPCR using primers NI-827/NI-828 and a diluted series of a standard. We did the second round of PCR using 1000 pM of PCR-I product for 7 cycles with dual indexes (provided by UCSF CAT). Libraries purified using the Zymo clean and concentrator kit (Zymo #D4004) with 5:1 protocol. Samples were quantified using Qubit 1X dsDNA HS Assay Kit (Thermo Scientific #Q33230) and Agilent Tapestation 2200 instrument. Libraries were pooled and concentrated using PCR Cleanup Beads (UCB DNA Sequencing Facility). Libraries were sequenced

Following step-1 PCR, samples were purified by spin column and eluted in 50 µL water. Half the elution was used as input for step-2 PCR with Illumina-compatible dual index primers containing unique dual indexes (provided by UCSF CAT), using 8 cycles for the CL1-YFP sample and 7 cycles for all other transcripts. Amplicons were then purified using AMPure XP beads (Beckman Coulter, A63882) using a 1:1 bead:PCR ratio, washed once with 180 µL 80% EtOH and eluted in 15 µL water. Samples were quantified using qPCR using DyNAmo HS SYBR Green qPCR (ThermoFisher, F410L) on a Stratagene Mx300P instrument, pooled, and further analyzed by automated electrophoresis using an Agilent Tapestation 2200. Pooled libraries were sequenced on an Illumina Novaseq-X with paired-end 150 basepair reads.

Sequencing reads were trimmed using cutadapt to remove Illumina adapter sequences (Martin 2011). Samtools software was used to process and prepare the alignment and reads were counted using HTSeq-count (Li et al. 2009; Anders, Pyl, and Huber 2015). Differential expression analysis was performed with DESeq2 (Love, Huber, and Anders 2014).

*Growth Assays*

Cells were grown overnight in minimal media to saturation. Cells were back-diluted to 0.2 and grown to mid-log phase (typically 5 mL culture at $OD_{600}$ 0.5 - 1.0), and then further back-diluted to $OD_{600}$ 0.01 in triplicate in a 96-well plate. For SM dose response curve, SM was added to cells upon plate setup. For tetracycline dose response curve, tetracycline was added to cells upon plate setup. Absorbance measurements at $OD_{595}$ were taken every 15 minutes, with shaking in between measurements, and temperature maintained at 30°C (Tecan SPARK Multimode Microplate Reader). Growth rates were fit using the R package 'growthcurver' (Sprouffske and Wagner 2016).

*RT-qPCR*

For guide validation, cells were grown to saturation overnight in minimal media. Cells were back-diluted to $OD_{600}$ of 0.1 until it reaches mid-log phase ($OD_{600}$ 0.5-0.8). Cells are back-diluted to $OD_{600}$ of 0.025 for 5mL culture without tetracycline and 60 mL culture with 500 ng/mL tetracycline. After ~17.5 hours, 5 mL culture without tetracycline is harvested as pre-induction sample and 5 mL culture with tetracycline is harvested as post-guide induction sample. 25mL culture is split into two pre-warmed flasks and one flask is treated with low dose SM (0.56µM) and one flask is treated with high dose SM (14µM). Cells from each treatment dose are collected at .25 hours, 1 hour, and 4 hour timepoints.

RNA was extracted from cell pellets using phenol/chloroform method in (Ares 2012). Complementary DNA was synthesized using ProtoScript II reverse transcriptase (NEB #M0368L) and oligo $d(T)_{23}VN$ according to manufacturers protocol. Quantitative PCR was conducted using the Luna universal qPCR master mix (NEB #M3003L) and the primers listed in Table 4.3 (BioRad-CFX96 qPCR System instrument).

*Sucrose Gradients*

Cells were grown to mid-log phase in a volume of at least 150 mL ($OD_{600}$ ~0.5 - 1.0). Cells were harvested by vacuum filtrated with 0.45 µM Whatman cellulose nitrate membrane filters (Fisher Scientific #09-744-75). Yeast cells were immediately scraped off with a pre-chilled metal spatula and plunged into a conical tube with holes poked into the cap and filled with liquid nitrogen. Drip 2 mL of freshly prepared ice cold polysome buffer (20 mM Tris-HCl pH 7.4, 150 mM NaCl, 5 mM MgCl2, 1 mM DTT, 1% Triton X-100, .02 U/µl Turbo DNase) into conical tube with cells so that it forms droplets. Store conical tubes in -80℃ overnight.

Frozen yeast and polysome buffer were lysed by cryogrinding with the MM400 Mixer mill (Retsch #20.745.0001). Cryogrinding yeast for six cycles of 3 minutes at 15 Hz. The powder was moved from the grinding chamber using a pre-chilled metal spatula into a conical tube with holes poked into the cap, filled with liquid nitrogen. Store conical in -80℃ overnight. Lysates were thawed slowly on an ice bucket (~2 hours). Lysates were clarified by centrifuging conical tube at 3000g/5min/4℃. Supernatant was transferred to Eppendorf tubes and clarified at 14000rpm/15min/4℃. Supernatant was transferred to Eppendorf tubes. Lysate was quantified by isolating 100µl RNA using a Direct-zol RNA Purification Kit (Zymo #R2060) and treating with TurboDNase for 15 minutes. Clarified lysates were used for sucrose gradients.

Sucrose gradients were prepared using a Gradient Master (BioComp Instruments) using Seton Open-Top Polyclear Centrifuge Tubes (Seton Scientific #7030). Normalized lysates (220µl) were loaded onto a 10-50% sucrose gradient prepared in polysome buffer. Gradients were centrifuged at 35000rpm/3 hours/4℃ in a Beckman SW41 Ti rotor using an XL-70 ultracentrifuge (Beckman Coulter). The sucrose gradients were run through the gradient master system and the absorbance was monitored using a UV monitor (BioRad EM-1 Econo UV monitor). Short density gradients followed the same protocol except using 5-30% sucrose concentrations.

### 4.4 Profiling the adaptive nature of the ISR and selectively screening genetic perturbations that effect these dynamics using CiBER-seq

In budding yeast, the ISR drives adaptive up-regulation of amino acid biosynthesis genes in response to amino acid limitation. The herbicide sulfometuron methyl (SM) is a titratable inhibitor of branched amino acid synthesis that activates the ISR in budding yeast (Jia et al. 2000). Lower doses of SM cause transient ISR activation followed by resumed growth, while high doses of SM lead to persistent ISR activation and growth arrest (Jia et al. 2000). Indeed, we found that yeast grown in minimal media showed a dose-dependent growth inhibition upon SM treatment (Figure 4.1A, Figure S4.1A). To measure ISR activation, we developed a reporter using the native promoter of *PCL5*, a strong transcriptional target of the yeast ISR transcription factor Gcn4. We observed a rapid, dose-dependent induction of endogenous *PCL5* that is mimicked by our citrine reporter driven by the *PCL5* promoter (Figure 4.1B). High dose (14 µM) SM treatment led to full ISR activation within 15 minutes that persisted over 4 hours. In contrast, low dose (0.56 µM) SM treatment caused slower ISR activation that gradually declined. This dose-dependent, adaptive response offers a setting to learn how genetic changes alter ISR dynamics.

We then set out to profile how genetic perturbations affect ISR dynamics by using an approach we developed that combines CRISPRi gene knockdown with barcoded expression readout sequencing (CiBER-seq) (Muller et al. 2020). CiBER-seq, and similar techniques, can provide time-resolved measurements of molecular phenotypes, such as ISR reporter expression, across thousands of genetic perturbations in parallel (Muller et al. 2020; Alford et al. 2021). The guide RNAs that induce these genetic perturbations are delivered to cells along with transcriptional reporters that measure their phenotypic effects. The reporter transcript contains a unique, guide-specific barcode sequence. The RNA abundance of each guide-specific barcode reflects the transcription level of the reporter in cells that contain the associated guide. By sequencing and quantifying expressed RNA barcodes, it is possible to measure reporter expression across many different perturbations in a single, bulk sequencing sample. To correct for variation in the number of cells containing different barcodes, we use two distinct reporters delivered together: the *PCL5* ISR reporter along with a reporter based on the *UBC6* promoter, which maintains very consistent expression levels across many different conditions. We have found that comparisons between two different expression reporters yields lower background and less technical noise than normalization of expressed reporter RNA against barcode DNA abundance (Muller et al. 2020; Lobel and Ingolia 2024).

We previously used CiBER-seq to profile ISR activity, along with other reporters for amino acid metabolism, in static conditions. We chose over 200 CRISPRi guides that displayed strong and significant effects in prior screens. A majority of guides were selected based on their effect on the classic ISR target *HIS4* either in unperturbed cells or in cells treated with the ISR activating drug 3-AT, with or without deletion of the ISR signaling kinase Gcn2 (Muller et al. 2020). Additional guides were chosen because of their effect on *MET6*, which encodes a methionine biosynthesis enzyme (Muller et al. 2020). A final set of guides were chosen due to their effect on a reporter for the catabolic enzyme gene *ARO10* (Diamond, McGlincy, and Ingolia 2024). A small number of guides were added by hand, along with six negative control guides targeting the *HO* endonuclease, for an overall set of 224 guides targeting 185 distinct genes (Figure 4.1C).

To profile a broader range of perturbations and identify genetic interactions in the ISR, we created a library of pairwise combinations between these guides. Expressing two different CRISPRi guides in the same cell yields strong knockdown of both targets. Importantly, our dual-guide library provided measurements of single-guide phenotypes by pairing each guide with one of several negative controls with no effect. With 224 guides and two guide pairs, we screened 24,976 guide pairs.

We delivered our dual-guide CiBER-seq library into a yeast strain engineered to facilitate ISR dynamics measurements. Budding yeast is naturally prototrophic for amino acids, but common laboratory strains were rendered auxotrophic to facilitate selective growth. We were concerned that amino acid auxotrophies would distort the ISR, and so we created a strain that would be fully prototrophic in the context of our CiBER-seq library. This strain also expressed the CRISPRi effector (dCas9-Mxi) and the tetracycline repressor (TetR) to provide tetracycline-inducible guide RNA expression. Finally, it contained a genomic “landing pad” that enables high-efficiency genomic integration mediated by the serine recombinase Bxb1. Integration of plasmids from the guide library into this landing pad reconstitutes a split *URA3* marker cassette,

allowing selection for integrants and restoring full prototrophy to the strain. We carried out four independent integrations and collected $3.0x10^5$ – $2.4 \times 10^6$ independent transformants.

The transformed populations were grown in minimal media and treated with tetracycine to induce guide expression. We sampled cells before guide expression and then 17.5 hours after guide induction. Each of the cultures were divided in half and treated with either a low dose or high dose of SM. We took samples 0.25 hours, 1 hour, and 4 hours after SM addition. We extracted RNA from each sample, created barcode sequencing libraries from 4 µg RNA per sample, and sequenced the barcode libraries (Figure 4.1D). We also quantified *PCL5* reporter expression in our libraries by RT-qPCR (Figure S4.1C). We saw substantial ISR activation even prior to SM treatment, which likely reflects the fact that a large fraction of guides in our library activate the ISR in the absence of external stress.

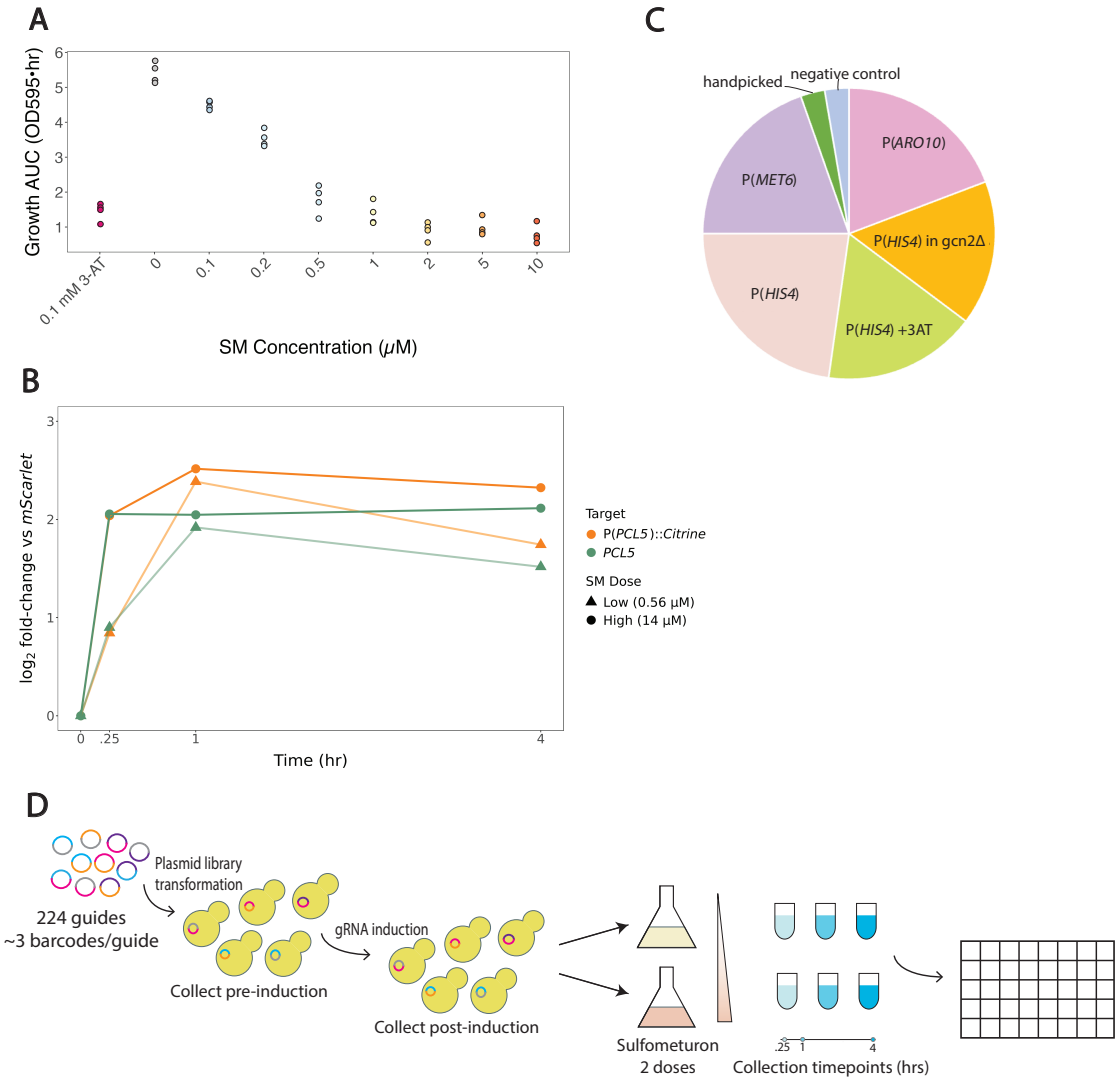

**Figure 4.1: Sulfometuron methyl titratable response and CiBER-seq screen setup (A)** Growth AUC (Area Under Logistic Curve) reflects relative growth rate for fitted growth curves for cells maintained in 3-AT or SM. **(B)** RT-qPCR for cells treated with low SM dose (●) or high SM dose (▲) for 0, .25, 1, or 4 hours, normalized to P(*UBC6*)::mScarlet reporter. Endogenous *PCL5* expression shows dose and time-dependent effect. P(*PCL5*)::Citrine reporter expression shows similar dose and time-dependent effect. **(C)** Pie chart of prior CiBER-seq screens guides were chosen from; guides were chosen based on their strength and significance in these screens. **(D)** Schematic of CiBER-seq screen setup. We integrated plasmid libraries containing guides into yeast using a *Bxb1* integrase system. We collected the pre-guide induction sample; induced guides with 500 ng/mL tetracycline and collected post-guide induction sample. The culture was divided into two flasks for treatment with low SM dose or high SM dose and cells were collected at 0.25, 1, or 4 hours post-treatment. ISR dynamics were mapped by DESeq2 analysis.

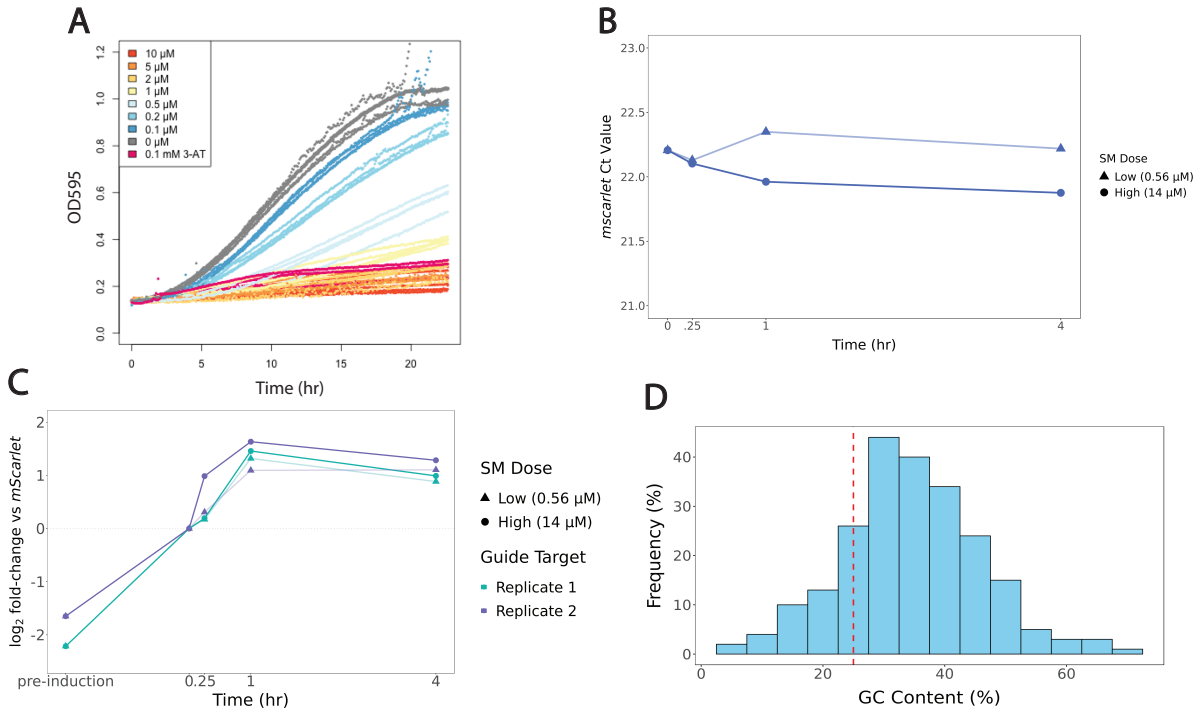


**Figure S4.1 Additional pilot data (A)** Raw data growth curves from Figure 4.1A **(B)** RT-qPCR for mScarlet normalizer reporter shows minimal variability in Ct values for low SM dose (●) or high SM dose (▲) treated cells after 0, .25, 1, or 4 hours. **(C)** RT-qPCR of ISR reporter normalized to mScarlet for CiBER-seq libraries. Two biological replicates for low and high dose SM treatment. **(D)** Histogram of percentage of GC content in 224 CiBER-seq spacer sequences. Dashed line represents 25% cutoff mark; spacer sequences that fell below this threshold were not followed-up on due to increased likelihood of off-target effects (Konstantakos et al. 2022).

## 4.5 Analysis of CiBER-seq screen to identify time-sensitive or dose-sensitive changes in ISR dynamics

We analyzed sequencing data to infer ISR activity and growth phenotypes for each individual genetic perturbation. Guide RNAs that change cell growth will lead to differences in the number of cells harboring that guide RNA, which will in turn change the abundance of the normalizer barcode driven by the housekeeping *UBC6* promoter. Guide RNAs that increase ISR activity will cause higher levels of the *PCL5* reporter barcode, relative to the matched *UBC6* barcode; guides that decrease ISR activity will lower the relative barcode levels. We inferred these ISR activity and growth rate jointly at all timepoints in a general linear modeling framework, combining all barcodes for a given genetic perturbation by weighted averaging.

The growth and ISR activity phenotypes we measured after guide induction but prior to SM treatment replicated known features of the yeast ISR. Most notably, many genetic perturbations that compromised protein synthesis by reducing the availability of charged tRNA led to slower growth and ISR activation (Figure 4.2A). Knockdown of aminoacyl-tRNA synthetases (AARS), components of RNA polymerase III (which transcribes tRNAs), and subunits of the tRNA processing enzyme RNase P all showed this effect, along with knockdown of proteins comprising the translation initiation factors eIF2 and eIF2B. There was a striking correlation between ISR activation and growth defect, suggesting that steady-state ISR activity directly tracks the extent to which protein synthesis limits cell growth (Figure 4.2A). The only exception to this trend was *PCL5*, which encodes a negative feedback regulator of the ISR transcription factor Gcn4. Knockdown of *PCL5* activates the ISR without causing a growth defect, presumably by reducing this feedback loop. Importantly, this *PCL5* guide does not affect our ISR reporter, which is based on the *PCL5* promoter. Our library included a second *PCL5* guide that does target the reporter itself as well as the endogenous *PCL5* gene, and strongly reduces reporter expression.

In contrast, many guides reduced basal ISR activity, with varying effects on growth. Consistent with our earlier CiBER-seq experiments, we saw that knockdown of proteasome components reduced ISR activity (Figure 4.2B). Likewise, guides targeting subunits of the ARP2/3 complex, an essential actin regulator, reduced cellular fitness and decreased basal ISR signaling (Figure 4.2C). Guides targeting ribosome biogenesis (RiBi) genes mostly grouped together, led to cellular defects and decreased basal ISR signaling due to the lack of ribosome availability (Figure 4.2D). More broadly, guides targeting functionally related genes tended to show similar phenotypes (Figure S4.2A). We next analyzed the single-guide ISR phenotypes across timecourses of SM treatment at two different doses. The similarity of dynamic ISR phenotypes between different guides targeting the same gene and between guides with shared function was quite strong.

We were interested in identifying genetic perturbations that change the dynamics of ISR activation. While most genetic perturbations showed a proportionate response to high-dose SM treatment between 0.25 hour and 1 hour, we noticed that several guides targeting ribosome biogenesis factors deviate from this trend and have increased ISR activation at the 1 hour timepoint (Figure 4.2E). Comparison between low and high SM doses at each individual timepoint also demonstrate that most guides show a proportionate response, although more guides lead to dose-dependent differences with increasing length of treatment time. Guides

targeting ribosome biogenesis factors again stand out in this comparison, with increased ISR activation at a high SM dose relative to a low SM dose at every treatment timepoint, with the activation increasing over treatment time (Figures 4.2F-H). Guides targeting the proteasome show a similar, albeit weaker, trend.

We also analyzed dual-guide phenotypes and found that they generally fall within the range delineated by the single guides. In particular, many guide pairs cause proportionate ISR activation and fitness defects (Figures S4.2B,C). We will present further analysis of these pairwise perturbations elsewhere.

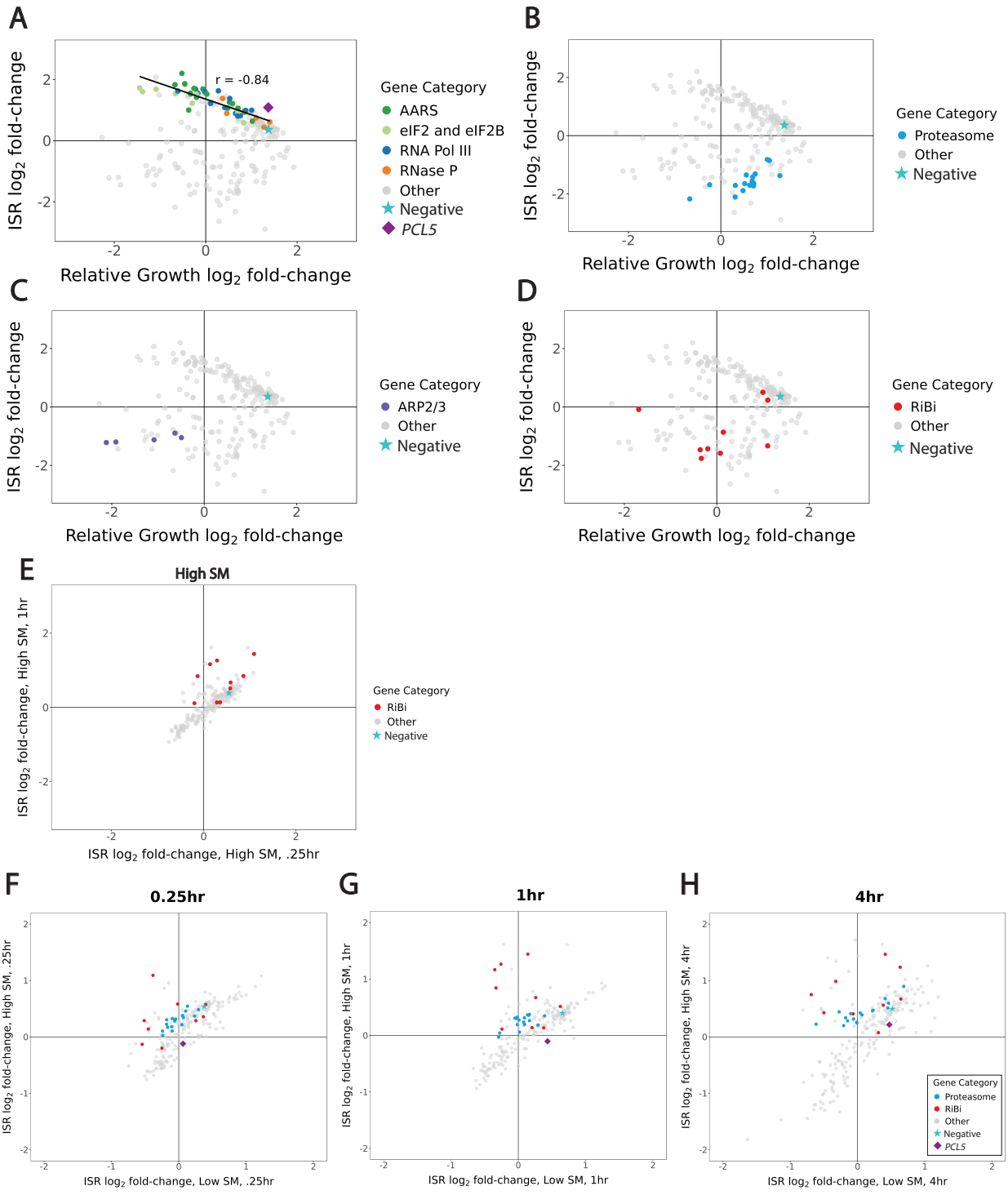
A
r = -0.84
ISR log2 fold-change
Relative Growth log2 fold-change
Gene Category
AARS
eIF2 and eIF2B
RNA Pol III
RNase P
Other
Negative
PCL5
B
ISR log2 fold-change
Relative Growth log2 fold-change
Gene Category
Proteasome
Other
Negative
C
ISR log2 fold-change
Relative Growth log2 fold-change
Gene Category
ARP2/3
Other
Negative
D
ISR log2 fold-change
Relative Growth log2 fold-change
Gene Category
RiBi
Other
Negative
E
High SM
ISR log2 fold-change, High SM, 1hr
ISR log2 fold-change, High SM, .25hr
Gene Category
RiBi
Other
Negative
F
0.25hr
ISR log2 fold-change, High SM, .25hr
ISR log2 fold-change, Low SM, .25hr
G
1hr
ISR log2 fold-change, High SM, 1hr
ISR log2 fold-change, Low SM, 1hr
H
4hr
ISR log2 fold-change, High SM, 4hr
ISR log2 fold-change, Low SM, 4hr
Gene Category
Proteasome
RiBi
Other
Negative
PCL5

**Figure 4.2: DESeq2 analysis of single mutants show dynamic ISR phenotypes (A-D)** Scatterplots show guides targeting functionally related genes have similar phenotypes; ISR $log_2$ fold-change versus growth $log_2$ fold-change after guide-induction **(A)** Guides targeting eIF2 and eIF2B, aminoacyl-tRNA synthetases (AARS), RNA Pol III, and RNaseP components proportionately slow growth and reduces ISR activation. Solid line represents correlation between these guides (r =-0.84). Negative guide (⋆) is used as a reference point for growth and ISR effects. *PCL5* targeted guide (◆) activates the ISR without causing a growth defect. **(B)** Knockdown of proteasome components reduces ISR activity. **(C)** Guides targeting subunits of the ARP2/3 complex reduced cellular fitness and decreased basal ISR signaling. **(D)** Guides targeting Ribosome Biogenesis (RiBi) factors mostly grouped together and led to slower growth and reduced ISR activation. **(E)** Scatterplot of high SM treated cells .25hr versus 1hr shows increase in ISR expression; guides targeting RiBi genes increase ISR activation after 1 hour treatment. **(F-H)** Scatterplots of low versus high dose for each timepoint of SM treatment. Guides targeting ribosome biogenesis increase activation at high SM dose relative to low SM dose at each timepoint. Activation increases over treatment time. Guides targeting proteasome components show a similar but weaker ISR activation.

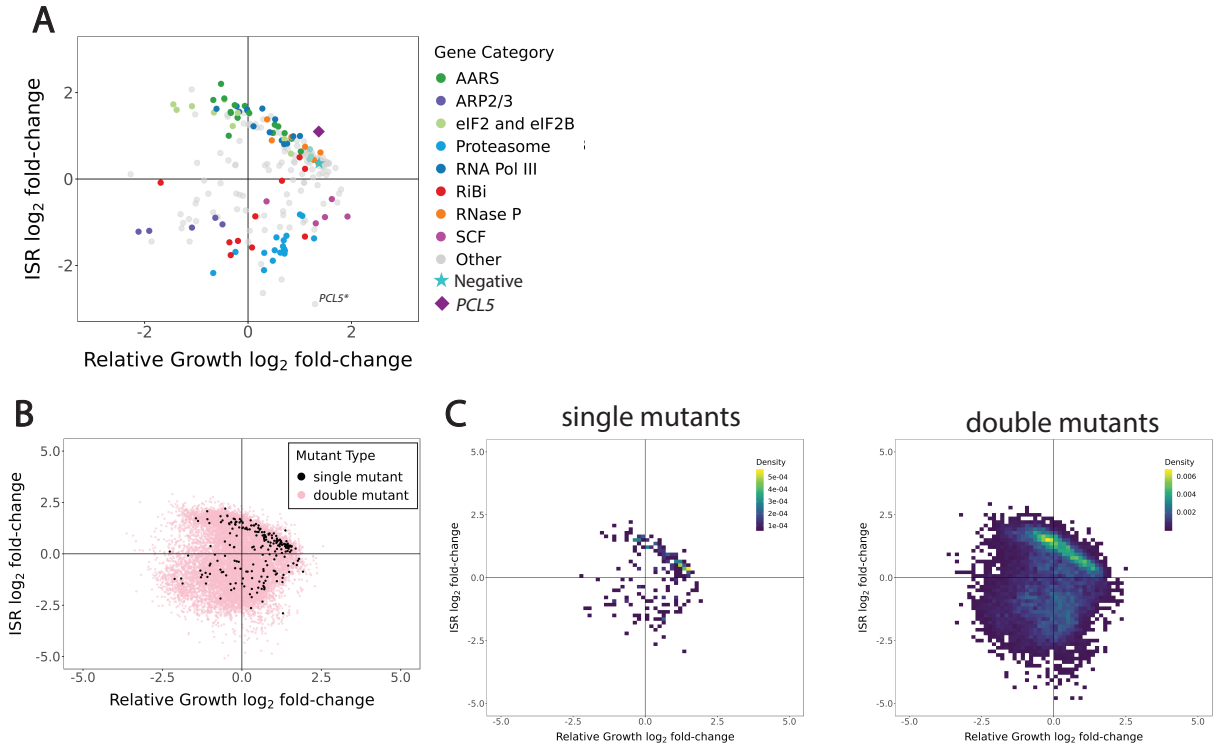


**Figure S4.2: Categorized single mutant analysis and double mutant analysis (A)** Guides targeting functionally related genes show similar growth and ISR activation phenotypes after guide-induction. **(B)** Dual-guide phenotypes (pink) and single-guide phenotypes (black) from DESeq2 analysis **(C)** Single-guide (left) and double-guide density plots (right) show similar density patterns within the range of the single-mutant phenotypes. Many guides activate the ISR and cause cellular fitness defects in a proportionate way.

### 4.6 Ribosome biogenesis transcripts *RRP42* and *PNO1* regulate the ISR in a dose-dependent manner

While we observed a wide range of ISR activity phenotypes, knockdown of ribosome biogenesis factors stood out for changing ISR dynamics in a dose- and time-dependent manner. We wished to understand the basis for this distinctive phenotype. Perturbations of ribosome biogenesis genes *RRP40*, *RRP42*, *RRP45*, *PNO1* and *CBF5* led to similar fitness defects and reduction in basal ISR activity (Figure 4.3A). We validated the effect of *RRP42* knockdown levels on cell fitness by titrating the concentration of tetracycline which regulates the knockdown level. Knockdown efficiency had an inverse relationship with the growth rate, highlighting the importance of the ribosome biogenesis factor *RRP42* in maintaining cell fitness (Figures S4.3A,B). ISR activity remained low when yeast were exposed to low doses of SM, but high doses led to strong but delayed ISR activation (Figure 4.3B). *RRP40*, *RRP42*, and *RRP45* encode components of the RNA exosome, a multifunctional RNA exonuclease that processes pre-rRNAs. *PNO1* and *CBF5* both encode dedicated ribosome biogenesis factors involved in ribosomal RNA processing. We carried out targeted validation experiments to confirm the phenotypes we measured for these guides in our screen. Knockdown of *RRP42* followed SM treatment confirmed that perturbed cells did not greatly activate the ISR after a low-dose SM treatment, but did reach nearly wildtype levels after 1 hour of high-dose treatment (Figure 4.3C and Figures S4.3C,E,G). Knockdown of *PNO1* likewise impaired ISR activation at a low SM dose that is overcome when cells are treated with a high SM dose—surpassing wildtype ISR activation (Figure 4.3D, Figures S4.3D,F,H). Knockdown of *CBF5* showed a similar pattern of weak ISR activity at low SM doses with robust responses at a higher dose (Figures S4.4A-D).

To further characterize how *RRP42* knockdown affects the response to SM, we measured ISR activation at 1 hour across a range of concentrations. *RRP42* knockdown cells show decreased basal ISR activity that does not increase below a threshold of 0.2 μM SM, whereas wildtype cells induce the ISR at these doses. Overall, *RRP42* knockdown cells appear 4–5-fold less sensitive to SM (Figure 4.3E). We observed a similar trend when measuring the endogenous ISR target *HIS4* (Figure S4.3I).

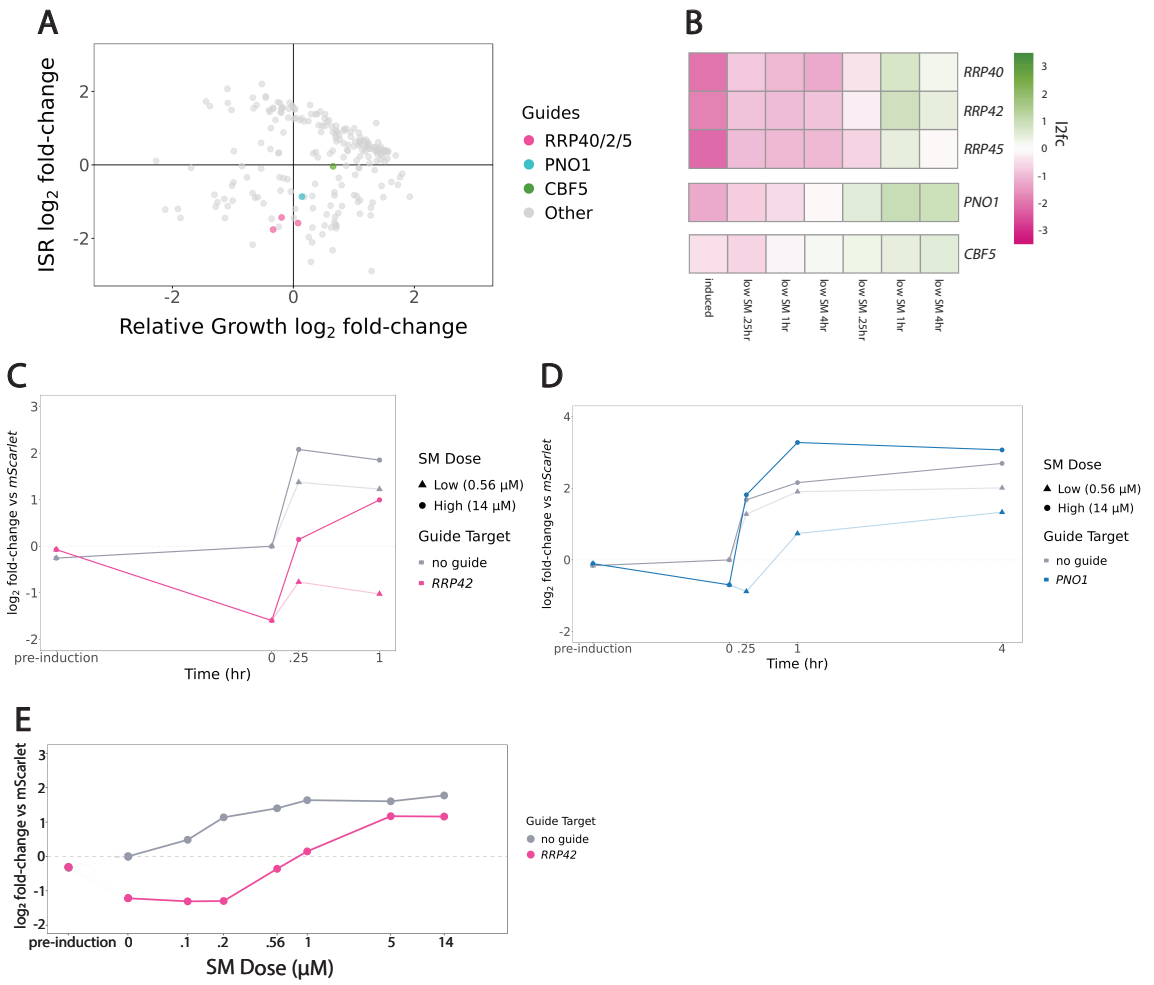


**Figure 4.3: Knockdown of RiBi factors *RRP42* and *PNO1* lead to SM treatment dose-dependent response (A)** Scatterplot highlighting *RRP40/2/5*, *PNO1*, and *CBF5* targeted guides. Guides targeting these RiBi genes slows cell growth and decreases ISR activation. **(B)** Heatmap for *RRP40*, *RRP42*, *RRP45*, *PNO1, and CBF5* mutants shows ISR $\log_2$ fold-change normalized to negative guide reference. Reduced ISR activity after low SM dose treatment; high ISR activity after high SM dose treatment. **(C)** RT-qPCR of ISR reporter for wildtype and *RRP42* knockdown cells, replicate 1. ISR reporter normalized to mScarlet for pre-guide induction, post-guide induction and 0, .25, and 1 hour low or high SM treated cells. Low SM dose reduces ISR activation and high SM dose strengthens ISR activation. **(D)** RT-qPCR of ISR reporter for wildtype and *PNO1* knockdown cells, replicate 1. ISR reporter normalized to mScarlet for pre-guide induction, post-guide induction and 0, .25, 1, and 4 hours low or high SM treated cells. Low SM dose reduces ISR activation and high SM dose strengthens ISR activation. **(E)** RT-qPCR for ISR reporter in wildtype or *RRP42* knock-down cells in pre-guide induction, post-guide induction, and SM treatment doses after 1 hour of treatment. *RRP42* knockdown decreases ISR SM response.

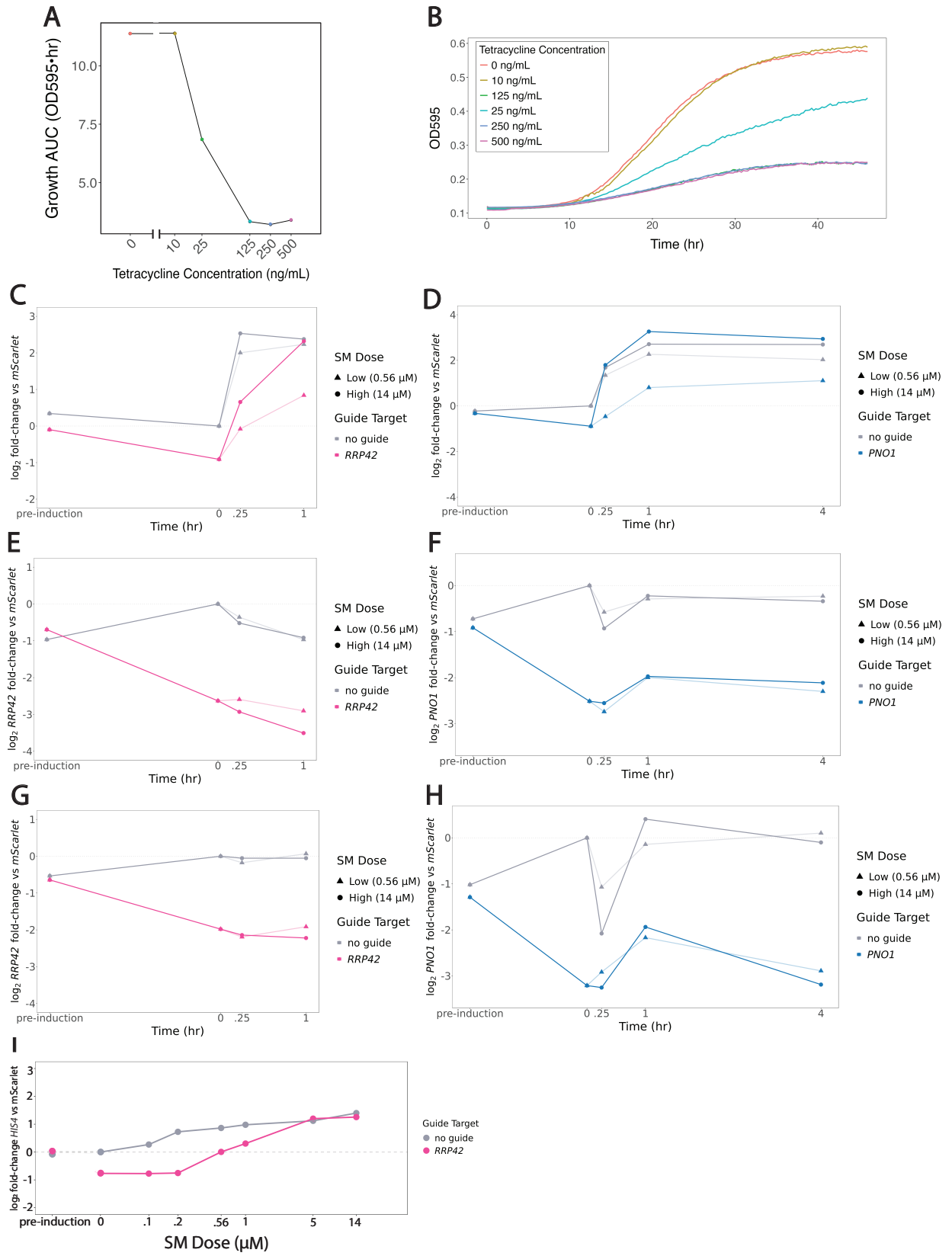


**Figure S4.3: Replicates of *RRP42* and *PNO1* lead to SM treatment dose-dependent response**

**(A**) Growth AUC (Area Under Logistic Curve) reflects relative growth rate for fitted growth curves for tetracycline guide-induction dose response. Growth rate slows with increased knockdown efficiency. **(B)** Raw growth curves from (A). **(C)** RT-qPCR of ISR reporter for wildtype and *RRP42* knockdown cells, replicate 2 of Figure 4.3C. **(D)** RT-qPCR of ISR reporter for wildtype and *PNO1* knockdown cells, replicate 2 of Figure 4.3D. **(E)** RT-qPCR *RRP42* knockdown-efficiency of data from Figure 4.3C **(F)** RT-qPCR *PNO1* knockdown-efficiency of Figure 4.3D. **(G)** RT-qPCR *RRP42* knockdown-efficiency of data from Figure S4.3C. **(H)** RT-qPCR *PNO1* knockdown-efficiency of data from Figure S4.3D. **(I)** RT-qPCR for endogenous *HIS4* target for SM dose response from Figure 4.3E. *HIS4* expression in *RRP42* knockdown cells shows similar decrease to ISR reporter.

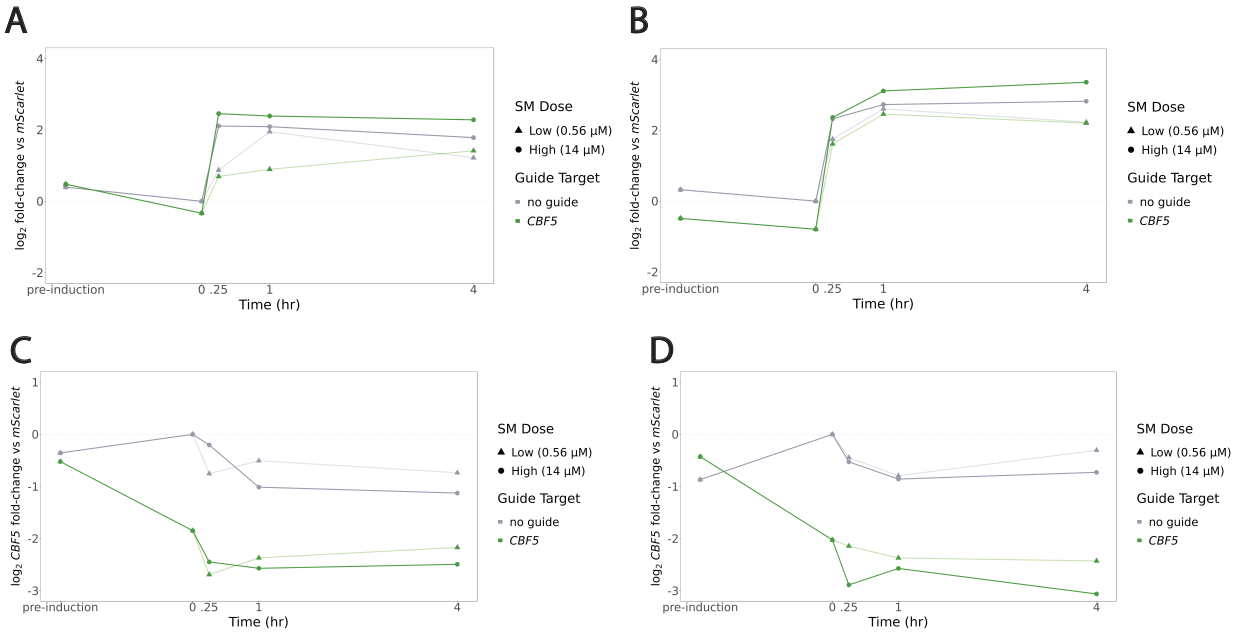


**Figure S4.4: Knockdown of RiBi gene *CBF5* SM dose-dependent effect (A)** RT-qPCR of ISR reporter for wildtype and *PNO1* knockdown cells, replicate 1. ISR reporter normalized to mScarlet for pre-guide induction, post-guide induction and 0, .25, 1 and 4 hour low or high SM treated cells. Low SM dose reduces ISR activation and high SM dose strengthens ISR activation. **(B)** RT-qPCR of ISR reporter for wildtype and *CBF5* knockdown cells, replicate 2 of Figure S4.4B. **(C)** RT-qPCR *CBF5* knockdown-efficiency of data from Figure S4.4A. **(D)** RT-qPCR *CBF5* knockdown-efficiency of data from Figure S4.4B.

## 4.7 Cellular defects in 40S ribosome biogenesis reshape the dynamics of the ISR

To directly measure the impact of *RRP42* and *PNO1* knockdown on translation, we analyzed polysomes in these cells. We generated matched lysates from knockdown and control cells (Figures 4.4A,C) and performed polysome profiling by sucrose density gradient ultracentrifugation. Both *RRP42* and *PNO1* knockdown demonstrated a loss of 40S subunits in comparison with wildtype cells (Figures 4.4B,D). *RRP42* knockdown led to some loss of polysomes and an increase in free 60S subunits (Figure 4.4B). *PNO1* knockdown caused stronger polysome collapse and a dramatic increase in the 60S:80S suggesting reduced overall translation (Figure 4.4D). We validated the loss of 40S subunits on shallower density gradients with better resolution of individual subunits (Figures S4.5A-B).

Since these polysome traces demonstrate that defects in 40S ribosome biogenesis reshape the dynamics of the ISR, we turned to our dataset to understand whether this effect was specific to the small ribosomal subunit. We evaluated guides targeting protein components of the 40S subunit (*RPS2*, *RPS5*, and *RPS28A*) and the 60S subunit (*RPL3*, *RPL25*, *RPL30*, and *RPL32*). In nearly all cases, knockdown of these subunits showed a strong growth defect and mild reduction in ISR activation (Figure 4.4E). Ribosomal protein depletion did not show the same strong ISR dynamics phenotype that we observed from disrupting ribosomal RNA processing. While we do observe that ribosomal protein alters dose-dependent ISR activation at 4 hours, this phenotype is not clearly different between guides targeting the small and large subunits (Figures 4.4F-G). This suggests that this is not a subunit specific response, but more likely a consequence of limited ribosome availability.

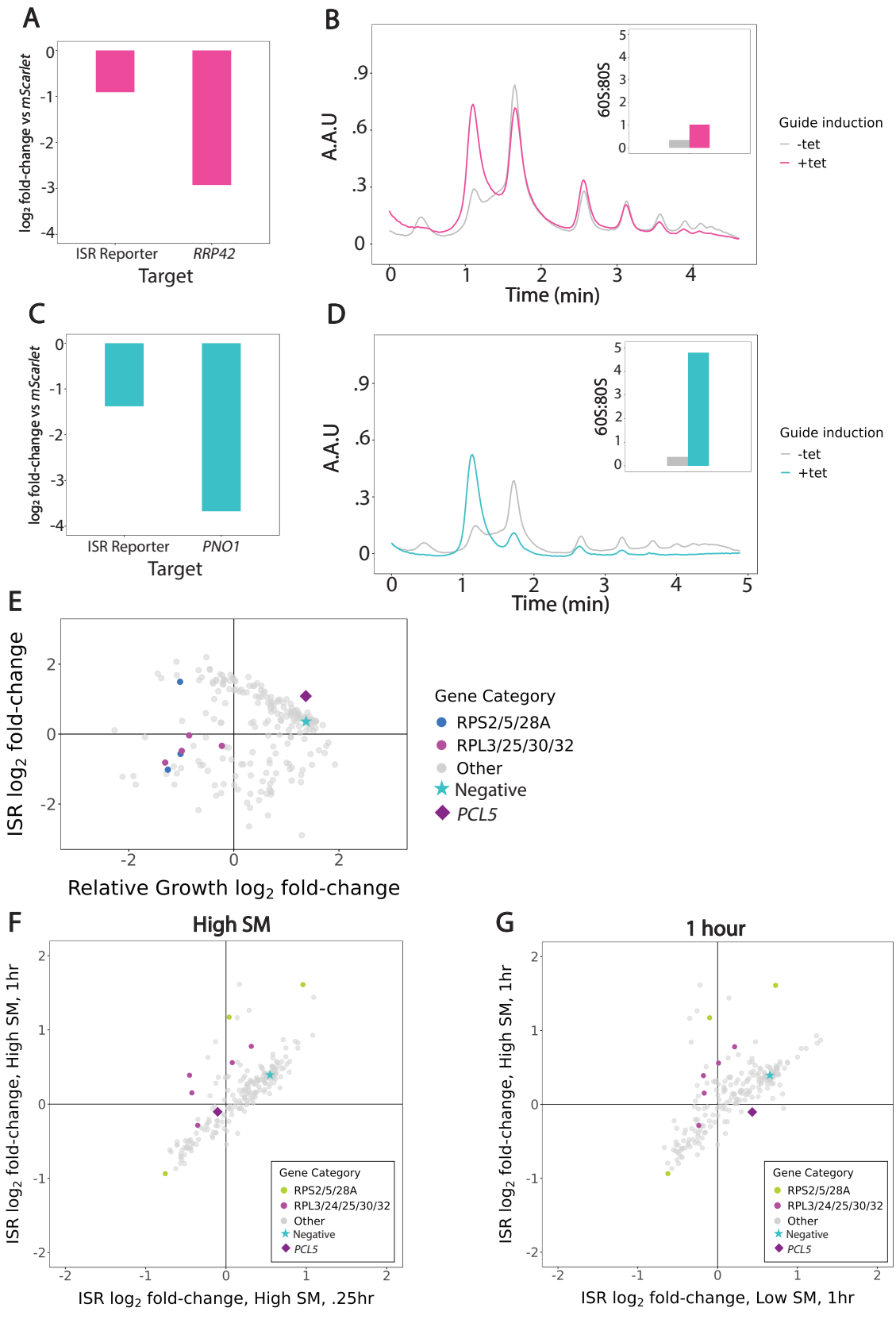
A
log2 fold-change vs mScarlet
0
-1
-2
-3
-4
ISR Reporter
RRP42
Target
B
A.A.U
.9
.6
.3
0
0
1
2
3
4
Time (min)
60S:80S
5
4
3
2
1
0
Guide induction
-tet
+tet
C
log2 fold-change vs mScarlet
0
-1
-2
-3
-4
ISR Reporter
PNO1
Target
D
A.A.U
.9
.6
.3
0
0
1
2
3
4
5
Time (min)
60S:80S
5
4
3
2
1
0
Guide induction
-tet
+tet
E
ISR log2 fold-change
2
0
-2
-2
0
2
Relative Growth log2 fold-change
Gene Category
RPS2/5/28A
RPL3/25/30/32
Other
Negative
PCL5
F
High SM
ISR log2 fold-change, High SM, 1hr
2
1
0
-1
-2
-2
-1
0
1
2
ISR log2 fold-change, High SM, .25hr
Gene Category
RPS2/5/28A
RPL3/24/25/30/32
Other
Negative
PCL5
G
1 hour
ISR log2 fold-change, High SM, 1hr
2
1
0
-1
-2
-2
-1
0
1
2
ISR log2 fold-change, Low SM, 1hr
Gene Category
RPS2/5/28A
RPL3/24/25/30/32
Other
Negative
PCL5

**Figure 4.4: Knockdown of *RRP42* and *PNO1* leads to defects in 40S ribosome biogenesis that reshape the dynamics of the ISR (A)** RT-qPCR data pre- and post-guide induction for *RRP42* knockdown lysate. *RRP42* knock-down reduced ISR reporter expression; *RRP42* shows robust knock-down efficiency. **(B)** 10-50% sucrose gradients in pre and post guide tet-induction in *RRP42* cells. Time (min) versus Absorbance Arbitrary Units (A.A.U). 60S:80S ratio for -/+ knockdown shows increase in ratio after knockdown. **(C)** RT-qPCR data pre- and post-guide induction for *PNO1* knockdown lysate. *PNO1* knock-down reduced ISR reporter expression; *PNO1* shows robust knock-down efficiency. **(D)** 10-50% sucrose gradients in pre- and post guide tet-induction in *PNO1* cells. Time (min) versus Absorbance Arbitrary Units (A.A.U). 60S:80S ratio for -/+ knockdown shows increase in ratio after knockdown. **(E)** Scatterplot highlighting guides targeting small and large ribosomal subunits shows strong growth defect and mild reduction of ISR activation. **(F)** Scatterplot highlighting guides targeting small and large ribosomal subunits after high SM dose treatment at .25hr versus 1hr shows similar dose-dependent ISR effect. **(G)** Scatterplot highlighting guides targeting small and large ribosomal subunits after 1hr low versus high dose SM treatment shows similar time-dependent ISR effect.

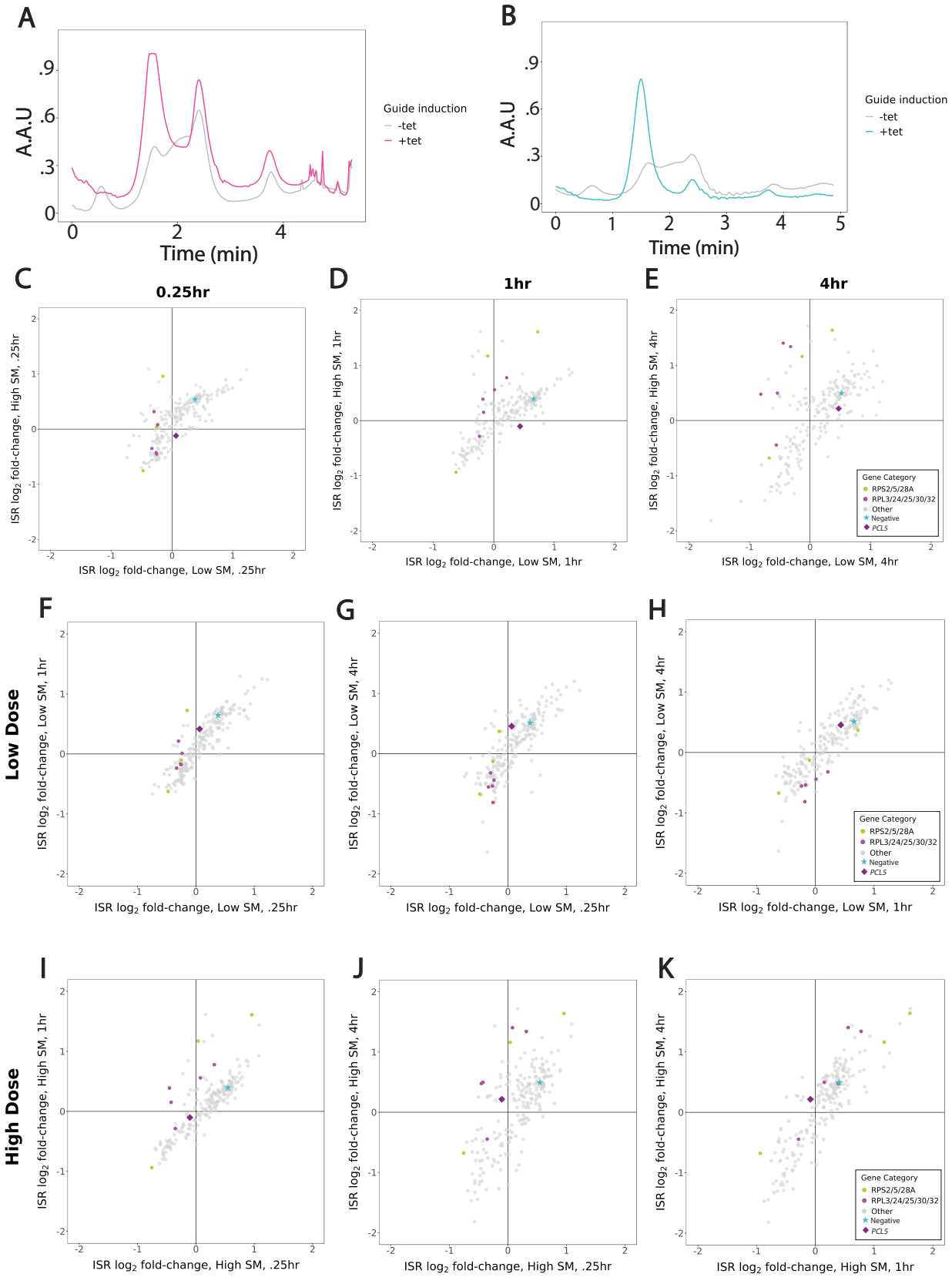
A
A.A.U
Time (min)
Guide induction
-tet
+tet
B
A.A.U
Time (min)
Guide induction
-tet
+tet
C
0.25hr
D
1hr
E
4hr
Low Dose
High Dose
F
G
H
I
J
K
ISR log2 fold-change, High SM, .25hr
ISR log2 fold-change, Low SM, .25hr
ISR log2 fold-change, High SM, 1hr
ISR log2 fold-change, Low SM, 1hr
ISR log2 fold-change, High SM, 4hr
ISR log2 fold-change, Low SM, 4hr
Gene Category
RPS2/5/28A
RPL3/24/25/30/32
Other
Negative
PCL5

**Figure S4.5: Targeting ribosomal genes effects ISR dynamics (A-B)** Short 5-30% sucrose gradients for (A) *RRP42* knockdown and (B) *PNO1* knockdown lysates. **(C-E)** Scatterplots highlighting guides targeting small and large ribosome subunits for low versus high SM treatment dose for (C) .25 hour (D) 1 hour (E) 4 hours. **(F-H)** Scatterplots highlighting guides targeting small and large ribosome subunits for low dose SM treatment (F) .25hr versus 1hr timepoints (G) .25hr versus 4hr timepoints (H) 1hr versus 4 hour timepoints. **(I-K)** Scatterplots highlighting guides targeting small and large ribosome subunits for high dose SM treatment (I) .25hr versus 1hr timepoints (J) .25hr versus 4hr timepoints (K) 1hr versus 4 hour timepoints.

## 4.8 Discussion

We successfully profiled ISR dynamics using CiBER-seq to identify genetic perturbations that regulate the behavior of the ISR. By perturbing 185 genes known to regulate the ISR, we learned how each of these individual genes help shape the dynamics of this response.

We observed a relationship between ribosome levels, amino acid demand and ISR activation. We propose that ribosome levels impact ISR dynamics—ribosome biogenesis mutants decrease the availability of ribosomes, reducing cellular demand for amino acids. At a low SM dose, wildtype cells can maintain amino acid levels by activating the ISR and thereby inducing amino acid biosynthetic genes. In contrast, ribosome biogenesis mutants have weaker demand for amino acids due to lower ribosome availability, leading to weaker and slower ISR activation. At a high SM dose, ribosome biogenesis mutants do become limited for amino acids, which leads to higher ISR activation in a manner similar to that seen in wildtype cells (Figure 4.5).

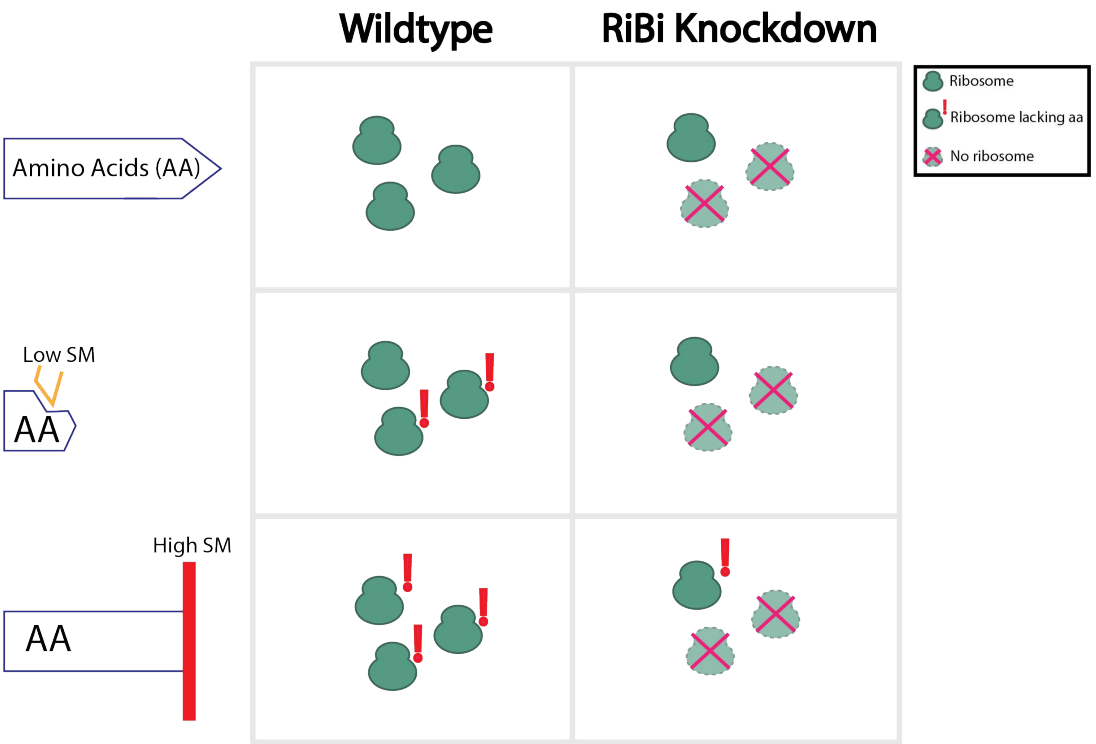

**Figure 4.5: Model of the effect of ribosome levels on reshaping ISR dynamics** Ribosome biogenesis mutants decrease the availability of ribosomes, reducing cellular demand for amino acids. **Low SM dose**: Wildtype cells can maintain amino acid levels by activating the ISR and inducing amino acid biosynthetic genes. Ribosome biogenesis mutants have weaker demand for amino acids due to lower ribosome availability, leading to weaker and slower ISR activation. **High SM dose**: Ribosome biogenesis mutants do become limited for amino acids, which leads to higher ISR activation in a manner similar to wildtype cells.

While this work focuses on single mutant phenotypes, we also generated data for double mutant phenotypes. We modeled the phenotype measurements for pairwise gRNA combinations as a function of the single mutant phenotypes using LOESS regression. This allowed us to identify pairwise combinations whose phenotype differs from the expected combination of single guide phenotypes. This analysis was performed to identify potential genetic interactions that impact ISR dynamics. However, experimental validation of the double mutant phenotypes showed discrepancies between the modeled and observed datasets. These inconsistencies indicate that our current model does not accurately capture the complexities of these epistatic interactions. Despite these challenges, our extended double mutant dataset provides a valuable resource for future work to identify potential epistatic interactions that contribute to dynamic ISR regulation.

**Table 4.1: Yeast strains used in this study.** All strains are derived from *S. cerevisiae* BY4741.

| Strain Number | Genotype | Source |
|---|---|---|
| NIY539 | MATa HIS3 leu2Δ0 LYS2 MET15 ura3Δ0 XII-2:kanMXsyn:dCas9-Mxi1:TetR X-3:KlLEU2:P(URA3)::URA3N-attP-2A-Bxb1-V5::T(ADH1) | Nick Ingolia |
| NIY559 | MATa HIS3 LEU2 LYS2 MET15 URA3 XII-2:kanMXsyn:dCas9-Mxi1:TetR X-3:KlLEU2:P(URA3)::URA3N-attP-2A-Bxb1-V5::T(ADH1)::Ura3N/C P(Pcl5)-Citrine/p(UBC6)-mScarlet | Nick Ingolia |
| NIY575 | MATa HIS3 LEU2 LYS2 MET15 URA3 XII-2:kanMXsyn:dCas9-Mxi1:TetR X-3:KlLEU2:P(URA3)::URA3N-attP-2A-Bxb1-V5::T(ADH1)::Ura3N/C P(Pcl5)-Citrine/p(UBC6)-mScarlet X-4::hphMX:sg(RRP42) | This work |
| NIY585 | MATa HIS3 LEU2 LYS2 MET15 URA3 XII-2:kanMXsyn:dCas9-Mxi1:TetR X-3:KlLEU2:P(URA3)::URA3N-attP-2A-Bxb1-V5::T(ADH1)::Ura3N/C P(Pcl5)-Citrine/p(UBC6)-mScarlet [sg(PNO1)] | This work |
| NIY587 | MATa HIS3 LEU2 LYS2 MET15 URA3 XII-2:kanMXsyn:dCas9-Mxi1:TetR X-3:KlLEU2:P(URA3)::URA3N-attP-2A-Bxb1-V5::T(ADH1)::Ura3N/C P(Pcl5)-Citrine/p(UBC6)-mScarlet X-4::hphMX:sg(CBF5) | This work |

**Table 4.2: Plasmids used in this study.**

| Plasmid Name | Description | Source |
|---|---|---|
| pNTI647 | Yeast dCas9-Mxi1 TetR KanMx | McGlincy et al. 2017 |
| pNTI829 | pCfB2189 (X-3 KlLEU2) Ura3N-intron/attP-Bxb1-V5::T_ADH1 | Lobel et al. 2024 |
| pNTI929 | T(ADH1)/BsmBI/P(UBC6)::mScarlet-KanR-attB-UraC-P(Pcl5)::Citrine-BsmBI/T(ACT1) SacB | This work |
| pNTI963 | sg(RRP42) Easyclone vector pCfB2194 | This work |
| pNTI972 | T(ADH1)/BsmBI/P(UBC6)::mScarlet-KanR-attB-UraC-P(Pcl5)::Citrine-BsmBI/T(ACT1) SacB sg(PNO1) | This work |
| pNTI974 | sg(CBF5) Easyclone vector pCfB2194 | This work |

**Table 4.3: Primers used in this study.**

| Oligo Number | Sequence | Notes | Source |
|---|---|---|---|
| NI-827 | CTCTTTCCCTACACGACGCTC | qPCR library quanitification primer | McGlincy et al. 2017 |
| NI-828 | GTGACTGGAGTTCAGACGTGTG | qPCR library quanitification primer | McGlincy et al. 2017 |
| NI-1243 | CCGGTGAAGGTGAAGGTGATGCT | Citrine RT-qPCR | Nick Ingolia |
| NI-1244 | ACCTTCTGGCATGGCAGACTTGA | Citrine RT-qPCR | Nick Ingolia |
| NI-1245 | TCCCAGGAGAAGGGAAGCGGTC | mScarlet RT-qPCR | Nick Ingolia |
| NI-1246 | GGGCAGCATGAACGGACACGAA | mScarlet RT-qPCR | Nick Ingolia |
| NI-1267 | ACTCTTTCCCTACACGACGCTCTTCCGATCTNNNNNNNNaTCCACATGTGCATTGCCTCG | ADH1-side RT N8 UMI | Nick Ingolia |
| NI-1268 | ACTCTTTCCCTACACGACGCTCTTCCGATCTNNNNNNNNcAGAGCTCGATCCAGTCACTC | ACT1-side RT N8 UMI | Nick Ingolia |
| NI-1271 | GTGACTGGAGTTCAGACGTGTGCTCTTCCGATCTatcgctgcaggtcgaaattcg | mScarlet library GSP | Nick Ingolia |
| NI-1272 | GTGACTGGAGTTCAGACGTGTGCTCTTCCGATCTgcgttacccaacGAtaatcgc | citrine library GSP | Nick Ingolia |
| NI-1273 | ACTCTTTCCCTACACGACGCT | GSP shared Rev | Nick Ingolia |
| qRB308 | CGGTACAAACTCTCGCATACA | *RRP42* RT-qPCR | This work |
| qRB309 | GACGACTTAGAGGTGGAAGAAC | *RRP42* RT-qPCR | This work |
| qRB319 | AGATCATGGTTCCACCACAC | *PNO1* RT-qPCR | This work |
| qRB320 | GCTCGACCAAAGGAGGATAAA | *PNO1* RT-qPCR | This work |
| qRB321 | TCTGCTGTCAATGCAGTATGT | *CBF5* RT-qPCR | This work |
| qRB322 | GGCTTCACCCTTGGTAGTTATC | *CBF5* RT-qPCR | This work |

**Table 4.4 Guide sequences used in this study.** Guide spacer sequences for targeted genes and GC content

| Guide | Systematic name | Standard Name | Spacer sequence | Spacer %GC content |
|---|---|---|---|---|
| Q0160_02 | Q0160 | SCEI | CTTTCATATATGTATATATA | 15 |
| YAL003W_07 | YAL003W | EFB1 | GTAAAAAGATAAAGAGTAGA | 25 |
| YAL003W_09 | YAL003W | EFB1 | ACCTTAAACTATTTATTTAG | 20 |
| YAL016C-B_06 | YAL016C-B | | GTATTTCTGCTTTTAAGGTA | 30 |
| YAL025C_04 | YAL025C | MAK16 | AAAAAAAATGAAAAAGTGAT | 15 |
| YBL033C_07 | YBL033C | RIB1 | ATATAAAGAAGTTGCTGTGC | 35 |
| YBL041W_09 | YBL041W | PRE7 | GATCGAGGAAACTCAAAGGG | 50 |
| YBL092W_05 | YBL092W | RPL32 | AAACCATACAATGCCTCCGC | 50 |
| YBR011C_03 | YBR011C | IPP1 | ATCCTGTTCTATAGACCTAA | 35 |
| YBR020W_06 | YBR020W | GAL1 | CGAATCAAATTAACAACCAT | 30 |
| YBR069C_06 | YBR069C | TAT1 | TCGTATATATCCCTGTTTTG | 35 |
| YBR078W_03 | YBR078W | ECM33 | ATGTTCTAAAAAGAAGAGAA | 25 |
| YBR078W_04 | YBR078W | ECM33 | TGTTCTAAAAAGAAGAGAAA | 25 |
| YBR103C-A_02 | YBR103C-A | | CCATAAAGAACAGAAAAAAG | 30 |
| YBR143C_06 | YBR143C | SUP45 | AAGAAATAAAGGTGTCGTTA | 30 |
| YBR166C_00 | YBR166C | TYR1 | ACTGGTATAACGCTTATTAG | 35 |
| YBR167C_07 | YBR167C | POP7 | TTCAATTCAACAGCCTGGTG | 45 |
| YBR211C_08 | YBR211C | AME1 | ACTAGTCCTTTAACAATATT | 25 |
| YBR234C_07 | YBR234C | ARC40 | GCCTTGCCTATAATGAAAAA | 35 |
| YBR248C_09 | YBR248C | HIS7 | CATGATCACCTAATTAGCCG | 45 |
| YBR257W_02 | YBR257W | POP4 | TACTCGATGACATGAATAAG | 35 |
| YBR288C_09 | YBR288C | APM3 | CCCTTGATGATGCTTTGTTT | 40 |
| YCL008C_06 | YCL008C | STP22 | TTTCTTAAAGTATAGATAAA | 15 |
| YCL030C_04 | YCL030C | HIS4 | TACTGTGTATATAATAGATA | 20 |
| YCL030C_05 | YCL030C | HIS4 | ACTGACTCTAATAGTGACTC | 40 |
| YCL034W_07 | YCL034W | LSB5 | CTTGATCACTTTACACGTCA | 40 |
| YCL048W-A_03 | YCL048W-A | | GAGAATGAAATAAAGAAAAG | 25 |
| YCR012W_01 | YCR012W | PGK1 | CAATGCAAGAAATACATATT | 25 |
| YCR012W_04 | YCR012W | PGK1 | ATGTAAATGTAAGTTTCACG | 30 |
| YCR059C_08 | YCR059C | YIH1 | GTTCCTTCTGCTTTTCAAAT | 35 |
| YDL029W_07 | YDL029W | ARP2 | ATTCTACAAGACGGGTAATA | 35 |
| YDL097C_07 | YDL097C | RPN6 | CTACCAACATTTGCCACCCT | 50 |

| | | | | |
|---|---|---|---|---|
| YDL111C_05 | YDL111C | RRP42 | AAAGAAACGTAGAGCTTATA | 30 |
| YDL132W_04 | YDL132W | CDC53 | GACACACATGAAGTGAAATG | 40 |
| YDL147W_06 | YDL147W | RPN5 | AAAATGCAAAGGGGAATCCA | 40 |
| YDL150W_02 | YDL150W | RPC53 | AGATAATGACCAGAGAATTA | 30 |
| YDL150W_08 | YDL150W | RPC53 | AAAAATTGGACTTTGCAGGG | 40 |
| YDL227C_00 | YDL227C | HO | GTAGTACAATTCAAAGTAGT | 30 |
| YDL227C_01 | YDL227C | HO | CGCGACTTTATTCGAAGTTA | 40 |
| YDL227C_02 | YDL227C | HO | CAGCTATTGCTACTCAAATG | 40 |
| YDL227C_04 | YDL227C | HO | AGAATTGATTGCTGCTTATG | 35 |
| YDL227C_05 | YDL227C | HO | AAATAAAAGCCATTTAGAAT | 20 |
| YDL227C_06 | YDL227C | HO | AAGTTATGGTGAACTTTTCG | 35 |
| YDR023W_09 | YDR023W | SES1 | ATATATTACAATTCGTGAAC | 25 |
| YDR160W_07 | YDR160W | SSY1 | TTGTGCAAAAAGTGAAGCCA | 40 |
| YDR187C_08 | YDR187C | | AGTTCCTTCTGCAAGTGGCC | 55 |
| YDR188W_04 | YDR188W | CCT6 | TGTGGAAAAGGTAAAGGTTA | 35 |
| YDR211W_02 | YDR211W | GCD6 | TTAAATCACCAATTCAAAGA | 25 |
| YDR211W_08 | YDR211W | GCD6 | TTTATACTTATCCCACAAGG | 35 |
| YDR271C_00 | YDR271C | | AAAATGAGATGGGAGTCTGG | 45 |
| YDR280W_05 | YDR280W | RRP45 | ATGTCTGAATATAAAGGAAT | 25 |
| YDR283C_04 | YDR283C | GCN2 | TTTATACATAGTATGTGTTA | 20 |
| YDR300C_06 | YDR300C | PRO1 | ATCTTGAAAGACCGTTTTGA | 35 |
| YDR328C_05 | YDR328C | SKP1 | GTTATATCTTTGCCAACGTT | 35 |
| YDR341C_05 | YDR341C | | CAATTTTCACAATGCATCTA | 30 |
| YDR341C_07 | YDR341C | | TCTATGGAGAGGATATTATA | 30 |
| YDR379C-A_08 | YDR379C-A | SDH6 | TATCTTTGTTAAGAATAATT | 15 |
| YDR380W_06 | YDR380W | ARO10 | TTGATACCTTCGGTAAGTGT | 40 |
| YDR380W_07 | YDR380W | ARO10 | CGGCGGAGCTTTGATACCTT | 55 |
| YDR392W_08 | YDR392W | SPT3 | TTGAAGACACTCTGAACCCG | 50 |
| YDR398W_08 | YDR398W | UTP5 | CTTTGATTGTCATTTAACAC | 30 |
| YDR448W_00 | YDR448W | ADA2 | GAAAAAATACTATAAATGTA | 15 |
| YDR454C_04 | YDR454C | GUK1 | TAGCATAAATGGATACACAA | 30 |
| YDR493W_03 | YDR493W | MZM1 | AGGAAAGAGAGGAAGAGAAA | 40 |
| YEL009C_00 | YEL009C | GCN4 | AAAATTTCCGACTTTAAATA | 20 |
| YEL026W_08 | YEL026W | SNU13 | AGTAGGACTTGAACACTAAG | 40 |
| YEL051W_06 | YEL051W | VMA8 | CGGGGATTGTTAAAAGACAA | 40 |
| YER001W_07 | YER001W | MNN1 | CGAAAACGTTGCAATGTATT | 35 |
| YER012W_09 | YER012W | PRE1 | GAACACCAATTACAAGAAAA | 30 |
| YER022W_04 | YER022W | SRB4 | ACTTTCTACATTCATAGACG | 35 |

| | | | | |
|---|---|---|---|---|
| YER025W_06 | YER025W | GCD11 | CTTTGCTTAGCTCCTGGTAC | 50 |
| YER025W_07 | YER025W | GCD11 | ATTTCATCTCGACCTGTACC | 45 |
| YER029C_01 | YER029C | SMB1 | TCGTGAGAAAAACAAGAACA | 35 |
| YER042W_00 | YER042W | MXR1 | ACGCACAAGATACAGTCGAC | 50 |
| YER091C_00 | YER091C | MET6 | CGATAGATGCACTAATTTAA | 30 |
| YER091C_01 | YER091C | MET6 | GAAACTAATGCTAGTAAAGA | 30 |
| YER092W_03 | YER092W | IES5 | ACAGAGTCGTACGTCAGGAC | 55 |
| YER094C_07 | YER094C | PUP3 | GTAGAAAGGCCAATTAAATC | 35 |
| YER165W_07 | YER165W | PAB1 | TCTCTTTCGCTCCAGTTCCA | 50 |
| YER171W_06 | YER171W | RAD3 | CCGTCGGCCATGATTAATAT | 45 |
| YFL022C_04 | YFL022C | FRS2 | TATATATATATGTATATATA | 5 |
| YFL039C_06 | YFL039C | ACT1 | AGGCGAGTTTGGTTTCAAAA | 40 |
| YFR002W_03 | YFR002W | NIC96 | TAATGCATTTGAAATCTTCT | 25 |
| YFR029W_03 | YFR029W | PTR3 | ATTTTCACACCTTTTTCAAG | 30 |
| YFR029W_07 | YFR029W | PTR3 | ATCATTGATGACTACTGTAA | 30 |
| YFR050C_09 | YFR050C | PRE4 | ACTATGTGGGTACGTATTTA | 35 |
| YGL030W_08 | YGL030W | RPL30 | GTAATGAACATTCCAACAAA | 30 |
| YGL030W_09 | YGL030W | RPL30 | TTTTCCTATTGGAGACGGAA | 40 |
| YGL058W_05 | YGL058W | RAD6 | CCAAGGAACAAATACATATT | 30 |
| YGL123W_01 | YGL123W | RPS2 | AAACTCTTACGTTACTACAG | 35 |
| YGL207W_09 | YGL207W | SPT16 | ATATTCTTTCGTTAGAAAAG | 25 |
| YGL245W_02 | YGL245W | GUS1 | AGGTTAAGGAAAGCATAGAA | 35 |
| YGL245W_05 | YGL245W | GUS1 | AATGACGAAACTATTTTCAA | 25 |
| YGR010W_05 | YGR010W | NMA2 | AGCAAAAAATGGCCAGAAAC | 40 |
| YGR030C_01 | YGR030C | POP6 | AACCAACCCCCGCACGCTCT | 65 |
| YGR030C_06 | YGR030C | POP6 | AAGATGAGGCCAAGATTGTT | 40 |
| YGR056W_00 | YGR056W | RSC1 | TATTGACGGAAAGAGGGTAA | 40 |
| YGR094W_02 | YGR094W | VAS1 | ACTTAGATGGTATGAATAAG | 30 |
| YGR094W_04 | YGR094W | VAS1 | AAGTAATTCCATAAATCTGA | 25 |
| YGR133W_05 | YGR133W | PEX4 | TTCGAAATCCTGAACGGAAG | 45 |
| YGR146C_01 | YGR146C | ECL1 | GGTGTTGAAACGGAAAAGAT | 40 |
| YGR156W_01 | YGR156W | PTI1 | AGCGACATGTTGGAAAGGTC | 50 |
| YGR195W_08 | YGR195W | SKI6 | GGTGAAATTGAAAAATTTTA | 20 |
| YGR198W_08 | YGR198W | YPP1 | TTTTCGAGATCCACCTATTG | 40 |
| YGR252W_01 | YGR252W | GCN5 | TTTACGCAGTATAATTGTTT | 25 |
| YGR264C_01 | YGR264C | MES1 | AATAAAACTTGAAAAAAAAG | 15 |
| YHL025W_04 | YHL025W | SNF6 | ATCCAGAAAGGGGAGGCTAA | 50 |
| YHR019C_08 | YHR019C | DED81 | AGGTAGAAGAAATTACGTTT | 30 |
| YHR020W_03 | YHR020W | | TACTTTTGCTAGATAGTTGC | 35 |

| | | | | |
|---|---|---|---|---|
| YHR032C-A_03 | YHR032C-A | | AAAATCAAAAACAAAAAAAG | 15 |
| YHR062C_05 | YHR062C | RPP1 | TTAGGTTAAGTATTTTCTAC | 25 |
| YHR062C_09 | YHR062C | RPP1 | TTTATGCGAGGTAAAATTCT | 30 |
| YHR069C_04 | YHR069C | RRP4 | CCAGTTTAAACCATAAGTAA | 30 |
| YHR069C_06 | YHR069C | RRP4 | ATGCAAGCAGTACTTAAGGA | 40 |
| YHR070C-A_08 | YHR070C-A | | AGAAGAATAAATTAGGAAGT | 25 |
| YHR071W_02 | YHR071W | PCL5 | GTTATAACTATATCGAACCT | 30 |
| YHR196W_03 | YHR196W | UTP9 | CCCGGCGTTATATATTGCAA | 45 |
| YIL019W_07 | YIL019W | FAF1 | GTCTAGTGTGCAGAGTCATA | 45 |
| YIL028W_08 | YIL028W | | AATATACCTATAATGAAAAA | 15 |
| YIL046W_03 | YIL046W | MET30 | GAGGCTTGAGTATCGGTAAA | 45 |
| YIL046W_07 | YIL046W | MET30 | GTTAAAGAAGTTTAGAGAAG | 30 |
| YIL078W_02 | YIL078W | THS1 | TGTGTCATCTGAAAGATTAC | 35 |
| YIL142W_08 | YIL142W | CCT2 | AGAGCAGAGCAATAAAAAAG | 35 |
| YIR013C_01 | YIR013C | GAT4 | ATTTCAAAAAAAAAGAAAAA | 10 |
| YJL001W_02 | YJL001W | PRE3 | ATTTTAAACAAGTTGCGAGA | 30 |
| YJL005W_07 | YJL005W | CYR1 | GTATTTTGGAAGGAAAGCAG | 40 |
| YJL011C_01 | YJL011C | RPC17 | GCTTAACTTTCATAGATCGA | 35 |
| YJL011C_06 | YJL011C | RPC17 | ACTCAACTTCTCTTCTACTG | 40 |
| YJL143W_01 | YJL143W | TIM17 | TGGCATAAAAATGGAAACTT | 30 |
| YJL176C_02 | YJL176C | SWI3 | CGCGATATATTGGTACATCG | 45 |
| YJR007W_04 | YJR007W | SUI2 | ACTTTACTCTTTAATGACCT | 30 |
| YJR041C_09 | YJR041C | URB2 | ATGATCGCTAAGAGGGCACT | 50 |
| YJR045C_08 | YJR045C | SSC1 | CCAACGCCGGCTCGACGCTT | 70 |
| YJR065C_08 | YJR065C | ARP3 | CAAGAATTGGCCCTACCGTA | 50 |
| YJR123W_05 | YJR123W | RPS5 | TAAGCCTGCGGCGAAGGTAG | 60 |
| YKL012W_09 | YKL012W | PRP40 | GCCAAGCAAATAGAGGCTTT | 45 |
| YKL143W_06 | YKL143W | LTV1 | TAGACGCAAGAAGCGTTATT | 40 |
| YKR025W_02 | YKR025W | RPC37 | GTGCAAGGTGAAAGTGGAAT | 45 |
| YLL018C_01 | YLL018C | DPS1 | AAATTATTTAATGTCATATA | 10 |
| YLL031C_00 | YLL031C | GPI13 | AACAAAAACAAAAGATAGAG | 25 |
| YLR004C_09 | YLR004C | THI73 | AGAGACTATATTAACTAAGG | 30 |
| YLR008C_06 | YLR008C | PAM18 | AACTGATGTAAGTTGGAGAT | 35 |
| YLR065C_07 | YLR065C | ENV10 | GCAATGCTAGCTAGCTTTGT | 45 |
| YLR117C_01 | YLR117C | CLF1 | GTCTCATCACCCCAACTATT | 45 |
| YLR175W_00 | YLR175W | CBF5 | AATGATGAGATGTTTAGCTT | 30 |
| YLR190W_01 | YLR190W | MMR1 | TACGTTCATTCAAGACAAAG | 35 |

| | | | | |
|---|---|---|---|---|
| YLR246W_09 | YLR246W | ERF2 | TAAGGTAACAAGAAGAGAAA | 30 |
| YLR291C_09 | YLR291C | GCD7 | CAGACCATTCATTACTCGTG | 45 |
| YLR347C_07 | YLR347C | KAP95 | ATTTTGCTGGAAGGGCAATA | 40 |
| YLR355C_02 | YLR355C | ILV5 | AAAAGCCATTGAGTCAAGTT | 35 |
| YLR355C_05 | YLR355C | ILV5 | GATGACCTAACTTGACTCAA | 40 |
| YML007W_00 | YML007W | YAP1 | GAAAAAGAAAAGAGTAACCT | 30 |
| YML060W_07 | YML060W | OGG1 | GCTCATCTCTTAAAAATTTT | 25 |
| YML092C_01 | YML092C | PRE8 | CAATAAGCTGAGAGTGGAAT | 40 |
| YMR005W_04 | YMR005W | TAF4 | TTCCCATTTGAGCTATTACA | 35 |
| YMR009W_09 | YMR009W | ADI1 | GTATAAAAGAACAAAGAGGG | 35 |
| YMR060C_01 | YMR060C | SAM37 | TTTTCTTCTTAATTATTACA | 15 |
| YMR108W_01 | YMR108W | ILV2 | GAACTTGTATTTCTCTTATC | 30 |
| YMR108W_08 | YMR108W | ILV2 | TTTCTAATCTTCCATCTATT | 25 |
| YMR177W_04 | YMR177W | MMT1 | CGCGCTTTTCCACCTTCGAA | 55 |
| YMR273C_03 | YMR273C | ZDS1 | CAAACTCTGGTAGGAACTCC | 50 |
| YMR314W_05 | YMR314W | PRE5 | CCACGTCTACCTAAATGTAG | 45 |
| YMR314W_07 | YMR314W | PRE5 | ACCAAGACGCCACTACATTT | 45 |
| YMR319C_04 | YMR319C | FET4 | ATCAGATATAAGAAGGGAAA | 30 |
| YNL003C_08 | YNL003C | PET8 | ATGATCTCATATATTCTCGA | 30 |
| YNL141W_01 | YNL141W | AAH1 | TTGAAAAAAATTAACATATA | 10 |
| YNL151C_02 | YNL151C | RPC31 | TCTGTCGTGTTGTTTTCTAT | 35 |
| YNL151C_05 | YNL151C | RPC31 | TTCTATAGGTTGCTGCGATG | 45 |
| YNL221C_06 | YNL221C | POP1 | GGTGGCATGTCTTTGAAGAA | 45 |
| YNL236W_02 | YNL236W | SIN4 | GATGATAAATCTCGCTATTT | 30 |
| YNL247W_02 | YNL247W | | GCATAGAATAAGAACTTGAC | 35 |
| YNL247W_09 | YNL247W | | AAAAGAACAGTATTGCTAAT | 25 |
| YNL268W_08 | YNL268W | LYP1 | AGGTGACTATTTAACAAGGA | 35 |
| YNL303W_00 | YNL303W | | TAACAAGATTGACCTTTATA | 25 |
| YNL330C_04 | YNL330C | RPD3 | ATTTGAAGTAATAACCATAA | 20 |
| YNR003C_01 | YNR003C | RPC34 | TAATACAATAAAAGATTTGA | 15 |
| YNR004W_01 | YNR004W | SWM2 | AACTAAAATTAAAAAAATAG | 10 |

| | | | | |
|---|---|---|---|---|
| YNR035C_06 | YNR035C | ARC35 | CAAGAAATACTATAAGCATA | 25 |
| YNR035C_07 | YNR035C | ARC35 | ACAAGAAATACTATAAGCAT | 25 |
| YOL038C-A_06 | YOL038C-A | | GAAAAGACATCATATATAGG | 30 |
| YOL038C-A_09 | YOL038C-A | | AAAGAAAAGACATCATATAT | 20 |
| YOL051W_04 | YOL051W | GAL11 | TTAGGCATTACCCTACATTG | 40 |
| YOL075C_02 | YOL075C | | AAGTGAAAAAAAAAAAAGGA | 20 |
| YOL115W_02 | YOL115W | PAP2 | AAAAATAAAATAAAAAAAAG | 5 |
| YOL127W_01 | YOL127W | RPL25 | AACGCAGTGAGGCAAGCCGA | 60 |
| YOL133W_08 | YOL133W | HRT1 | GAAGCCCATACGTCTATTGT | 45 |
| YOL133W_09 | YOL133W | HRT1 | GAAACCCACAATAGACGTAT | 40 |
| YOL134C_02 | YOL134C | | ATGCCATAATCCTTCTACCT | 40 |
| YOL135C_09 | YOL135C | MED7 | TGAAACCCACAATAGACGTA | 40 |
| YOL142W_07 | YOL142W | RRP40 | TATTAAACCAACAGCACAAA | 30 |
| YOR001W_04 | YOR001W | RRP6 | ACCCAAAAATATGAGGGCAT | 40 |
| YOR046C_09 | YOR046C | DBP5 | TAAAGGTCAACTGGTTTTAA | 30 |
| YOR063W_02 | YOR063W | RPL3 | ATAATGAGTAAAGAAAGATG | 25 |
| YOR116C_04 | YOR116C | RPO31 | AATATATGCAAAGAATAGTA | 20 |
| YOR116C_07 | YOR116C | RPO31 | ACCAGATCAAATAACAGAAG | 35 |
| YOR117W_02 | YOR117W | RPT5 | TTGGGTAAAAAGGGCACATC | 45 |
| YOR117W_08 | YOR117W | RPT5 | TTACCCAAGAGTTCATTAAT | 30 |
| YOR145C_08 | YOR145C | PNO1 | TGAGCATCGGTATGATAATA | 35 |
| YOR167C_06 | YOR167C | RPS28A | CATCGCAGGGTATAAAGATT | 40 |
| YOR187W_06 | YOR187W | TUF1 | ACCAGTTAGCAGCAAAAGGG | 50 |
| YOR207C_09 | YOR207C | RET1 | ACAAGTTAGGAAAGAATTAA | 25 |
| YOR208W_09 | YOR208W | PTP2 | TGATGATATATGGACAAGTT | 30 |
| YOR225W_05 | YOR225W | | AGACATTGCTGCGGTTGTTA | 45 |
| YOR260W_03 | YOR260W | GCD1 | GGGGGGGAGCTATCAACGGT | 65 |
| YOR290C_05 | YOR290C | SNF2 | ATTGTCCTACCGCCTCAGGA | 55 |
| YOR335C_01 | YOR335C | ALA1 | TAAAACAAGAAAAACGCAGT | 30 |
| YOR340C_07 | YOR340C | RPA43 | TACAATAAAATAGAGCCGAA | 30 |
| YOR362C_02 | YOR362C | PRE10 | GTGGCGGTAGAGGGTTTATT | 50 |
| YOR362C_07 | YOR362C | PRE10 | AAAGTAAGTGGTAATAGTGG | 35 |
| YPL063W_08 | YPL063W | TIM50 | TCTCTTCAGACGCTTTACAG | 45 |
| YPL082C_01 | YPL082C | MOT1 | CGCCAAGGGAACGGAATTGG | 60 |
| YPL082C_09 | YPL082C | MOT1 | CGCGCAAACCGCCAAGGGAA | 65 |
| YPL160W_04 | YPL160W | CDC60 | GTTTGAATAGAATATGCGTT | 30 |
| YPL237W_01 | YPL237W | SUI3 | GCGAGAAAAAGTGAAATTGA | 35 |

| | | | | |
|---|---|---|---|---|
| YPL237W_02 | YPL237W | SUI3 | TATTATATGACTGGTTGCCT | 35 |
| YPL268W_02 | YPL268W | PLC1 | ATCACGACATAAGCAGCCTC | 50 |
| YPR033C_02 | YPR033C | HTS1 | TAAGCAAGAGACGAGCAGAA | 45 |
| YPR033C_05 | YPR033C | HTS1 | CTATTCTAAAGTAACACATT | 25 |
| YPR067W_05 | YPR067W | ISA2 | GATGTTTAAACAAGTGACAC | 35 |
| YPR084W_07 | YPR084W | | TGGGATTAAAAAATAAAAGA | 20 |
| YPR103W_02 | YPR103W | PRE2 | GCAAGGTGAATTGTAAAGAA | 35 |
| YPR137W_02 | YPR137W | RRP9 | GATGCTTATTTGAATATTTA | 20 |
| YPR190C_02 | YPR190C | RPC82 | GAATTGCTGACACAGGAATA | 40 |
| YPR190C_08 | YPR190C | RPC82 | TTGGATCAAAATAATAATAG | 20 |

## References


Alford, Brian D., Eduardo Tassoni-Tsuchida, Danish Khan, Jeremy J. Work, Gregory Valiant, and Onn Brandman. 2021. "ReporterSeq Reveals Genome-Wide Dynamic Modulators of the Heat Shock Response across Diverse Stressors." *eLife* 10 (July):e57376. https://doi.org/10.7554/eLife.57376.

Anders, Simon, Paul Theodor Pyl, and Wolfgang Huber. 2015. "HTSeq—a Python Framework to Work with High-Throughput Sequencing Data." *Bioinformatics* 31 (2): 166–69. https://doi.org/10.1093/bioinformatics/btu638.

Aranda-Díaz, Andrés, Kieran Mace, Ignacio Zuleta, Patrick Harrigan, and Hana El-Samad. 2017. "Robust Synthetic Circuits for Two-Dimensional Control of Gene Expression in Yeast." *ACS Synthetic Biology* 6 (3): 545–54. https://doi.org/10.1021/acssynbio.6b00251.

Ares, Manuel. 2012. "Isolation of Total RNA from Yeast Cell Cultures." *Cold Spring Harbor Protocols* 2012 (10): 1082–86. https://doi.org/10.1101/pdb.prot071456.

Arribere, Joshua A., Jennifer A. Doudna, and Wendy V. Gilbert. 2011. "Reconsidering Movement of Eukaryotic mRNAs between Polysomes and P Bodies." *Molecular Cell* 44 (5): 745–58. https://doi.org/10.1016/j.molcel.2011.09.019.

Ashe, M. P., S. K. De Long, and A. B. Sachs. 2000. "Glucose Depletion Rapidly Inhibits Translation Initiation in Yeast." *Molecular Biology of the Cell* 11 (3): 833–48. https://doi.org/10.1091/mbc.11.3.833.

Barlit, Hanna, Antonia M. Romero, Ali Gülhan, Praveen K. Patnaik, Alexander Tyshkovskiy, María T. Martínez-Pastor, Vadim N. Gladyshev, Sergi Puig, and Vyacheslav M. Labunskyy. 2024. "Ribosome Profiling Reveals the Role of Yeast RNA-Binding Proteins Cth1 and Cth2 in Translational Regulation." *iScience* 27 (6): 109868. https://doi.org/10.1016/j.isci.2024.109868.

Bendrioua, Loubna, Maria Smedh, Joachim Almquist, Marija Cvijovic, Mats Jirstrand, Mattias Goksör, Caroline B. Adiels, and Stefan Hohmann. 2014. "Yeast AMP-Activated Protein Kinase Monitors Glucose Concentration Changes and Absolute Glucose Levels*." *Journal of Biological Chemistry* 289 (18): 12863–75. https://doi.org/10.1074/jbc.M114.547976.

Brothers, Molly, and Jasper Rine. 2019. "Mutations in the PCNA DNA Polymerase Clamp of Saccharomyces Cerevisiae Reveal Complexities of the Cell Cycle and Ploidy on Heterochromatin Assembly." *Genetics* 213 (2): 449–63. https://doi.org/10.1534/genetics.119.302452.

Canadell, David, José García-Martínez, Paula Alepuz, José E. Pérez-Ortín, and Joaquín Ariño. 2015. "Impact of High pH Stress on Yeast Gene Expression: A Comprehensive Analysis of mRNA Turnover during Stress Responses." *Biochimica Et Biophysica Acta* 1849 (6): 653–64. https://doi.org/10.1016/j.bbagrm.2015.04.001.

Chan, Leon Y., Christopher F. Mugler, Stephanie Heinrich, Pascal Vallotton, and Karsten Weis. 2018. "Non-Invasive Measurement of mRNA Decay Reveals Translation Initiation as the Major Determinant of mRNA Stability." *eLife* 7 (September):e32536. https://doi.org/10.7554/eLife.32536.

Chen, Yang S., Wanfu Hou, Sharon Tracy, Alex T. Harvey, Vince Harjono, Fan Xu, James J. Moresco, John R. Yates, and Brian M. Zid. 2022. "Rvb1/Rvb2 Proteins Couple

Transcription and Translation during Glucose Starvation." *eLife* 11 (September):e76965. https://doi.org/10.7554/eLife.76965.

Costanzo, Michael, Benjamin VanderSluis, Elizabeth N. Koch, Anastasia Baryshnikova, Carles Pons, Guihong Tan, Wen Wang, et al. 2016. "A Global Genetic Interaction Network Maps a Wiring Diagram of Cellular Function." *Science (New York, N.Y.)* 353 (6306): aaf1420. https://doi.org/10.1126/science.aaf1420.

Diamond, Paige D., Nicholas J. McGlincy, and Nicholas T. Ingolia. 2024. "Depletion of Cap-Binding Protein eIF4E Dysregulates Amino Acid Metabolic Gene Expression." *Molecular Cell* 84 (11): 2119-2134.e5. https://doi.org/10.1016/j.molcel.2024.05.008.

Durrant, Matthew G., Alison Fanton, Josh Tycko, Michaela Hinks, Sita S. Chandrasekaran, Nicholas T. Perry, Julia Schaepe, et al. 2023. "Systematic Discovery of Recombinases for Efficient Integration of Large DNA Sequences into the Human Genome." *Nature Biotechnology* 41 (4): 488–99. https://doi.org/10.1038/s41587-022-01494-w.

Fleischer, Tracey C., Connie M. Weaver, K. Jill McAfee, Jennifer L. Jennings, and Andrew J. Link. 2006. "Systematic Identification and Functional Screens of Uncharacterized Proteins Associated with Eukaryotic Ribosomal Complexes." *Genes & Development* 20 (10): 1294. https://doi.org/10.1101/gad.1422006.

Gasch, Audrey P., Paul T. Spellman, Camilla M. Kao, Orna Carmel-Harel, Michael B. Eisen, Gisela Storz, David Botstein, and Patrick O. Brown. 2000. "Genomic Expression Programs in the Response of Yeast Cells to Environmental Changes." *Molecular Biology of the Cell* 11 (12): 4241. https://doi.org/10.1091/mbc.11.12.4241.

Gerstberger, Stefanie, Markus Hafner, and Thomas Tuschl. 2014. "A Census of Human RNA-Binding Proteins." *Nature Reviews Genetics* 15 (12): 829–45. https://doi.org/10.1038/nrg3813.

Gibson, Daniel G., Lei Young, Ray-Yuan Chuang, J. Craig Venter, Clyde A. Hutchison, and Hamilton O. Smith. 2009. "Enzymatic Assembly of DNA Molecules up to Several Hundred Kilobases." *Nature Methods* 6 (5): 343–45. https://doi.org/10.1038/nmeth.1318.

Gietz, R. Daniel, and Robert H. Schiestl. 2007. "High-Efficiency Yeast Transformation Using the LiAc/SS Carrier DNA/PEG Method." *Nature Protocols* 2 (1): 31–34. https://doi.org/10.1038/nprot.2007.13.

Gimeno, C. J., P. O. Ljungdahl, C. A. Styles, and G. R. Fink. 1992. "Unipolar Cell Divisions in the Yeast S. Cerevisiae Lead to Filamentous Growth: Regulation by Starvation and RAS." *Cell* 68 (6): 1077–90. https://doi.org/10.1016/0092-8674(92)90079-r.

Giordano, Nils, Francis Mairet, Jean-Luc Gouzé, Johannes Geiselmann, and Hidde De Jong. 2016. "Dynamical Allocation of Cellular Resources as an Optimal Control Problem: Novel Insights into Microbial Growth Strategies." Edited by Oleg A Igoshin. *PLOS Computational Biology* 12 (3): e1004802. https://doi.org/10.1371/journal.pcbi.1004802.

Godard, Patrice, Antonio Urrestarazu, Stéphan Vissers, Kevin Kontos, Gianluca Bontempi, Jacques van Helden, and Bruno André. 2007. "Effect of 21 Different Nitrogen Sources on Global Gene Expression in the Yeast Saccharomyces Cerevisiae." *Molecular and Cellular Biology* 27 (8): 3065–86. https://doi.org/10.1128/MCB.01084-06.

Goldstein, A. L., and J. H. McCusker. 1999. "Three New Dominant Drug Resistance Cassettes for Gene Disruption in Saccharomyces Cerevisiae." *Yeast (Chichester, England)* 15 (14):

1541–53. https://doi.org/10.1002/(SICI)1097-0061(199910)15:14<1541::AID-YEA476>3.0.CO;2-K.
Hedbacker, Kristina, and Marian Carlson. 2006. “Regulation of the Nucleocytoplasmic Distribution of Snf1-Gal83 Protein Kinase.” *Eukaryotic Cell* 5 (12): 1950–56. https://doi.org/10.1128/EC.00256-06.
Heinrich, Stephanie, Maria Hondele, Désirée Marchand, Carina Patrizia Derrer, Mostafa Zedan, Alexandra Oswald, Liliana Malinovska, et al. 2024. “Glucose Stress Causes mRNA Retention in Nuclear Nab2 Condensates.” *Cell Reports* 43 (1): 113593. https://doi.org/10.1016/j.celrep.2023.113593.
Hentges, Pierre, Benoit Van Driessche, Lionel Tafforeau, Jean Vandenhaute, and Antony M. Carr. 2005. “Three Novel Antibiotic Marker Cassettes for Gene Disruption and Marker Switching in Schizosaccharomyces Pombe.” *Yeast* 22 (13): 1013–19. https://doi.org/10.1002/yea.1291.
Hinnebusch, A G. 1984. “Evidence for Translational Regulation of the Activator of General Amino Acid Control in Yeast.” *Proceedings of the National Academy of Sciences of the United States of America* 81 (20): 6442–46.
Hinnebusch, Alan G. 2005. “Translational Regulation of GCN4 and the General Amino Acid Control of Yeast.” *Annual Review of Microbiology* 59 (1): 407–50. https://doi.org/10.1146/annurev.micro.59.031805.133833.
Hofman-Bang, J. 1999. “Nitrogen Catabolite Repression in Saccharomyces Cerevisiae.” *Molecular Biotechnology* 12 (1): 35–73. https://doi.org/10.1385/MB:12:1:35.
Huh, Won-Ki, James V. Falvo, Luke C. Gerke, Adam S. Carroll, Russell W. Howson, Jonathan S. Weissman, and Erin K. O’Shea. 2003. “Global Analysis of Protein Localization in Budding Yeast.” *Nature* 425 (6959): 686–91. https://doi.org/10.1038/nature02026.
Ishimura, Ryuta, Gabor Nagy, Ivan Dotu, Huihao Zhou, Xiang-Lei Yang, Paul Schimmel, Satoru Senju, Yasuharu Nishimura, Jeffrey H. Chuang, and Susan L. Ackerman. 2014. “RNA Function. Ribosome Stalling Induced by Mutation of a CNS-Specific tRNA Causes Neurodegeneration.” *Science (New York, N.Y.)* 345 (6195): 455–59. https://doi.org/10.1126/science.1249749.
Jia, M. H., R. A. Larossa, J. M. Lee, A. Rafalski, E. Derose, G. Gonye, and Z. Xue. 2000. “Global Expression Profiling of Yeast Treated with an Inhibitor of Amino Acid Biosynthesis, Sulfometuron Methyl.” *Physiological Genomics* 3 (2): 83–92. https://doi.org/10.1152/physiolgenomics.2000.3.2.83.
Kief, D. R., and J. R. Warner. 1981. “Coordinate Control of Syntheses of Ribosomal Ribonucleic Acid and Ribosomal Proteins during Nutritional Shift-up in Saccharomyces Cerevisiae.” *Molecular and Cellular Biology* 1 (11): 1007. https://doi.org/10.1128/mcb.1.11.1007.
Kim, Daehwan, Ben Langmead, and Steven L. Salzberg. 2015. “HISAT: A Fast Spliced Aligner with Low Memory Requirements.” *Nature Methods* 12 (4): 357–60. https://doi.org/10.1038/nmeth.3317.
Kim, Jinoh, Kerui Huang, Pham Thuy Tien Vo, Ting Miao, Jacinta Correia, Ankur Kumar, Mirre J P Simons, and Hua Bai. 2024. “Peroxisomal Import Stress Activates Integrated Stress Response and Inhibits Ribosome Biogenesis.” *PNAS Nexus* 3 (10): pgae429. https://doi.org/10.1093/pnasnexus/pgae429.

Konstantakos, Vasileios, Anastasios Nentidis, Anastasia Krithara, and Georgios Paliouras. 2022. "CRISPRedict: A CRISPR-Cas9 Web Tool for Interpretable Efficiency Predictions." *Nucleic Acids Research* 50 (W1): W191–98. https://doi.org/10.1093/nar/gkac466.

Lee, Michael E., William C. DeLoache, Bernardo Cervantes, and John E. Dueber. 2015. "A Highly Characterized Yeast Toolkit for Modular, Multipart Assembly." *ACS Synthetic Biology* 4 (9): 975–86. https://doi.org/10.1021/sb500366v.

Li, Heng, Bob Handsaker, Alec Wysoker, Tim Fennell, Jue Ruan, Nils Homer, Gabor Marth, Goncalo Abecasis, and Richard Durbin. 2009. "The Sequence Alignment/Map Format and SAMtools." *Bioinformatics* 25 (16): 2078–79. https://doi.org/10.1093/bioinformatics/btp352.

Lobel, Joseph H., and Nicholas T. Ingolia. 2024. "Precise Measurement of Molecular Phenotypes with Barcode-Based CRISPRi Systems." *bioRxiv: The Preprint Server for Biology*, June, 2024.06.21.600132. https://doi.org/10.1101/2024.06.21.600132.

Love, Michael I., Wolfgang Huber, and Simon Anders. 2014. "Moderated Estimation of Fold Change and Dispersion for RNA-Seq Data with DESeq2." *Genome Biology* 15 (12): 550. https://doi.org/10.1186/s13059-014-0550-8.

Magasanik, Boris, and Chris A Kaiser. 2002. "Nitrogen Regulation in Saccharomyces Cerevisiae." *Gene* 290 (1–2): 1–18. https://doi.org/10.1016/S0378-1119(02)00558-9.

Martin, Marcel. 2011. "Cutadapt Removes Adapter Sequences from High-Throughput Sequencing Reads." *EMBnet.Journal* 17 (1): 10–12. https://doi.org/10.14806/ej.17.1.200.

Matreyek, Kenneth A., Jason J. Stephany, Melissa A. Chiasson, Nicholas Hasle, and Douglas M. Fowler. 2020. "An Improved Platform for Functional Assessment of Large Protein Libraries in Mammalian Cells." *Nucleic Acids Research* 48 (1): e1. https://doi.org/10.1093/nar/gkz910.

Matreyek, Kenneth A., Jason J. Stephany, and Douglas M. Fowler. 2017. "A Platform for Functional Assessment of Large Variant Libraries in Mammalian Cells." *Nucleic Acids Research* 45 (11): e102. https://doi.org/10.1093/nar/gkx183.

Mattiazzi Usaj, Mojca, Nil Sahin, Helena Friesen, Carles Pons, Matej Usaj, Myra Paz D. Masinas, Ermira Shuteriqi, et al. 2020. "Systematic Genetics and Single-Cell Imaging Reveal Widespread Morphological Pleiotropy and Cell-to-Cell Variability." *Molecular Systems Biology* 16 (2): e9243. https://doi.org/10.15252/msb.20199243.

McGeachy, Anna M., Zuriah A. Meacham, and Nicholas T. Ingolia. 2019. "An Accessible Continuous-Culture Turbidostat for Pooled Analysis of Complex Libraries." *ACS Synthetic Biology* 8 (4): 844–56. https://doi.org/10.1021/acssynbio.8b00529.

Miller, Darach, Nathan Brandt, and David Gresham. 2018. "Systematic Identification of Factors Mediating Accelerated mRNA Degradation in Response to Changes in Environmental Nitrogen." *PLoS Genetics* 14 (5): e1007406. https://doi.org/10.1371/journal.pgen.1007406.

Muller, Ryan, Zuriah A. Meacham, Lucas Ferguson, and Nicholas T. Ingolia. 2020. "CiBER-Seq Dissects Genetic Networks by Quantitative CRISPRi Profiling of Expression Phenotypes." *Science* 370 (6522): eabb9662. https://doi.org/10.1126/science.abb9662.

Ott, Martin. 2016. "Choreography of Protein Synthesis." *Nature* 533 (7604): 472–73. https://doi.org/10.1038/nature18436.

Puig, Sergi, Eric Askeland, and Dennis J. Thiele. 2005. “Coordinated Remodeling of Cellular Metabolism during Iron Deficiency through Targeted mRNA Degradation.” *Cell* 120 (1): 99–110. https://doi.org/10.1016/j.cell.2004.11.032.

Puig, Sergi, Sandra V. Vergara, and Dennis J. Thiele. 2008. “Cooperation of Two mRNA-Binding Proteins Drives Metabolic Adaptation to Iron Deficiency.” *Cell Metabolism* 7 (6): 555–64. https://doi.org/10.1016/j.cmet.2008.04.010.

Reynaud, Kendra, Anna M. McGeachy, David Noble, Zuriah A. Meacham, and Nicholas T. Ingolia. 2023. “Surveying the Global Landscape of Post-Transcriptional Regulators.” *Nature Structural & Molecular Biology* 30 (6): 740–52. https://doi.org/10.1038/s41594-023-00999-5.

Rytka, J. 1975. “Positive Selection of General Amino Acid Permease Mutants in Saccharomyces Cerevisiae.” *Journal of Bacteriology* 121 (2): 562–70. https://doi.org/10.1128/jb.121.2.562-570.1975.

Scheffler, I. E., B. J. de la Cruz, and S. Prieto. 1998. “Control of mRNA Turnover as a Mechanism of Glucose Repression in Saccharomyces Cerevisiae.” *The International Journal of Biochemistry & Cell Biology* 30 (11): 1175–93. https://doi.org/10.1016/s1357-2725(98)00086-7.

Schofield, Jeremy A., Erin E. Duffy, Lea Kiefer, Meaghan C. Sullivan, and Matthew D. Simon. 2018. “TimeLapse-Seq: Adding a Temporal Dimension to RNA Sequencing through Nucleoside Recoding.” *Nature Methods* 15 (3): 221. https://doi.org/10.1038/nmeth.4582.

Schure, E. G. ter, N. A. van Riel, and C. T. Verrips. 2000. “The Role of Ammonia Metabolism in Nitrogen Catabolite Repression in Saccharomyces Cerevisiae.” *FEMS Microbiology Reviews* 24 (1): 67–83. https://doi.org/10.1111/j.1574-6976.2000.tb00533.x.

Shachrai, Irit, Alon Zaslaver, Uri Alon, and Erez Dekel. 2011. “Cost of Unneeded Proteins in E. Coli Is Reduced after Several Generations in Exponential Growth.” *Molecular Cell* 42 (3): 401. https://doi.org/10.1016/j.molcel.2011.04.009.

Sprouffske, Kathleen, and Andreas Wagner. 2016. “Growthcurver: An R Package for Obtaining Interpretable Metrics from Microbial Growth Curves.” *BMC Bioinformatics* 17 (April):172. https://doi.org/10.1186/s12859-016-1016-7.

Stovicek, Vratislav, Gheorghe M. Borja, Jochen Forster, and Irina Borodina. 2015. “EasyClone 2.0: Expanded Toolkit of Integrative Vectors for Stable Gene Expression in Industrial Saccharomyces Cerevisiae Strains.” *Journal of Industrial Microbiology & Biotechnology* 42 (11): 1519–31. https://doi.org/10.1007/s10295-015-1684-8.

Tye, Blake W, Nicoletta Commins, Lillia V Ryazanova, Martin Wühr, Michael Springer, David Pincus, and L Stirling Churchman. 2019. “Proteotoxicity from Aberrant Ribosome Biogenesis Compromises Cell Fitness.” Edited by Alan G Hinnebusch, Naama Barkai, and David Tollervey. *eLife* 8 (March):e43002. https://doi.org/10.7554/eLife.43002.

West, Sean M., Desirea Mecenas, Michelle Gutwein, David Aristizábal-Corrales, Fabio Piano, and Kristin C. Gunsalus. 2018. “Developmental Dynamics of Gene Expression and Alternative Polyadenylation in the Caenorhabditis Elegans Germline.” *Genome Biology* 19 (1): 8. https://doi.org/10.1186/s13059-017-1369-x.

Wiame, J. M., M. Grenson, and H. N. Arst. 1985. “Nitrogen Catabolite Repression in Yeasts and Filamentous Fungi.” *Advances in Microbial Physiology* 26:1–88. https://doi.org/10.1016/s0065-2911(08)60394-x.

Winters, Matthew J., and Peter M. Pryciak. 2018. “Analysis of the Thresholds for Transcriptional Activation by the Yeast MAP Kinases Fus3 and Kss1.” *Molecular Biology of the Cell* 29 (5): 669–82. https://doi.org/10.1091/mbc.E17-10-0578.

Wu, Colin Chih-Chien, Amy Peterson, Boris Zinshteyn, Sergi Regot, and Rachel Green. 2020. “Ribosome Collisions Trigger General Stress Responses to Regulate Cell Fate.” *Cell* 182 (2): 404-416.e14. https://doi.org/10.1016/j.cell.2020.06.006.

Zid, Brian M., and Erin K. O’Shea. 2014. “Promoter Sequences Direct Cytoplasmic Localization and Translation of mRNAs during Starvation in Yeast.” *Nature* 514 (7520): 117–21. https://doi.org/10.1038/nature13578.